TIME-DOMAIN PROPAGATOR FULL-WAVE NUMERICAL METHOD FOR ELECTROMAGNETIC FIELDS

A Dissertation

by

JONGCHUL SHIN

Submitted to the Office of Graduate and Professional Studies of
Texas A&M University
in partial fulfillment of the requirements for the degree of

DOCTOR OF PHILOSOPHY

Chair of Committee,	Robert D. Nevels
Committee Members,	Krzysztof A. Michalski
	Ehsani Mehrdad
	Stephen A. Fulling
Head of Department,	Miroslav M. Begovic

December 2018

Major Subject: Electrical Engineering

ABSTRACT

This dissertation aims at developing a new time-domain Propagator numerical method for full-wave electromagnetic wave propagation and scattering. An analytical and numerical solution of the full-wave time-domain Propagator method for electromagnetic fields is presented. A propagator is a subclass of Green's function that, when integrated against the present time field throughout a volume of space, produces the field at a pre-determined later time. A primary advantage of the Propagator method is that all electromagnetic field components are calculated at each numerical grid point and all components are in time synchronization. The numerical expressions, provided in one-, two-, and three-dimensions, are obtained by discretizing electric and magnetic field propagator integrals. The Propagator method discussed includes: (1) an extrapolation procedure in time, necessary to maintain constant spatial and time increments throughout an inhomogeneous numerical space, (2) boundary conditions, (3) a simple and effective first order absorbing boundary condition (ABC), described as the null boundary condition, (4) numerical dispersion relations and stability conditions providing the complete stable numerical equations, and (5) the total-field scattered-field formulation. Examples include plane wave reflection from and transmission through a planar boundary, and scattering and radar cross sections for multiple canonical dielectric objects. The proposed method shows good agreement with exact solutions and the results computed by other numerical methods including the Finite-Difference Time-Domain (FDTD) and Method of Moment (MoM).

DEDICATION

To my wife, Hyunju Hwang and son, Jaden Mingyu Shin,

for being with me.

To my parents,

for unconditional love and support.

ACKNOWLEDGEMENTS

I would like to express my deepest gratitude to my advisor, Dr. Robert D. Nevels, for his support and guidance throughout my Ph.D. study at Texas A&M University. He has provided a lot of invaluable advice and devoted much time for this work. I would not have completed this work without his support. I would also like to thank Dr. Krzysztof A. Michalski, Dr. Ehsani Mehrdad, and Dr. Stephen A. Fulling for being my committee members. Their comments are very helpful for the improvement of my dissertation and future research.

Thanks also go to my colleagues, Hasan Tahir Abbas, Muhammad Al-Khalidi, and Caleb Grimms for sharing technical discussions and making my life pleasurable. I would like to extend my thanks to my friend, Kyeong-Rok Ryu, for his sincere advice, support, and encouragement. I am also thankful to Texas ladies, Vera R. Wallem and Carolyn E. McDaniel, for taking care of my family during a stay in Texas.

I would like to thank my parents, parents-in-law, brothers, and sister-in-law family for their consistent love, support, and encouragement. Finally, I would like to thank my dear wife, Hyunju Hwang, for her patience and love during my Ph.D. study. Without her support, this work would not have been possible.

CONTRIBUTORS AND FUNDING SOURCES

Contributors

This work was supervised by a dissertation committee consisting of Professor Robert D. Nevels, Krzysztof A. Michalski, and Ehsani Mehrdad of the Department of Electrical & Computer Engineering and Professor Stephen A. Fulling of the Department of Mathematics.

All other work conducted for the dissertation was completed by the student independently.

Funding Sources

This graduate study was supported by Graduate Teaching Assistantships in the Department of Electrical and Computer Engineering at Texas A&M University.

TABLE OF CONTENTS

LIST OF FIGURES

LIST OF TABLES

1. INTRODUCTION

Numerical techniques in computational electromagnetics fall into two categories: a frequency-domain method such as the Method of Moments (MoM) [1] and the Finite Element Method (FEM) [2] and a time-domain method such as the Finite-Difference Time-Domain (FDTD) method [3]. Each numerical method has its advantages and disadvantages. For example, the FDTD method is simple to implement a variety of electromagnetic phenomena, however, based upon its grid scheme, known as Yee's algorithm [4], it has limitations, primarily due to its interleaving structure in which the electric and magnetic fields are not spatially coincident and they exist at different instances in time. The proposed time-domain Propagator method has a distinguishing advantage, all six electromagnetic field components are coincident in both time and space. Time coincidence and spatial collocation offer the potential for more precise calculation of high frequency circuit parameters and the equivalent electric and magnetic currents used for finding radar cross section (RCS) of a scatterer. Probably the most important advantage is that numerical expressions for other equations of science, such as Schrödinger's equation of quantum mechanics [5] and the bio-heat equation for biological applications [6], combine seamlessly at every numerical grid point in the Propagator method mesh.

A propagator is widely used in quantum mechanics [5], quantum electrodynamics [7], quantum chromodynamics [8], plasmonics [9], acoustic surface waves [10], ocean waves [11], geophysical waves [12], polymer physics [13], and almost every scientific discipline involving wave motion [14], [15], but it is virtually untouched in

electromagnetics literature due to complexities of the vector nature of the electromagnetic field. A complete time-domain propagator and corresponding dyadic Green's function for Maxwell's equations were first derived in [16], [17], along with analytical examples demonstrating the correctness of the result. The integral equation that completed the analytical development of the electromagnetic field Green's function propagator expression was then derived in [18]. Based upon this work, the time-domain Propagator numerical method has been successfully applied to one-dimensional transmission line problems, such as nonuniform transmission lines [19], [20], multiconductor quasi-TEM line [21], and inhomogeneous transmission lines [22]. Although the complete closed form of the time-domain propagator has been derived, time-domain numerical expressions in two- and three-dimensions have only recently been developed in [23]–[30].

A propagator is a subclass of Green's functions that, when integrated against the field throughout a volume of space, produces the field at a pre-determined later time [31]. The Propagator method requires an integration that can be either analytical, involving a spatial integration of the propagator multiplied by the field that exists throughout a given region of space, or numerical, involving a numerical volume integration over the product of the discretized propagator function and field. In either case the integral operator produces the field that exists in a region of space after a given time increment. This can also be a recursive procedure, the present time field integrated against the propagator becomes a new present time field that is used to continue the process. For the electromagnetic field, the Green's function propagator is found by a direct solution of Maxwell's equations, yielding a 6×6 second order tensor expression [16], [17] that when

multiplied by the six previous time electric and magnetic field components and integrated, produces the six current time field components.

Because the time-domain Propagator method involves an evaluation of an integral over known quantities, the Green's function propagator and the initial field, it is best described as an evolution operator technique rather than the integral equation method such as the MoM [1] or FEM [2], or the differential equation method such as the FDTD [3]. It is also a direct calculation of the present time field from the previous time field without intermediate steps, as compared to for example the Method of Moments Marching on in Time [32] where the current must be found first and the field then calculated from the current.

1.1 Outline

In this section, the structure of this dissertation is briefly summarized.

Chapter 2 reviews in detail a derivation of the analytical closed-form of propagator and Green's function for Maxwell's equation. Based upon the integral equation of electromagnetic Green's function propagator, the full-dimensional numerical expressions are derived by evaluating numerically the surface integration and derivatives on the causal boundary.

Chapter 3 presents numerical theories including the concept of physical time step that requires an extrapolation technique in time, the introduction of a simple absorbing boundary condition (ABC) and the analysis of boundary condition, numerical dispersion relations, and stability conditions.

In chapter 4, the total-field/scattered-field (TF/SF) formulation for the full-wave Propagator method is described in detail. Advantages of the TF/SF formulation include generation of a plane wave source, wide computational range and absorbing boundary condition.

Chapter 5 illustrates numerical examples that include computation of reflection and transmission coefficients in one-dimensional structures and radar cross sections (RCS) of several dielectric objects in two- and three-dimensional space lattices. In order to demonstrate accuracy, the computed results are compared with other numerical method codes and exact solutions.

Chapter 6 provides concluding remarks and recommended future research work.

2. TIME DOMAIN PROPAGATOR METHOD FOR MAXWELL'S EQUATIONS*

2.1 Introduction

This chapter is intended to present a complete time-domain propagator solution for Maxwell's equations in terms of a Green's function, which can be found by means of a propagator. The Green's function is a solution to an inhomogeneous differential equation, whereas the propagator is a solution to a homogeneous equation. Although the dyadic Green's function can be found by an eigenfunction expansion method [33], solving the propagator with the relation between the Green's function and propagator that causality is enforced is much more straightforward than the eigenfunction expansion.

In this chapter, we review the introduction of a compact integral form of the propagator solution for the time-domain Maxwell's equations and the derivation of its propagator and Green's function found in [16]–[18]. Based upon the derived Green's function propagator, we obtain numerical expressions in each dimension. The present time field is found by simply evaluating the integral of the field-propagator product. Although the one-dimensional (1-D) propagator numerical expression is also an exact solution of Maxwell's equations, the numerical two-dimensional (2-D) and three-dimensional (3-D) propagator expressions have a small numerical error due to numerical approximation of partial derivatives and a surface integration over a causal boundary. Since our objective is to use the direct Maxwell's equations, which has a form that is different from the Green's

function obtained with the standard solution to Maxwell's equations via potentials, we refer to our Green's function as a propagator in this literature.

2.2 Time domain Propagator solution for Maxwell's equations

The time-domain Maxwell's curl equations in a homogeneous region in terms of the electric and magnetic field intensities, $\mathbf{E}$ and $\mathbf{H}$, and the electric and magnetic current densities $\mathbf{J}_{\mathrm{e}}$ and $\mathbf{J}_{\mathrm{m}}$, are given by

$$\varepsilon \frac{\partial \mathbf{E}}{\partial t} = \nabla \times \mathbf{H} - \mathbf{J}_{\mathrm{e}} \tag{2.1a}$$

$$\mu \frac{\partial \mathbf{H}}{\partial t} = -\nabla \times \mathbf{E} - \mathbf{J}_{\mathrm{m}} \tag{2.1b}$$

where ε and μ are the region permittivity and permeability, respectively. Equations (2.1) can be expressed as a general matrix equation, given by

$$\frac{\partial \mathbf{F}}{\partial t} - \bar{\mathbf{S}} \cdot \mathbf{F} = -\mathbf{J} \tag{2.2}$$

which has a vector field **F** and vector current **J**, defined by

$$\mathbf{F} = \begin{bmatrix} E_x & E_y & E_z & H_x & H_y & H_z \end{bmatrix}^{\mathrm{T}}, \quad \mathbf{J} = \begin{bmatrix} \dfrac{\mathbf{J}_{\mathrm{e}}}{\varepsilon} & \dfrac{\mathbf{J}_{\mathrm{m}}}{\mu} \end{bmatrix}^{\mathrm{T}} \tag{2.3}$$

and a 6×6 matrix of differential operator $\bar{\mathbf{S}}$, represented by

$$\bar{\mathbf{S}} = \begin{bmatrix} 0 & \dfrac{1}{\varepsilon} \nabla \times \\ -\dfrac{1}{\mu} \nabla \times & 0 \end{bmatrix} \tag{2.4}$$

Equation (2.2) can be solved by finding a free space dyadic Green's function $\bar{\mathbf{G}}(\mathbf{r},t|\mathbf{r}',t')$ by means of a propagator. Once $\bar{\mathbf{G}}$ is found, a present time field $\mathbf{F}(\mathbf{r},t)$ is determined by [18]

$$\begin{aligned}\mathbf{F}(\mathbf{r},t) = &\int_v\int_{t_0}^{t} \bar{\mathbf{G}}(\mathbf{r},t\,|\,\mathbf{r}',t')\cdot\mathbf{J}(\mathbf{r}',t')dt'd\mathbf{r}' + \int_{v'} \bar{\mathbf{G}}(\mathbf{r},t\,|\,\mathbf{r}',t_0)\cdot\mathbf{F}_0(\mathbf{r}',t_0)d\mathbf{r}' \\ &+\int_s\int_{t_0}^{t} \bar{\mathbf{G}}(\mathbf{r},t\,|\,\mathbf{r}',t')\cdot\begin{bmatrix}\frac{1}{\varepsilon}\hat{\mathrm{n}}\times\mathbf{H}(\mathbf{r}',t') \\ \frac{1}{\mu}\mathbf{E}(\mathbf{r}',t')\times\hat{\mathrm{n}}\end{bmatrix}dt'd\mathbf{s}', \quad (t>t_0)\end{aligned} \tag{2.5}$$

The first integral in (2.5) is the contribution due to the current source $\mathbf{J}(\mathbf{r}',t_0)$ and the second integral is contribution to the present time field due to the initial field $\mathbf{F}_0(\mathbf{r}',t_0)$. The third integral is the contribution from the field on the surface *s* bounding the volume of space in which the present time field is to be found. In a sourceless region, the current $\mathbf{J}$ is zero and, due to the radiation condition, the third contribution goes to zero by extending the volume to infinity.

The propagator is a solution to the homogeneous differential equation

$$\frac{\partial\bar{\mathbf{K}}}{\partial t} - \bar{\mathbf{S}}\cdot\bar{\mathbf{K}} = 0, \;\; t>t' \tag{2.6}$$

subject to

$$\bar{\mathbf{K}}(\mathbf{r},t|\mathbf{r}',t') = \bar{\mathbf{I}}\delta(\mathbf{r}-\mathbf{r}'), \;\; \text{at time } t=t' \tag{2.7}$$

and the Sommerfeld condition $\bar{\mathbf{K}}\to 0$ as $|\mathbf{r}|\to\infty$. However, a Green's function is a solution to the nonhomogeneous differential equation

$$\frac{\partial\bar{\mathbf{G}}}{\partial t} - \bar{\mathbf{S}}\cdot\bar{\mathbf{G}} = \bar{\mathbf{I}}\delta(\mathbf{r}-\mathbf{r}')\delta(t-t') \tag{2.8}$$

The relation between the propagator and Green's function is

$$\bar{\mathbf{G}}\left(\mathbf{r},t\left|\mathbf{r}',t'\right.\right)=U\left(t-t'\right)\bar{\mathbf{K}}\left(\mathbf{r},t\left|\mathbf{r}',t'\right.\right) \tag{2.9}$$

where *U* is the unit step function that enforces causality in the sense that the wave traveling forward in time is determined by the $t>t'$ part of the propagator.

The 6×6 Green's function propagator $\bar{\mathbf{G}}$ for free space Maxwell's equations can be expressed in compact dyadic form in terms of 3×3 submatrices as [16], [18]

$$\bar{\mathbf{G}}=\begin{bmatrix}\bar{\mathbf{G}}_{11} & \bar{\mathbf{G}}_{12}\\ \bar{\mathbf{G}}_{21} & \bar{\mathbf{G}}_{22}\end{bmatrix} \tag{2.10}$$

with

$$\bar{\mathbf{G}}_{11}=\bar{\mathbf{G}}_{22}=\frac{\delta'(c\tau-R)}{4\pi R}\bar{\mathbf{I}}-\nabla\nabla\frac{[U(c\tau-R)-U(-R)]}{4\pi R} \tag{2.11a}$$

$$\bar{\mathbf{G}}_{12}=-\eta^2\bar{\mathbf{G}}_{21}=\eta\nabla\times\frac{\delta(c\tau-R)}{4\pi R}\bar{\mathbf{I}} \tag{2.11b}$$

where $\tau=t-t'$ is the time increment between the initial time t' and present time *t*, $\bar{\mathbf{I}}$ is the identity matrix, and δ is the Dirac delta function. A key observation is that the $\nabla\nabla$ operator in (2.11a) only contributes to the field in the source region, otherwise it can be neglected [34]. Therefore, if the initial field is given in a sourceless volume region, only the first terms in (2.11a) and (2.11b) are required to propagate the field for one time step. If all that needs to be found is the sourceless time evolving field in an open region, it is sufficient to evaluate the only second integral in (2.5). Therefore, the present time field $\mathbf{F}(\mathbf{r},t)$ is found by evaluating the propagator equation,

$$\mathbf{F}(\mathbf{r},t)=\int_{v'}\bar{\mathbf{G}}(\mathbf{r},t\,|\,\mathbf{r}',t_0)\cdot\mathbf{F}_0(\mathbf{r}',t_0)d\mathbf{r}',\quad t>t_0 \tag{2.12}$$

where a zero in the subscript represents the initial time and field. Equation (2.12) is the most compact closed-form of the time-domain propagator solution for Maxwell's equations. The initial field $\mathbf{F}_0$ can be a plane wave, an antenna current, a waveguide mode, an aperture source, or any given field in the volume. Below we extend the scalar propagator method, found in for example [31], to a full vector propagator method, and derive the tensor propagator for Maxwell's equations.

2.3 Propagator and Green's function for Maxwell's equations

In order to find the time evolving field using (2.12), the Green's function (2.10) for Maxwell's equations must be found. The Green's function can be found by means of a propagator. To find the Green's function, we first find the propagator $\bar{\mathbf{K}}$, the solution of homogeneous Maxwell's equations, by solving (2.6). To solve (2.6), the propagator $\bar{\mathbf{K}}$ is expressed as a Fourier integral in terms of spectral dependence $\mathbf{k}$,

$$\bar{\mathbf{K}}\left(\mathbf{r},t\left|\mathbf{r}',t'\right.\right)=\int_{-\infty}^{\infty}\bar{\mathbf{K}}_p\left(\mathbf{k},t\left|\mathbf{r},t'\right.\right)e^{j\mathbf{k}\cdot\mathbf{r}}d\mathbf{k} \tag{2.13}$$

where in Cartesian coordinates $\mathbf{k}=k_x\hat{x}+k_y\hat{y}+k_z\hat{z}$ and the differential $d\mathbf{k}=dk_xdk_ydk_z$ are in terms of the spatial frequency components, and $\mathbf{r}=x\hat{x}+y\hat{y}+z\hat{z}$. Substituting (2.13) into (2.6) gives

$$\int_{-\infty}^{\infty}\left[\frac{\partial\bar{\mathbf{K}}_p}{\partial t}-\bar{\mathbf{S}}_p\bar{\mathbf{K}}_p\right]e^{j\mathbf{k}\cdot\mathbf{r}}d\mathbf{k}=0 \tag{2.14}$$

where the 6×6 matrix operator $\bar{\mathbf{S}}_p$, the spectral domain form of (2.4), can be expressed symbolically by

$$\bar{\mathbf{S}}_p(\mathbf{k}) = \begin{bmatrix} 0 & \frac{1}{\varepsilon}\mathbf{k}\times \\ -\frac{1}{\mu}\mathbf{k}\times & 0 \end{bmatrix} \tag{2.15}$$

Equation (2.14) yields the time dependence of $\bar{\mathbf{K}}_p$ through

$$\frac{\partial \bar{\mathbf{K}}_p}{\partial t} - \bar{\mathbf{S}}_p \bar{\mathbf{K}}_p = 0 \tag{2.16}$$

A solution to (2.16) is

$$\bar{\mathbf{K}}_p = e^{\bar{\mathbf{S}}_p t}\, \bar{\mathbf{K}}_0 \tag{2.17}$$

Substituting (2.17) into (2.13) and enforcing (2.7) gives

$$\int_{-\infty}^{\infty} e^{\bar{\mathbf{S}}_p t'} \bar{\mathbf{K}}_0 e^{j\mathbf{k}\cdot\mathbf{r}}\, d\mathbf{k} = \delta(\mathbf{r}-\mathbf{r}') \tag{2.18}$$

Using the standard Fourier transform representation of the delta function, (2.18) can be written as

$$\int_{-\infty}^{\infty} e^{\bar{\mathbf{S}}_p t'} \bar{\mathbf{K}}_0 e^{j\mathbf{k}\cdot\mathbf{r}}\, d\mathbf{k} = \frac{1}{(2\pi)^3} \int_{-\infty}^{\infty} e^{j\mathbf{k}\cdot(\mathbf{r}-\mathbf{r}')} d\mathbf{k} \tag{2.19}$$

Equating coefficients of $\exp(j\mathbf{k}\cdot\mathbf{r})$ in (2.19) gives

$$e^{\bar{\mathbf{S}}_p t'} \bar{\mathbf{K}}_0 = \frac{1}{(2\pi)^3} e^{-j\mathbf{k}\cdot\mathbf{r}'} \tag{2.20}$$

Substituting (2.20) into (2.17) yields

$$\bar{\mathbf{K}}_p = \frac{1}{(2\pi)^3} e^{\bar{\mathbf{S}}_p \tau} e^{-j\mathbf{k}\cdot\mathbf{r}'} \tag{2.21}$$

where $\tau = t - t'$ is the time increment. By substituting (2.21) into (2.13), the propagator can be obtained by

$$\bar{\mathbf{K}} = \frac{1}{(2\pi)^3} \int_{-\infty}^{\infty} e^{\bar{\mathbf{S}}_p \tau} e^{j\mathbf{k}\cdot(\mathbf{r}-\mathbf{r}')} d\mathbf{k} \tag{2.22}$$

To solve (2.22), the exponential matrix term $e^{\bar{\mathbf{S}}_p \tau}$ is expanded in the power series

$$e^{\bar{\mathbf{S}}_p \tau} = \bar{\mathbf{I}} + \bar{\mathbf{S}}_p \tau + \frac{\bar{\mathbf{S}}_p^2 \tau^2}{2!} + \frac{\bar{\mathbf{S}}_p^3 \tau^3}{3!} + \cdots \tag{2.23}$$

Summing the matrices on the right hand side of (2.23) creates a new 6×6 evolution operator matrix $e^{\bar{\mathbf{S}}_p \tau} = \bar{\mathbf{A}}(t, \mathbf{k})$. The power series formed by summing the components of the $\bar{\mathbf{A}}$ matrix yield surprisingly simple closed form expressions

$$\begin{aligned}
A_{11} = A_{44} &= \frac{\left[k_x^2 + (k_y^2 + k_z^2)\cos(kc\tau)\right]}{k^2} \\
A_{22} = A_{55} &= \frac{\left[k_y^2 + (k_x^2 + k_z^2)\cos(kc\tau)\right]}{k^2} \\
A_{33} = A_{66} &= \frac{\left[k_z^2 + (k_x^2 + k_y^2)\cos(kc\tau)\right]}{k^2} \\
A_{12} = A_{21} = A_{45} = A_{54} &= \frac{k_x k_y \left[1 - \cos(kc\tau)\right]}{k^2} \\
A_{13} = A_{31} = A_{46} = A_{64} &= \frac{k_x k_z \left[1 - \cos(kc\tau)\right]}{k^2} \\
A_{23} = A_{32} = A_{56} = A_{65} &= \frac{k_y k_z \left[1 - \cos(kc\tau)\right]}{k^2} \\
A_{15} = -A_{24} = -\eta^2 A_{42} = \eta^2 A_{51} &= -\frac{jk_z \eta \sin(kc\tau)}{k}
\end{aligned} \tag{2.24}$$

$$A_{16} = -A_{34} = -\eta^2 A_{43} = \eta^2 A_{61} = \frac{jk_y \eta \sin(kc\tau)}{k}$$
$$A_{26} = -A_{35} = -\eta^2 A_{53} = \eta^2 A_{62} = -\frac{jk_x \eta \sin(kc\tau)}{k}$$
$$A_{14} = A_{25} = A_{36} = A_{41} = A_{52} = A_{63} = 0$$

where $k^2 = k_x^2 + k_y^2 + k_z^2$, and $c = 1/\sqrt{\mu\varepsilon}$ and $\eta = \sqrt{\mu/\varepsilon}$ are respectively the phase velocity and intrinsic impedance of the homogeneous medium.

The goal is now to find $\bar{\mathbf{K}}$ by (2.22), i.e.,

$$\bar{\mathbf{K}}(\mathbf{r}, t|\mathbf{r}', t') = \frac{1}{(2\pi)^3} \int_{-\infty}^{\infty} \bar{\mathbf{A}}(t, \mathbf{k}) e^{j\mathbf{k}\cdot(\mathbf{r}-\mathbf{r}')} d\mathbf{k} \tag{2.25}$$

Once the propagator $\bar{\mathbf{K}}$ is evaluated by (2.25) using the evolution operator matrix $\bar{\mathbf{A}}(t, \mathbf{k})$, the Green's function propagator $\bar{\mathbf{G}}$ can be found by (2.9).

The evolution operator matrix $\bar{\mathbf{A}}$ for the 1-D and 2-D cases can be found by respectively setting two and one of the spectral variables k_x, k_y, and k_z in (2.24) to zero. However, the 3-D propagator needs to be evaluated by (2.25) with all spectral variables. We first solve the 3-D propagator, and obtain for example,

$$\begin{aligned} K_{11}^{(3)} &= \frac{1}{(2\pi)^3} \int_0^{\infty} \left[\frac{k_x^2 + (k_x^2 + k_x^2)\cos(kc\tau)}{k^2} \right] e^{j\mathbf{k}\cdot(\mathbf{r}-\mathbf{r}')} dk_x dk_y dk_z \\ &= \left[\frac{\delta(c\tau + R) - 2\delta(R) + \delta(c\tau - R)}{4\pi R^2} + \frac{\mathrm{sgn}(R) U(c\tau - |R|)}{4\pi R^3} \right] \left[1 - \frac{3(x-x')^2}{R^2} \right] \\ &+ \left[\frac{\delta'(c\tau + R) - 2\delta'(R) - \delta'(c\tau - R)}{4\pi R} \right] \frac{(x-x')^2}{R^2} - \left[\frac{\delta'(c\tau + R)}{4\pi R} - \frac{\delta'(c\tau - R)}{4\pi R} \right] \end{aligned} \tag{2.26}$$

where

$$\begin{aligned}
&\mathbf{r}-\mathbf{r}' = (x-x')\hat{x}+(y-y')\hat{y}+(z-z')\hat{z} \\
&R = \sqrt{(x-x')^2+(y-y')^2+(z-z')^2} \\
&\text{sgn}(R) = \begin{cases} +1, & R>0 \\ -1, & R<0 \end{cases}
\end{aligned} \tag{2.27}$$

By rejecting nonphysical solutions, where $R<0$, and removing factors of 2 in front of the delta functions acting at the origin due to the spatial symmetry, we get

$$\begin{aligned}
K_{11}^{(3)} = &\left[\frac{\delta(c\tau-R)-\delta(R)}{4\pi R^2}+\frac{U(c\tau-R)-U(-R)}{4\pi R^3}\right]\left[1-\frac{3(x-x')^2}{R^2}\right] \\
&+\left[\frac{-\delta'(c\tau-R)-\delta'(R)}{4\pi R}\right]\frac{(x-x')^2}{R^2}+\frac{\delta'(c\tau-R)}{4\pi R}
\end{aligned} \tag{2.28}$$

Other components of the propagator matrix $\bar{\mathbf{K}}^{(3)}$ can be similarly found. Finally, all components of the 3-D Green's function propagator matrix using (2.9) are

$$\begin{aligned}
G_{11}^{(3)} &= G_{44}^{(3)} = L\left[1-\frac{3(x-x')^2}{R^2}\right]+S\left(\frac{x-x'}{R}\right)^2+T \\
G_{22}^{(3)} &= G_{55}^{(3)} = L\left[1-\frac{3(y-y')^2}{R^2}\right]+S\left(\frac{y-y'}{R}\right)^2+T \\
G_{33}^{(3)} &= G_{66}^{(3)} = L\left[1-\frac{3(z-z')^2}{R^2}\right]+S\left(\frac{z-z'}{R}\right)^2+T \\
G_{12}^{(3)} &= G_{21}^{(3)} = G_{45}^{(3)} = G_{54}^{(3)} \\
&= -L\left[\frac{3(x-x')(y-y')}{R^2}\right]+S\left[\frac{(x-x')(y-y')}{R^2}\right] \\
G_{13}^{(3)} &= G_{31}^{(3)} = G_{46}^{(3)} = G_{64}^{(3)} \\
&= -L\left[\frac{3(x-x')(z-z')}{R^2}\right]+S\left[\frac{(x-x')(z-z')}{R^2}\right]
\end{aligned} \tag{2.29}$$

$$
\begin{aligned}
G_{23}^{(3)} &= G_{32}^{(3)} = G_{56}^{(3)} = G_{65}^{(3)} \\
&= -L\left[\frac{3(y-y')(z-z')}{R^2}\right] + S\left[\frac{(y-y')(z-z')}{R^2}\right] \\
G_{15}^{(3)} &= -G_{24}^{(3)} = -\eta^2 G_{42}^{(3)} = \eta^2 G_{51}^{(3)} = \eta P\frac{(z-z')}{R} \\
G_{16}^{(3)} &= -G_{34}^{(3)} = -\eta^2 G_{43}^{(3)} = \eta^2 G_{61}^{(3)} = -\eta P\frac{(y-y')}{R} \\
G_{26}^{(3)} &= -G_{35}^{(3)} = -\eta^2 G_{53}^{(3)} = \eta^2 G_{62}^{(3)} = \eta P\frac{(x-x')}{R} \\
G_{14}^{(3)} &= G_{25}^{(3)} = G_{36}^{(3)} = G_{41}^{(3)} = G_{52}^{(3)} = G_{63}^{(3)} = 0
\end{aligned}
$$

where

$$
\begin{aligned}
L &= U(\tau)\left[\frac{\delta(c\tau-R)-\delta(R)}{4\pi R^2} + \frac{U(c\tau-R)-U(-R)}{4\pi R^3}\right] \\
S &= U(\tau)\left[\frac{-\delta'(c\tau-R)-\delta'(R)}{4\pi R}\right] \\
T &= \frac{U(\tau)\delta'(c\tau-R)}{4\pi R} \\
P &= U(\tau)\left[\frac{\delta(c\tau-R)}{4\pi R^2} + \frac{\delta'(c\tau-R)}{4\pi R}\right]
\end{aligned}
\tag{2.30}
$$

We next obtain the 2-D Green's function propagator. As an example, take the 2-D transverse magnetic (TM) to *z* case where all fields are zero except E_z, H_x and H_y. The field vector is expressed as

$$
\mathbf{F} = \begin{bmatrix} E_z & H_x & H_y \end{bmatrix}^T \tag{2.31}
$$

The 1st, 2nd and 6th row components of the 6×6 evolution operator matrix $\bar{\mathbf{A}}$ do not contribute because the field components E_x, E_y, and H_z are all zero. Setting $k_z = 0$ gives $A_{31} = A_{32} = A_{42} = A_{46} = A_{51} = A_{56} = 0$ in (2.24). Replacing $1/(2\pi)^3 \to 1/(2\pi)^2$,

$A_{33} \to A_{11}^{(2)}$, $A_{34} \to A_{12}^{(2)}$, $A_{35} \to A_{13}^{(2)}$, $A_{43} \to A_{21}^{(2)}$, $A_{44} \to A_{22}^{(2)}$, $A_{45} \to A_{23}^{(2)}$, $A_{53} \to A_{31}^{(2)}$, $A_{54} \to A_{32}^{(2)}$, and $A_{55} \to A_{33}^{(2)}$ results in the creation of a 3×3 2-D evolution operator matrix $\bar{\mathbf{A}}^{(2)}$. Each component of the evolution operator matrix determines a corresponding 2-D propagator matrix $\bar{\mathbf{K}}_{\mathrm{mn}}^{(2)}$ acquired by solving (2.25). For example, by substituting $A_{11}^{(2)}$ into (2.25), the propagator matrix element $K_{11}^{(2)}$ can be expressed as

$$K_{11}^{(2)} = \frac{1}{(2\pi)^2} \int_{-\infty}^{\infty} \int_{-\infty}^{\infty} A_{11}^{(2)} d\mathbf{k} = \frac{1}{(2\pi)^2} \int_{-\infty}^{\infty} \int_{-\infty}^{\infty} \cos(kc\tau) e^{jk_x(x-x')} e^{jk_y(y-y')} dk_x dk_y \qquad (2.32)$$

where $k = \sqrt{k_x^2 + k_y^2}$. When (2.32) is evaluated, the Green's function propagator $G_{11}^{(2)}$ becomes

$$G_{11}^{(2)} = U(\tau) K_{11}^{(2)} = \frac{U(\tau)}{2\pi} \left[\frac{\delta(c\tau - \rho)}{\sqrt{(c\tau)^2 - \rho^2}} - \frac{(c\tau) U(c\tau - \rho)}{\left\{(c\tau)^2 - \rho^2\right\}^{3/2}} \right] \qquad (2.33)$$

The remaining terms of the 2-D Green's function matrix, which can be obtained with the help of integral identities [35], [36], are

$$G_{12}^{(2)} = \frac{\eta U(\tau)}{2\pi} \left[\frac{\delta(c\tau - \rho)}{\sqrt{(c\tau)^2 - \rho^2}} - \frac{\rho U(c\tau - \rho)}{\left\{(c\tau)^2 - \rho^2\right\}^{3/2}} \right] \sin\phi$$

$$G_{13}^{(2)} = \frac{\eta U(\tau)}{2\pi} \left[\frac{-\delta(c\tau - \rho)}{\sqrt{(c\tau)^2 - \rho^2}} + \frac{\rho U(c\tau - \rho)}{\left\{(c\tau)^2 - \rho^2\right\}^{3/2}} \right] \cos\phi$$

$$G_{21}^{(2)} = G_{31}^{(2)} = \frac{G_{13}^{(2)}}{\eta^2}$$

$$
\begin{aligned}
G_{22}^{(2)} &= \frac{\delta(\rho)U(\tau)\cos^2\phi}{2\pi\rho} + \frac{U(\tau)\sin^2\phi}{2\pi}\left[\frac{\delta(c\tau-\rho)}{\sqrt{(c\tau)^2-\rho^2}} - \frac{(c\tau)U(c\tau-\rho)}{\left\{(c\tau)^2-\rho^2\right\}^{3/2}}\right] \\
&\quad - \frac{\cos(2\phi)}{2\pi}\left[\frac{1}{\rho^2} + \frac{U(c\tau-\rho)}{\sqrt{(c\tau)^2-\rho^2}\left\{c\tau+\sqrt{(c\tau)^2-\rho^2}\right\}}\right] \\
G_{23}^{(2)} &= \frac{U(\tau)\sin(2\phi)}{2\pi}\left[\frac{\delta(\rho)}{2\rho} + \frac{\delta(c\tau-\rho)}{2\sqrt{(c\tau)^2-\rho^2}} - \frac{(c\tau)U(c\tau-\rho)}{2\left\{(c\tau)^2-\rho^2\right\}^{3/2}}\right. \\
&\quad \left. - \frac{1}{\rho^2} - \frac{U(c\tau-\rho)}{\sqrt{(c\tau)^2-\rho^2}\left\{c\tau+\sqrt{(c\tau)^2-\rho^2}\right\}}\right] \\
G_{32}^{(2)} &= G_{23}^{(2)} \\
G_{33}^{(2)} &= \frac{\delta(\rho)U(\tau)\sin^2\phi}{2\pi\rho} + \frac{U(\tau)\cos^2\phi}{2\pi}\left[\frac{\delta(c\tau-\rho)}{\sqrt{(c\tau)^2-\rho^2}} - \frac{(c\tau)U(c\tau-\rho)}{\left\{(c\tau)^2-\rho^2\right\}^{3/2}}\right] \\
&\quad + \frac{U(\tau)\cos(2\phi)}{2\pi}\left[\frac{1}{\rho^2} + \frac{U(c\tau-\rho)}{\sqrt{(c\tau)^2-\rho^2}\left\{c\tau+\sqrt{(c\tau)^2-\rho^2}\right\}}\right]
\end{aligned}
\tag{2.34}
$$

Although we derived a relatively compact analytical form in 2-D, the Green's function propagator is not analytically integrable across the singularities at $\rho = 0$ and $\rho = c\tau$. However, it will be shown that it is possible to obtain a 2-D propagator numerical expression.

2.4 Time Domain Propagator Numerical Expression

The analytical time-domain propagator solution for Maxwell's equations has been reviewed above. Given the analytical solution, we now derive the 1-D, 2-D, and 3-D Propagator method numerical expressions by solving the integral form (2.12) containing the derived each Green's function propagator and the initial field. Although the 1-D Propagator equation has been derived in [16], for completeness we first review its derivation. We then present the derivation of 3-D and 2-D Propagator numerical equations, respectively.

2.4.1 One-dimensional expression

In order to derive the 1-D Propagator equation, consider the case in which $k_x = k_y = 0$. Because this is a 1-D case, $k \to k_z$, $1/(2\pi)^3 \to 1/(2\pi)$ and

$$\mathbf{F} = \begin{bmatrix} E_x & H_y \end{bmatrix}^T \tag{2.35}$$

The evolution operator matrix elements except A_{11}, A_{15}, A_{51}, and A_{55} do not contribute because nonzero fields for this case are only E_x and H_y. By substituting $k_x = k_y = 0$ into above four elements in (2.24), (2.25) becomes

$$\bar{\mathbf{K}}^{(1)} = \frac{1}{(2\pi)} \int_{-\infty}^{\infty} \begin{bmatrix} \cos(k_z c\tau) & -j\eta \sin(k_z c\tau) \\ \frac{-j}{\eta} \sin(k_z c\tau) & \cos(k_z c\tau) \end{bmatrix} e^{jk_z(z-z')} dk_z \tag{2.36}$$

When (2.36) is substituted into (2.9), the Green's function propagator can be easily evaluated analytically, yielding

$$G_{11}^{(1)} = G_{55}^{(1)} = \frac{U(\tau)}{2}\left[\delta(\mathbf{z}+c\tau)+\delta(\mathbf{z}-c\tau)\right] \tag{2.37a}$$

$$G_{15}^{(1)} = \eta^2 G_{51}^{(1)} = -\eta\frac{U(\tau)}{2}\left[\delta(\mathbf{z}+c\tau)-\delta(\mathbf{z}-c\tau)\right] \tag{2.37b}$$

where δ represents the Dirac delta function, and we define $\mathbf{z} = z - z'$ for brevity.

The time-updating electric and magnetic field can be found by solving (2.12) analytically with the 1-D Green's function propagator $\bar{\mathbf{G}}^{(1)}$ and the initial field at the previous time *t'*, giving

$$E_x(z,t) = \int_{z'}\left[G_{11}^{(1)}E_{x0} + G_{15}^{(1)}H_{y0}\right]dz' \tag{2.38a}$$

$$H_y(z,t) = \int_{z'}\left[G_{51}^{(1)}E_{x0} + G_{55}^{(1)}H_{y0}\right]dz' \tag{2.38b}$$

where a zero in the subscript designates the initial field. Substituting the Green's function propagator (2.37) into (2.38), the time-updating field components are written as

$$E_x(z,t) = \frac{1}{2}\int_{-\infty}^{\infty} U(\tau)\left[E_{x0}\left[\delta(\mathbf{z}+c\tau)+\delta(\mathbf{z}-c\tau)\right]-\eta H_{y0}\left[\delta(\mathbf{z}+c\tau)-\delta(\mathbf{z}-c\tau)\right]\right]dz' \tag{2.39a}$$

$$H_y(z,t) = \frac{1}{2}\int_{-\infty}^{\infty} U(\tau)\left[-\frac{E_{x0}}{\eta}\left[\delta(\mathbf{z}+c\tau)-\delta(\mathbf{z}-c\tau)\right]+H_{y0}\left[\delta(\mathbf{z}+c\tau)+\delta(\mathbf{z}-c\tau)\right]\right]dz' \tag{2.39b}$$

Because the spatial dependence of the 1-D Green's function propagator is entirely contained in the delta function, (2.39) can be easily evaluated, resulting in

$$E_x(z,t) = \frac{1}{2}\left[E_{x0}(z+\Delta z)+E_{x0}(z-\Delta z)\right]-\frac{\eta}{2}\left[H_{y0}(z+\Delta z)-H_{y0}(z-\Delta z)\right] \tag{2.40a}$$

$$H_y(z,t) = \frac{1}{2}\left[H_{y0}(z+\Delta z)+H_{y0}(z-\Delta z)\right]-\frac{1}{2\eta}\left[E_{x0}(z+\Delta z)-E_{x0}(z-\Delta z)\right] \tag{2.40b}$$

where $\eta = \sqrt{\mu / \varepsilon}$ is the intrinsic impedance at the point *z* and $\Delta z = c\tau$ is the numerical spatial increment. Equation (2.40) is the 1-D Propagator method equation. This representation can be described as the D'Alembert solution for a coupled set of first order homogeneous differential equations. Therefore, (2.40) is both a numerical expression and an exact solution to (2.2). In this expression, the numerical time step and spatial increment are fixed with the relation $\Delta t = \Delta z / c$, where *c* is the speed of light. Equation (2.40) can be also interpreted as the present time field found by combinations of the previous time fields traveling at the speed of light from the causal boundary, which is at $z \pm \Delta z$. Fig. 2.1 illustrates the 1-D numerical scheme for the present and previous time electric and magnetic fields in both time and space. Vertical and horizontal axes represent respectively time and space. The previous time fields at $z \pm \Delta z$ will contribute to the current time field at the grid point *z* by traveling at the speed of light.

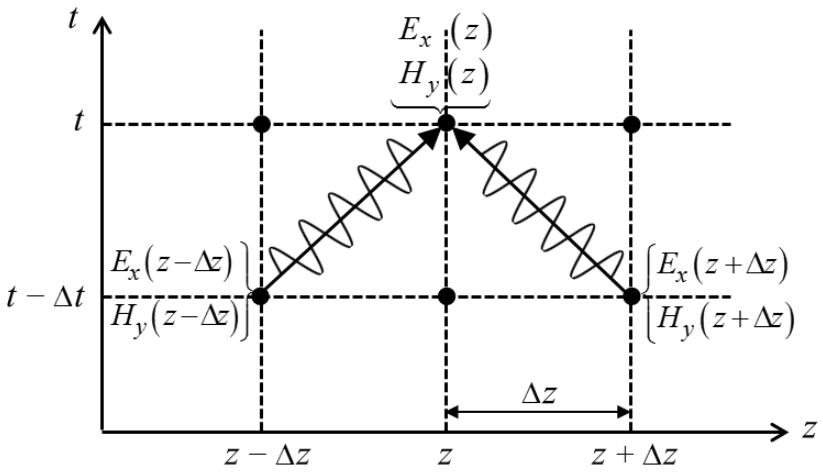

Figure 2.1: 1-D Propagator numerical scheme of the present and previous time fields in time and space.

2.4.2 Three-dimensional expression

The 3-D numerical expressions for the time-domain Propagator method can be found by evaluating the integral expression (2.12) with all components of the 3-D Green's function propagator. As an example, the *x*-component of electric field is written as

$$E_x(\mathbf{r},t)=\int_{v'}\left[G_{11}^{(3)}E_{x0}+G_{12}^{(3)}E_{y0}+G_{13}^{(3)}E_{z0}+G_{14}^{(3)}H_{x0}+G_{15}^{(3)}H_{y0}+G_{16}^{(3)}H_{z0}\right]d\mathbf{r}' \quad (2.41)$$

Here the components G_{12}, G_{13}, and G_{14} in (2.41) will not contribute to the future time E_x field because the *L* and *S* terms in (2.30), which belong to the $\nabla\nabla$ operator, are zero outside a source free region. Substituting each component G_{11}, G_{15}, and G_{16} into (2.41), the time-updating electric field is represented as

$$\begin{aligned}E_x(\mathbf{r},t)=&\int_{v'}\left[U(\tau)\frac{\delta'(r_0-R)}{4\pi R}\right]E_{x0}dv'\\&+\int_{v'}\left\{\eta U(\tau)\left[\frac{\delta(r_0-R)}{4\pi R^2}+\frac{\delta'(r_0-R)}{4\pi R}\right]\frac{(z-z')}{R}\right\}H_{y0}dv'\\&+\int_{v'}\left\{-\eta U(\tau)\left[\frac{\delta(r_0-R)}{4\pi R^2}+\frac{\delta'(r_0-R)}{4\pi R}\right]\frac{(y-y')}{R}\right\}H_{z0}dv'\end{aligned} \quad (2.42)$$

where $r_0=c\tau$, $\tau=t-t_0$, $R=\sqrt{(x-x')^2+(y-y')^2+(z-z')^2}$, and the square bracket in the first integral and curly brackets in the second and third integrals contain respectively G_{11}, G_{15}, and G_{16}. In order to compactly evaluate (2.42), the Cartesian coordinates are transformed to spherical coordinates. Expressing the resulting equation in spherical coordinates gives

$$
\begin{aligned}
E_x(\mathbf{r},t) = {} & \frac{1}{4\pi}\int_{r'=-\infty}^{\infty}\int_{\theta'=0}^{\pi}\int_{\phi'=0}^{2\pi} U(\tau)\left[r'\delta'(r_0-r')\right]E_{x0}\sin\theta' dr' d\phi' d\theta' \\
& -\frac{\eta}{4\pi}\int_{r'=-\infty}^{\infty}\int_{\theta'=0}^{\pi}\int_{\phi'=0}^{2\pi} U(\tau)\left[\delta(r_0-r')+r'\delta'(r_0-r')\right]H_{y0}\cos\theta'\sin\theta' dr' d\phi' d\theta' \\
& +\frac{\eta}{4\pi}\int_{r'=-\infty}^{\infty}\int_{\theta'=0}^{\pi}\int_{\phi'=0}^{2\pi} U(\tau)\left[\delta(r_0-r')+r'\delta'(r_0-r')\right]H_{z0}\sin\phi'\sin\theta'^2 dr' d\phi' d\theta'
\end{aligned}
\tag{2.43}
$$

where the initial fields are a function of r', θ', and ϕ'. Evaluating the Dirac delta function in (2.43) at r_0 reduces the volume integral to the spherical surface integral with a radius r_0 and the unit step function enforces causality. The following three mathematical properties of the derivative of the delta function are used,

$$
\begin{aligned}
&\delta'(r_0-r) = -\delta'(r-r_0) \\
&r\delta'(r-r_0) = -\delta(r-r_0) + r_0\delta'(r-r_0) \\
&\int \delta^{(k)}(x-x_0) f(x)\,dx = (-1)^k f^{(k)}(x_0)
\end{aligned}
\tag{2.44}
$$

where the superscript k in the parenthesis represents the k^{th} derivative. Upon substituting (2.44) into (2.43), after simplifications, the time-evolving electric field becomes

$$
\begin{aligned}
E_x(\mathbf{r},t) = {} & \frac{1}{4\pi}\int_{\theta'=0}^{\pi}\int_{\phi'=0}^{2\pi}\left[E_{x0}(\mathbf{r}') + r_0\frac{\partial}{\partial r'}E_{x0}(\mathbf{r}')\right]_{r'=r_0}\sin\theta' d\phi' d\theta' \\
& -\frac{\eta}{4\pi}\int_{\theta'=0}^{\pi}\int_{\phi'=0}^{2\pi}\left[2H_{y0}(\mathbf{r}') + r_0\frac{\partial}{\partial r'}H_{y0}(\mathbf{r}')\right]_{r'=r_0}\cos\theta'\sin\theta' d\phi' d\theta' \\
& +\frac{\eta}{4\pi}\int_{\theta'=0}^{\pi}\int_{\phi'=0}^{2\pi}\left[2H_{z0}(\mathbf{r}') + r_0\frac{\partial}{\partial r'}H_{z0}(\mathbf{r}')\right]_{r'=r_0}\sin\phi'\sin^2\theta' d\phi' d\theta'
\end{aligned}
\tag{2.45}
$$

The integration and derivative of the initial fields, which are a function of the position $\mathbf{r}'$, in (2.45), cannot be analytically evaluated, however it can be numerically evaluated.

First, a numerical integration for a spherical surface integral that conveniently fits into a square grid lattice is provided by the weighted sum

$$\frac{1}{4\pi r_0^2}\int_{\text{surf}} f(\mathbf{r}')\,ds' = \sum_{m=1}^{6} w_m f(\mathbf{r}'_m) + R\left(r_0^4\right);\quad w_m = \frac{1}{6} \tag{2.46}$$

where *m* denotes each position of six points on the spherical surface. Equation (2.46) has a small error factor, the fourth power of the radius of the sphere, and it includes values of the integrand at six equally spaced node points on the surface surrounding the point **r** where the updated field resides as shown in Fig. 2.2. To incorporate (2.46), we multiply and divide by r_0^2 on the right side of (2.45). The result is

$$\begin{aligned} E_x(\mathbf{r},t) = {} & \frac{1}{4\pi r_0^2}\int_{\theta'=0}^{\pi}\int_{\phi'=0}^{2\pi}\left[E_{x0}(\mathbf{r}') + r_0\frac{\partial}{\partial r'}E_{x0}(\mathbf{r}')\right]_{r'=r_0} r_0^2\sin\theta'\,d\phi'd\theta' \\ & -\frac{\eta}{4\pi r_0^2}\int_{\theta'=0}^{\pi}\int_{\phi'=0}^{2\pi}\left[2H_{y0}(\mathbf{r}') + r_0\frac{\partial}{\partial r'}H_{y0}(\mathbf{r}')\right]_{r'=r_0}\cos\theta' r_0^2\sin\theta'd\phi'd\theta' \\ & +\frac{\eta}{4\pi r_0^2}\int_{\theta'=0}^{\pi}\int_{\phi'=0}^{2\pi}\left[2H_{z0}(\mathbf{r}') + r_0\frac{\partial}{\partial r'}H_{z0}(\mathbf{r}')\right]_{r'=r_0}\sin\phi'\sin\theta' r_0^2\sin\theta'd\phi'd\theta' \end{aligned} \tag{2.47}$$

In the spherical coordinate, a differential surface area *ds* is $r^2\sin\theta d\phi d\theta$. Substituting the differential surface area *ds* into (2.47) gives

$$E_x(\mathbf{r},t)=\frac{1}{4\pi r_0^2}\int_{\theta'=0}^{\pi}\int_{\phi'=0}^{2\pi}\left[E_{x0}(\mathbf{r}')+r_0\frac{\partial}{\partial r'}E_{x0}(\mathbf{r}')\right]_{r'=r_0}ds'$$

$$-\frac{\eta}{4\pi r_0^2}\int_{\theta'=0}^{\pi}\int_{\phi'=0}^{2\pi}\left[2H_{y0}(\mathbf{r}')+r_0\frac{\partial}{\partial r'}H_{y0}(\mathbf{r}')\right]_{r'=r_0}\cos\theta' ds' \qquad (2.48)$$

$$+\frac{\eta}{4\pi r_0^2}\int_{\theta'=0}^{\pi}\int_{\phi'=0}^{2\pi}\left[2H_{z0}(\mathbf{r}')+r_0\frac{\partial}{\partial r'}H_{z0}(\mathbf{r}')\right]_{r'=r_0}\sin\phi'\sin\theta' ds'$$

With (2.46), the numerical expression of (2.48) becomes

$$E_x(\mathbf{r},t)=\frac{1}{6}\sum_{m=1}^{6}\left[E_{x0}(\mathbf{r}'_m)+r_0\frac{\partial}{\partial r'}E_{x0}(\mathbf{r}'_m)\right]_{r'=r_0}$$

$$-\frac{\eta}{6}\sum_{m=1}^{6}\left[2H_{y0}(\mathbf{r}'_m)+r_0\frac{\partial}{\partial r'}H_{y0}(\mathbf{r}'_m)\right]_{r'=r_0}\cos\theta' \qquad (2.49)$$

$$+\frac{\eta}{6}\sum_{m=1}^{6}\left[2H_{z0}(\mathbf{r}'_m)+r_0\frac{\partial}{\partial r'}H_{z0}(\mathbf{r}'_m)\right]_{r'=r_0}\sin\phi'\sin\theta'+O(r_0^4)$$

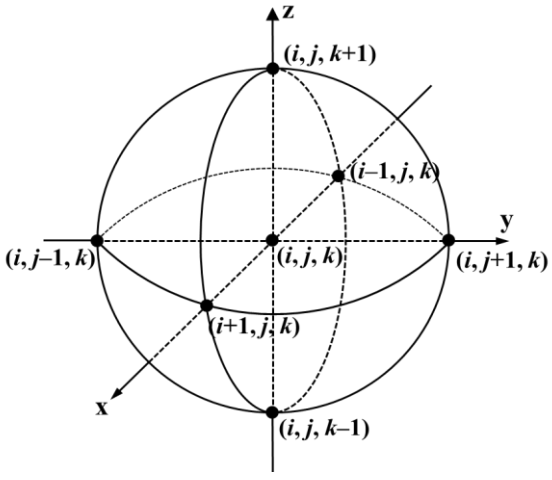

Figure 2.2: A spherical volume in a square grid serves both as the region of integration for each field component and as the Propagator method numerical cell.

Next, partial derivatives with respect to r' of the initial time **E** and **H** fields in (2.49) are approximated by a three-point backward finite differencing, having the second order accuracy, given by

$$f'(r') = \frac{3f(r_0) - 4f(r_0 - h) + f(r_0 - 2h)}{2r_0} + O(h^2) \tag{2.50}$$

where h is a grid spacing. In the second summation in (2.49), when $\theta' = 0,\ \pi$, the $\cos\theta'$ term restricts respectively the H_y fields to $(i, j, k+1)$ and $(i, j, k-1)$ in z-axis on the spherical surface shown in Fig. 2.2. Similarly in the third summation in (2.49), the $\sin\phi'\sin\theta'$ term restricts the H_z fields to $(i, j+1, k)$ and $(i, j-1, k)$ in y-axis when $\theta' = \pi/2$ and $\phi' = \pi/2,\ 3\pi/2$. Every set of coefficients we obtained using standard numerical differentiation and integration resulted in instability or significant dispersion either when a plane wave propagated in a homogeneous region or when it scattered from an object. Then we selected a 'best guess' set of trial coefficients, $1/6$ for the electric field components and $1/2$ for the magnetic field components, and proceeded with a dispersion and stability analysis. The $1/6$ and $1/2$ coefficients were chosen because they provide the expected dispersion equation. With those coefficients, (2.49) is numerically expressed as

$$\begin{aligned} E_x\big|_{i,j,k}^{n} = \frac{1}{6}\Big[& E_x\big|_{i+1,j,k}^{n-1} + E_x\big|_{i-1,j,k}^{n-1} + E_x\big|_{i,j+1,k}^{n-1} + E_x\big|_{i,j-1,k}^{n-1} + E_x\big|_{i,j,k+1}^{n-1} + E_x\big|_{i,j,k-1}^{n-1} \Big] \\ & - \frac{\eta}{2}\Big[H_y\big|_{i,j,k+1}^{n-1} - H_y\big|_{i,j,k-1}^{n-1} \Big] + \frac{\eta}{2}\Big[H_z\big|_{i,j+1,k}^{n-1} - H_z\big|_{i,j-1,k}^{n-1} \Big] \end{aligned} \tag{2.51}$$

where i, j and k represent grid points of the x-, y-, and z-axes respectively, and n is the time step. However, we observed that the numerical expression (2.51) still leads to instability.

Based upon the stability analysis that will be discussed in detail in section 3.6, it was found that the magnetic field in (2.51) must be multiplied by the factor $1/\sqrt{3}$ in order to satisfy the 3-D stability condition.

Finally, (2.51) for the *x*-component of the electric field reduces to a stable numerical equation, given by

$$\begin{aligned} E_x\big|_{i,j,k}^{n} = \frac{1}{6}\Big[& E_x\big|_{i+1,j,k}^{n-1} + E_x\big|_{i-1,j,k}^{n-1} + E_x\big|_{i,j+1,k}^{n-1} + E_x\big|_{i,j-1,k}^{n-1} + E_x\big|_{i,j,k+1}^{n-1} + E_x\big|_{i,j,k-1}^{n-1} \Big] \\ & - \frac{\eta}{2\sqrt{3}}\Big[H_y\big|_{i,j,k+1}^{n-1} - H_y\big|_{i,j,k-1}^{n-1} \Big] + \frac{\eta}{2\sqrt{3}}\Big[H_z\big|_{i,j+1,k}^{n-1} - H_z\big|_{i,j-1,k}^{n-1} \Big] \end{aligned} \tag{2.52}$$

Other components of electric and magnetic field take a form similar to (2.52). After evaluating each field component in (2.12) in the manner presented above:

$$\begin{aligned} E_y\big|_{i,j,k}^{n} = \frac{1}{6}\Big[& E_y\big|_{i+1,j,k}^{n-1} + E_y\big|_{i-1,j,k}^{n-1} + E_y\big|_{i,j+1,k}^{n-1} + E_y\big|_{i,j-1,k}^{n-1} + E_y\big|_{i,j,k+1}^{n-1} + E_y\big|_{i,j,k-1}^{n-1} \Big] \\ & - \frac{\eta}{2\sqrt{3}}\Big[H_z\big|_{i+1,j,k}^{n-1} - H_z\big|_{i-1,j,k}^{n-1} \Big] + \frac{\eta}{2\sqrt{3}}\Big[H_x\big|_{i,j,k+1}^{n-1} - H_x\big|_{i,j,k-1}^{n-1} \Big] \end{aligned} \tag{2.53a}$$

$$\begin{aligned} E_z\big|_{i,j,k}^{n} = \frac{1}{6}\Big[& E_z\big|_{i+1,j,k}^{n-1} + E_z\big|_{i-1,j,k}^{n-1} + E_z\big|_{i,j+1,k}^{n-1} + E_z\big|_{i,j-1,k}^{n-1} + E_z\big|_{i,j,k+1}^{n-1} + E_z\big|_{i,j,k-1}^{n-1} \Big] \\ & - \frac{\eta}{2\sqrt{3}}\Big[H_x\big|_{i,j+1,k}^{n-1} - H_x\big|_{i,j-1,k}^{n-1} \Big] + \frac{\eta}{2\sqrt{3}}\Big[H_y\big|_{i+1,j,k}^{n-1} - H_y\big|_{i-1,j,k}^{n-1} \Big] \end{aligned} \tag{2.53b}$$

$$\begin{aligned} H_x\big|_{i,j,k}^{n} = \frac{1}{6}\Big[& H_x\big|_{i+1,j,k}^{n-1} + H_x\big|_{i-1,j,k}^{n-1} + H_x\big|_{i,j+1,k}^{n-1} + H_x\big|_{i,j-1,k}^{n-1} + H_x\big|_{i,j,k+1}^{n-1} + H_x\big|_{i,j,k-1}^{n-1} \Big] \\ & + \frac{1}{2\sqrt{3}\eta}\Big[E_y\big|_{i,j,k+1}^{n-1} - E_y\big|_{i,j,k-1}^{n-1} \Big] - \frac{1}{2\sqrt{3}\eta}\Big[E_z\big|_{i,j+1,k}^{n-1} - E_z\big|_{i,j-1,k}^{n-1} \Big] \end{aligned} \tag{2.53c}$$

$$\begin{aligned} H_y\big|_{i,j,k}^{n} = \frac{1}{6}\Big[& H_y\big|_{i+1,j,k}^{n-1} + H_y\big|_{i-1,j,k}^{n-1} + H_y\big|_{i,j+1,k}^{n-1} + H_y\big|_{i,j-1,k}^{n-1} + H_y\big|_{i,j,k+1}^{n-1} + H_y\big|_{i,j,k-1}^{n-1} \Big] \\ & + \frac{1}{2\sqrt{3}\eta}\Big[E_z\big|_{i+1,j,k}^{n-1} - E_z\big|_{i-1,j,k}^{n-1} \Big] - \frac{1}{2\sqrt{3}\eta}\Big[E_x\big|_{i,j,k+1}^{n-1} - E_x\big|_{i,j,k-1}^{n-1} \Big] \end{aligned} \tag{2.53d}$$

$$H_z\big|_{i,j,k}^{n} = \frac{1}{6}\left[H_z\big|_{i+1,j,k}^{n-1} + H_z\big|_{i-1,j,k}^{n-1} + H_z\big|_{i,j+1,k}^{n-1} + H_z\big|_{i,j-1,k}^{n-1} + H_z\big|_{i,j,k+1}^{n-1} + H_z\big|_{i,j,k-1}^{n-1} \right] + \frac{1}{2\sqrt{3}\eta}\left[E_x\big|_{i,j+1,k}^{n-1} - E_x\big|_{i,j-1,k}^{n-1} \right] - \frac{1}{2\sqrt{3}\eta}\left[E_y\big|_{i+1,j,k}^{n-1} - E_y\big|_{i-1,j,k}^{n-1} \right] \tag{2.53e}$$

Although the numerical surface integration (2.46) delivers a high order accuracy, (2.52)-(2.53) reduce to 2nd order accuracy due to the numerical approximation of the derivative (2.50). Equations (2.52)-(2.53) imply that the time-stepped **E** or **H** field can be found by numerical evaluation of the surface integration of the previous time field and the derivative of the **H** or **E** field at appropriate positions on the spherical surface.

2.4.3 Two-dimensional expression

It has been shown that the 2-D Green's function propagator cannot be analytically evaluated due to singularities at $\rho = 0$ and $\rho = c\tau$. However, 2-D numerical Propagator equations can be inferred by comparison with the derived 1-D and 3-D expressions. We hypothesize that the present time field at each grid point can be determined by a numerical surface integration and differentiation lying on a causal boundary surrounding that point. The causal boundary is a sphere in 3-D, a circle in 2-D and in 1-D it is two points, one on each side of the grid point being updated.

As an example, in the 2-D TM to *z* case, where the vector field components are E_z, H_x, and H_y, the numerical expressions are

$$E_z\big|_{i,j}^{n} = \frac{1}{4}\left[E_z\big|_{i+1,j}^{n-1} + E_z\big|_{i-1,j}^{n-1} + E_z\big|_{i,j+1}^{n-1} + E_z\big|_{i,j-1}^{n-1} \right] - \frac{\eta}{2\sqrt{2}}\left[H_x\big|_{i,j+1}^{n-1} - H_x\big|_{i,j-1}^{n-1} \right] + \frac{\eta}{2\sqrt{2}}\left[H_y\big|_{i+1,j}^{n-1} - H_y\big|_{i-1,j}^{n-1} \right] \tag{2.54a}$$

$$H_x\big|_{i,j}^{n} = \frac{1}{4}\left[H_x\big|_{i+1,j}^{n-1} + H_x\big|_{i-1,j}^{n-1} + H_x\big|_{i,j+1}^{n-1} + H_x\big|_{i,j-1}^{n-1} \right] - \frac{1}{2\sqrt{2}\eta}\left[E_z\big|_{i,j+1}^{n-1} - E_z\big|_{i,j-1}^{n-1} \right] \tag{2.54b}$$

$$H_y\big|_{i,j}^{n} = \frac{1}{4}\left[H_y\big|_{i+1,j}^{n-1} + H_y\big|_{i-1,j}^{n-1} + H_y\big|_{i,j+1}^{n-1} + H_y\big|_{i,j-1}^{n-1} \right] + \frac{1}{2\sqrt{2}\eta}\left[E_z\big|_{i+1,j}^{n-1} - E_z\big|_{i-1,j}^{n-1} \right] \tag{2.54c}$$

where *i* and *j* respectively represent grid points on the *x*-, and *y*-axes. Similarly with the 3-D equations, the coefficient $1/\sqrt{2}$ in (2.54) was added to meet the 2-D stability condition. This will be also shown in section 3.6.

Similarly, the Propagator equations for the 2-D transverse electric (TE) to *z*-direction case where all fields are zero except E_x, E_y, and H_z fields, are

$$E_x\big|_{i,j}^{n} = \frac{1}{4}\left[E_x\big|_{i+1,j}^{n-1} + E_x\big|_{i-1,j}^{n-1} + E_x\big|_{i,j+1}^{n-1} + E_x\big|_{i,j-1}^{n-1} \right] + \frac{\eta}{2\sqrt{2}}\left[H_z\big|_{i,j+1}^{n-1} - H_z\big|_{i,j-1}^{n-1} \right] \tag{2.55a}$$

$$E_y\big|_{i,j}^{n} = \frac{1}{4}\left[E_y\big|_{i+1,j}^{n-1} + E_y\big|_{i-1,j}^{n-1} + E_y\big|_{i,j+1}^{n-1} + E_y\big|_{i,j-1}^{n-1} \right] - \frac{\eta}{2\sqrt{2}}\left[H_z\big|_{i+1,j}^{n-1} - H_z\big|_{i-1,j}^{n-1} \right] \tag{2.55b}$$

$$H_z\big|_{i,j}^{n} = \frac{1}{4}\left[H_z\big|_{i+1,j}^{n-1} + H_z\big|_{i-1,j}^{n-1} + H_z\big|_{i,j+1}^{n-1} + H_z\big|_{i,j-1}^{n-1} \right] + \frac{1}{2\sqrt{2}\eta}\left[E_x\big|_{i,j+1}^{n-1} - E_x\big|_{i,j-1}^{n-1} \right] - \frac{1}{2\sqrt{2}\eta}\left[E_y\big|_{i+1,j}^{n-1} - E_y\big|_{i-1,j}^{n-1} \right] \tag{2.55c}$$

Fig. 2.3 illustrates a numerical grid scheme of the Propagator and FDTD method for the 2-D TM_z case. In the Propagator method, all three electric and magnetic field

components reside at each numerical grid point as shown in Fig. 2.3(a) and all time-stepping field components of E_z, H_x and H_y are computed from the one time step back fields at each time step. For example, at the current time $t = n$, both *E*- and *H*-fields are calculated at each grid in the numerical space from the previous time fields at $t = n-1$ located on the causal boundary.

On the other hand, in the FDTD grid scheme, *E*- and *H*-fields are interleaved in space as shown in Fig. 2.3(b) and exist at different instances in time with a half time increment. The FDTD equations with a square grid cell $\Delta_x = \Delta_y = \Delta$ for the 2-D TM_z case, for example, are

$$E_z\big|_{i,j}^{n+1/2} = E_z\big|_{i,j}^{n-1/2} + \frac{\Delta t}{\varepsilon_{i,j}\Delta}\left[H_y\big|_{i+1/2,j}^{n} - H_y\big|_{i-1/2,j}^{n} + H_x\big|_{i,j-1/2}^{n} - H_x\big|_{i,j+1/2}^{n} \right] \quad (2.56a)$$

$$H_x\big|_{i,j+1/2}^{n+1} = H_x\big|_{i,j+1/2}^{n} - \frac{\Delta t}{\mu_{i,j}\Delta}\left[E_z\big|_{i,j+1}^{n+1/2} - E_z\big|_{i,j}^{n+1/2} \right] \quad (2.56b)$$

$$H_y\big|_{i+1/2,j}^{n+1} = H_x\big|_{i+1/2,j}^{n} + \frac{\Delta t}{\mu_{i,j}\Delta}\left[E_z\big|_{i+1,j}^{n+1/2} - E_z\big|_{i,j}^{n+1/2} \right] \quad (2.56c)$$

To compute the time-updating fields, for instance, the $E_z(i, j)$ field at the current time $t = n+1/2$ is calculated from the $E_z(i, j)$ field at the previous time $t = n-1/2$ and the most recent values of H_x fields at $(i, j+1/2)$, $(i, j-1/2)$ and H_y fields at $(i+1/2, j)$, $(i-1/2, j)$ that encircle the $E_z(i, j)$ field. In the next time step $t = n+1$, the H_x and H_y fields are computed from their one time step back fields at $t = n$ and the recent stored values of E_z field at $t = n+1/2$, that exist a half spatial apart with them.

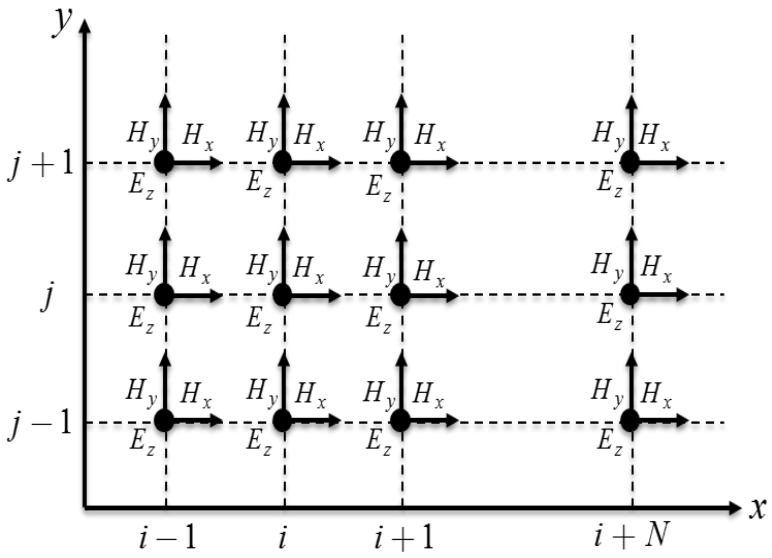

(a)

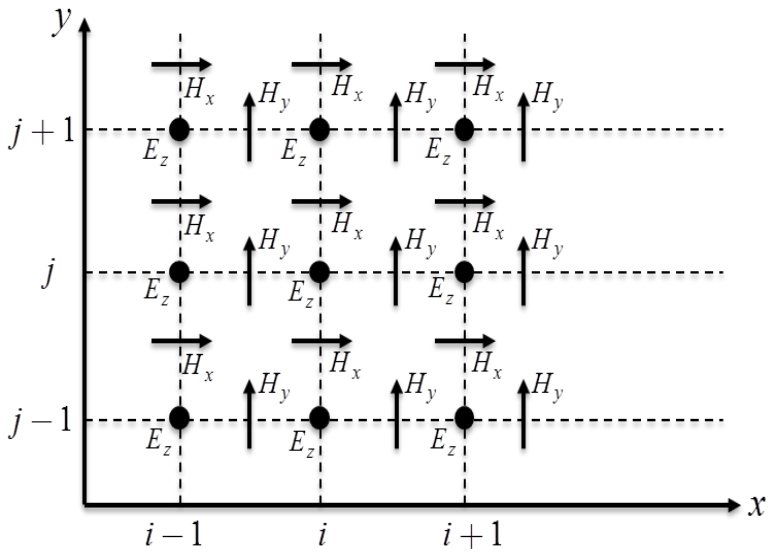

(b)

Figure 2.3: 2-D TM_z numerical grid scheme of (a) the Propagator method and (b) FDTD method.

2.5 Summary

This chapter presented the complete full-wave time-domain propagator equations for Maxwell's equations. The propagator equations in all dimensions have been derived by numerically evaluating the integral form of the propagator solution containing the each dimensional Green's function propagator and the initial field. The 2-D and 3-D propagator equations have been found by approximating the surface integration, respectively, over a circle and a sphere. It was shown that in the Propagator numerical scheme all electromagnetic field components are computed at each numerical grid point and at the same numerical time.

3. NUMERICAL METHOD THEORY*

3.1 Introduction

In the previous chapter, we presented the derivation of the time-domain Propagator solution of Maxwell's equations and its numerical expressions. However, numerical methods for implementing boundary conditions, absorbing boundary conditions (ABCs), numerical dispersion relations and stability conditions must be developed in order to model diverse electromagnetic problems. The FDTD method has attracted the attention of many researchers since these methods were established and it is now widely used in computational electromagnetics. The time-domain Propagator method algorithm also needs to establish similar numerical methods. One distinguishing feature of the Propagator method, a concept of a numerical and physical time step, is useful for modeling propagation in both homogeneous and inhomogeneous dielectric mediums.

This chapter introduces a numerical and physical time step along with an extrapolation technique in time, the development of boundary conditions in an inhomogeneous region including both the dielectric-dielectric and dielectric-perfect electric conductor (PEC) cases, and a simple absorbing boundary condition, described as the null boundary condition. The derivation of numerical dispersion relations from the nu-

---

* Reprinted with permission from "A Propagator analysis of transmission line on an inhomogeneous substrate" by J. Shin and R. D. Nevels, 2017, *Microwave and Optical Technology Letters*, vol. 59, pp. 1411-1416, Copyright 2017 by John Wiley and Sons.
* Reprinted with permission from "A time-domain Propagator numerical method for computational electromagnetics" by J. Shin and R. D. Nevels, 2018, *IEEE Journal on Multiscale and Multiphysics Computational Techniques*, vol. 3, pp. 80-87, Copyright 2018 by IEEE.

merical equations and the analysis of the stability conditions are also described. It is noted that in free space the 1-D equation has no dispersions, whereas the 2-D and 3-D numerical equations are subject to have numerical dispersion since they were numerically approximated.

3.2 Numerical and Physical Time

In the time-domain Propagator equations derived in the previous chapter, the previous time field contributes to the present time field at a grid point by traveling from the causal boundary at the velocity of light in the surrounding medium. However, the previous time field located in a dielectric material will contribute to the current time field with a proper phase velocity depending on a material property. In a homogeneous dielectric medium, having a constant relative permittivity ε_{r} and a relative permeability $\mu_{\mathrm{r}} = 1$, the phase velocity is

$$v = \frac{c}{\sqrt{\varepsilon_{\mathrm{r}}}} = \frac{\Delta r}{\sqrt{\varepsilon_{\mathrm{r}}}\Delta t} = \frac{\Delta r}{\Delta \tau} \tag{3.1}$$

where c is the speed of light, Δt is the numerical time increment and Δr, where r represents x, y, or z, is the spatial increment between grid points on the Cartesian axes. In order to maintain uniform numerical spacing Δr everywhere in the numerical grid, the time at which the field leaves the points $r \pm \Delta r$ must be $\Delta t\sqrt{\varepsilon_{\mathrm{r}}}$. We define this to be the physical time increment $\Delta\tau$. Newton's third order backward difference interpolation is adapted to find the fields leaving nearest neighbors at the previous physical time increment by using three surrounding known previous time values, and arriving at all grid points in the

numerical space at the same numerical time. Therefore the physical travel time between nearest neighbor points can be different as shown in Fig. 3.1 by the red lines, but the computational time increment is the same for all points in the numerical space. For instance, when a dielectric constant $\varepsilon_r = 5$, the corresponding electric field at the physical time increment $\Delta\tau = \sqrt{5}\Delta t$ is located between two and three steps back in the numerical time at the same point in space. This field component can be extrapolated by Newton's backwards difference interpolation in time.

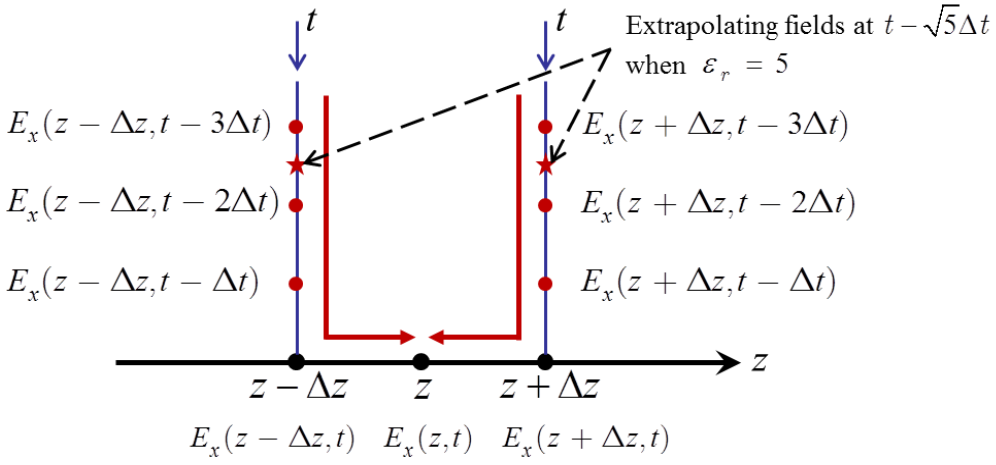

Figure 3.1: Example of the fields traveling nearest neighbors in the physical time period.

An example of Newton's third order backwards difference interpolation that finds a nearest neighbor electric and magnetic field with third order accuracy in a medium with a dielectric constant ε_r is

$$E(z,t-\Delta\tau) = \left[1+\beta+\frac{\beta(\beta+1)}{2}\right]E(z,t-\Delta t) + \left[\beta(\beta+2)\right]E(z,t-2\Delta t) + \left[\frac{\beta(\beta+1)}{2}\right]E(z,t-3\Delta t) \tag{3.2a}$$

$$H(z,t-\Delta\tau)=\left[1+\beta+\frac{\beta(\beta+1)}{2}\right]H(z,t-\Delta t) +\left[\beta(\beta+2)\right]H(z,t-2\Delta t)+\left[\frac{\beta(\beta+1)}{2}\right]H(z,t-3\Delta t) \tag{3.2b}$$

where $\beta=-\sqrt{\varepsilon_{\mathrm{r}}}+1$. The physical time electric and magnetic fields at a grid point in a dielectric medium are each extrapolated from the field values at three consecutive previous numerical times surrounding the physical time.

Extrapolation in time to determine the electric and magnetic field in a dielectric medium has three important features. First, it permits a fixed spatial grid and numerical time increment throughout the numerical space. Second, the specific condition for achieving an exact calculation of electric or magnetic field, i.e. D'Alembert solution, in any medium is to require the velocity of the wave in that medium to satisfy $v=\Delta z/\Delta\tau$. This condition is met by electric and magnetic field extrapolation in each distinct medium, as well as in a case where the dielectric constant changes from point to point. If there are multiple substrates, the medium with the lowest dielectric constant satisfies $v=\Delta z/\Delta t$ and therefore does not require extrapolation. Third, if the most recent three consecutive time steps are used in (3.2) then the allowed values of the dielectric constant are $1\le\varepsilon_{\mathrm{r}}\le 9$ because the extrapolated time $\sqrt{\varepsilon_{\mathrm{r}}}\Delta t$ lies within these three time steps, given by the square roots of 1, 4, and 9 multiplied by Δt. However, for a higher relative permittivity, the three consecutive numerical intervals must come from farther back in time. Therefore (3.2) can always be used for any dielectric constant by simply shifting the extrapolation calculation to greater previous time intervals. For example, if a relative permittivity of the

material surrounding a particular grid point is in the range of $25 \le \varepsilon_r \le 49$, the extrapolation equation becomes

$$E(t-\Delta\tau) = \left[1+\beta+\frac{\beta(\beta+1)}{2}\right]E(t-5\Delta t) + \left[\beta(\beta+2)\right]E(t-6\Delta t) + \left[\frac{\beta(\beta+1)}{2}\right]E(t-7\Delta t) \tag{3.3}$$

where $\beta = -\sqrt{\varepsilon_r} + 5$.

As an example for a high relative permittivity, reflection coefficients for a dielectric slab where $\varepsilon_r = 36$ are computed by the 1-D Propagator method along with the extrapolation equation (3.3). Fig. 3.2 illustrates a comparison of reflection coefficients between the 1-D Propagator method and the exact solution. This result ensures that the Propagator solution maintains same order of accuracy even for higher dielectric constant values.

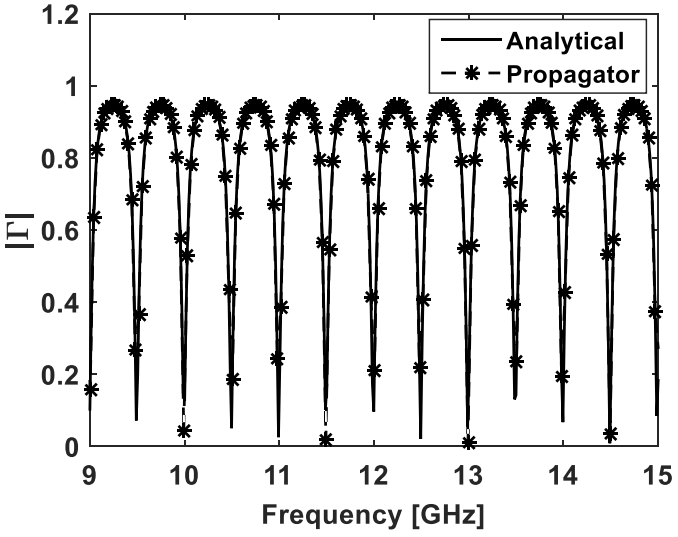

Figure 3.2: Comparison of reflection coefficients for a dielectric slab ($\varepsilon_r = 36$), between the Propagator method and exact solution.

In the above discussion of the extrapolation technique, Newton's backward difference polynomial has been used to extrapolate the previous time electric and magnetic field components. The natural cubic spline is also a widely used interpolation method [37], which can in principle be applied to the time-domain Propagator method instead of the backwards differencing interpolation. However, when implemented with the cubic spline interpolation, it was found that the amplitude of a Gaussian pulse gradually decreases as it propagates. Fig. 3.3 shows a comparison of Gaussian pulse peak electric field as a function of propagation time when the fields are computed by the backward difference and cubic spline extrapolation formula in a homogeneous dielectric medium with $\varepsilon_{\mathrm{r}} = 2$. In each case, the Gaussian pulse, given by

$$E_{\mathrm{s}} = \exp\left[-\left[\left(n - 4\kappa\right)/\kappa\right]^2\right] \tag{3.4}$$

propagates 500 time steps, where n is the time step and $\kappa = 20$. The value $\kappa = 20$ was chosen to minimize numerical dispersion. It is shown in Fig. 3.3(a) that the pulse computed by Newton's backward polynomial is well preserved, whereas the pulse computed by the cubic spline interpolation decays in amplitude and slightly widens. The decreasing amplitude of the pulse can be distinctly seen in Fig. 3.3(b). At 500 time steps, the amplitude decreases by 0.1% with Newton's backward extrapolation, but with the cubic spline extrapolation it decreases by 5%. An almost linear decay suggests that the cubic spline interpolation is lower than the exact value by the same amount at every time step. In light of these results, we conclude that Newton's backward difference method provides more suitable extrapolation of the physical time electric or magnetic field than does the cubic spline method.

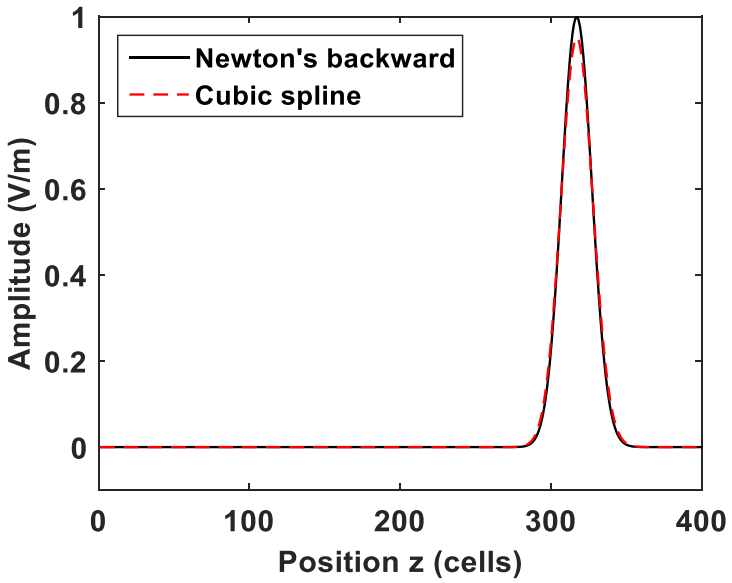

(a)

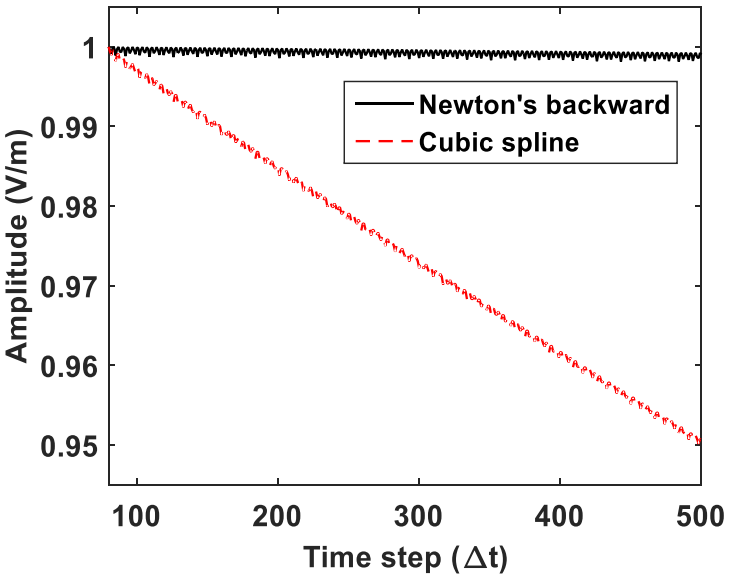

(b)

Figure 3.3: Comparison of (a) Gaussian pulse propagated in space and (b) peak amplitude of Gaussian pulse in time for Newton's backward and the cubic spline extrapolation in a homogeneous dielectric medium ($\varepsilon_r = 2$).

3.3 Boundary Condition

The Propagator method allows both electric and magnetic field components to compute at each node in a numerical space, including the node on the boundary between different mediums. Both the tangential and normal electromagnetic fields on an interface between two dissimilar contiguous mediums are subject to the boundary conditions that must be applied in a manner consistent with the numerical method. In the following, we derive a set of numerical boundary condition expressions for the Propagator method.

Fig. 3.4 illustrates the 1-D numerical grid scheme for electric and magnetic fields in two different dielectric mediums including the boundary between them. Here z_1 is the last grid point in region 1 and z_2 is the first grid point in region 2. The electric and magnetic fields at the grid points z_1 and z_2 are written as

$$E_x(z_1) = \frac{1}{2}\left[E_x(z_1+\Delta z) + E_x(z_1-\Delta z)\right] - \frac{\eta_1}{2}\left[H_y(z_1+\Delta z) - H_y(z_1-\Delta z)\right] \quad (3.5a)$$

$$H_y(z_1) = \frac{1}{2}\left[H_y(z_1+\Delta z) + H_y(z_1-\Delta z)\right] - \frac{1}{2\eta_1}\left[E_x(z_1+\Delta z) - E_x(z_1-\Delta z)\right] \quad (3.5b)$$

$$E_x(z_2) = \frac{1}{2}\left[E_x(z_2+\Delta z) + E_x(z_2-\Delta z)\right] - \frac{\eta_2}{2}\left[H_y(z_2+\Delta z) - H_y(z_2-\Delta z)\right] \quad (3.5c)$$

$$H_y(z_2) = \frac{1}{2}\left[H_y(z_2+\Delta z) + H_y(z_2-\Delta z)\right] - \frac{1}{2\eta_2}\left[E_x(z_2+\Delta z) - E_x(z_2-\Delta z)\right] \quad (3.5d)$$

where η_1 and η_2 are the respective intrinsic impedance of the two regions. Continuity of electric and magnetic field at the boundary is assured by requiring

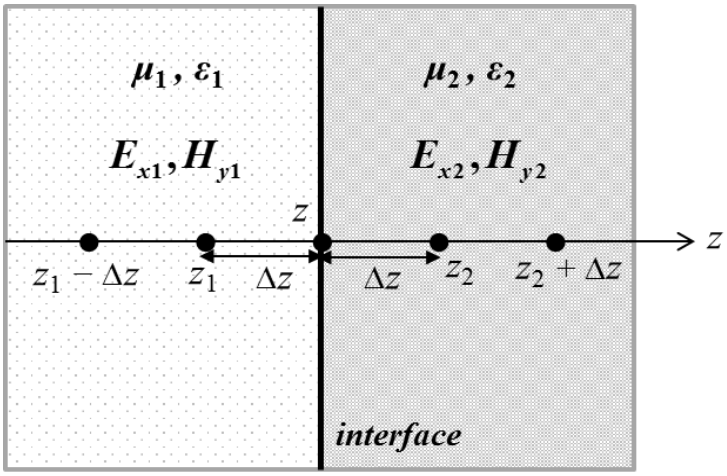

Figure 3.4: 1-D numerical grid scheme of two different mediums and interface.

$$\lim_{z_1 \to z} E_x(z_1) = \lim_{z_2 \to z} E_x(z_2) \approx E_x(z) \tag{3.6a}$$

$$\lim_{z_1 \to z} H_y(z_1) = \lim_{z_2 \to z} H_y(z_2) \approx H_y(z) \tag{3.6b}$$

First observe that in (3.5a) the electric field at $z_1 + \Delta z$ is on the boundary and must be equal to the electric field at $z_2 - \Delta z$ in (3.5c), which is also on the boundary. Therefore, these two electric fields cancel out before the limit is taken when (3.5a) and (3.5c) are substituted into (3.6a). By taking the limit $z_1, z_2 \to z$, we obtain the boundary equation for the magnetic field on the boundary as

$$H_y(z) = \frac{1}{\eta_1 + \eta_2}\left[\eta_2 H_y(z + \Delta z) + \eta_1 H_y(z - \Delta z)\right] - \frac{1}{\eta_1 + \eta_2}\left[E_x(z + \Delta z) - E_x(z - \Delta z)\right] \tag{3.7}$$

Similarly, substituting (3.5b) and (3.5d) into (3.6b) and taking the limit $z_1, z_2 \to z$, after simplifications, yield the boundary equation for the electric field:

$$E_x(z) = \frac{1}{\eta_1 + \eta_2}\left[\eta_1 E_x(z + \Delta z) + \eta_2 E_x(z - \Delta z)\right] - \frac{\eta_1 \eta_2}{\eta_1 + \eta_2}\left[H_y(z + \Delta z) - H_y(z - \Delta z)\right] \tag{3.8}$$

Equation (3.7) and (3.8) are the 1-D boundary equations for the electric and magnetic fields. As a check, assume that the medium is uniform, $\eta_1 = \eta_2 = \eta$, then (3.7) and (3.8) reduce to the general 1-D Propagator method equations (2.40).

An alternative boundary condition for a dielectric and PEC boundary is necessary. In the case where the second media is the PEC, the electric field must be totally reflected when it meets at the dielectric-PEC boundary. This can be realized numerically by setting the intrinsic impedance η_2 at grid points on the PEC boundary to zero and forcing both electric and magnetic fields at grid points inside the PEC region to zero. As seen in Fig. 3.5, application of these conditions in the case of a Gaussian plane wave in air and normally incident on a flat planar boundary results in a perfect reflection, with the reflection coefficient of $\Gamma = -1$, and a magnetic field that is doubled at the boundary as expected. This can be also mathematically proved that, by inserting $\eta_2 = 0$ and setting $E_x(z+\Delta z) = H_y(z+\Delta z) = 0$ in (3.7) and (3.8). The electric and magnetic field at the PEC boundary become

$$E_x(z) = 0 \tag{3.9a}$$

$$H_y(z) = H_y(z-\Delta z) + \frac{1}{\eta_1} E_x(z-\Delta z) = 2H_y(z-\Delta z) \tag{3.9b}$$

with $E_x = \eta H_y$.

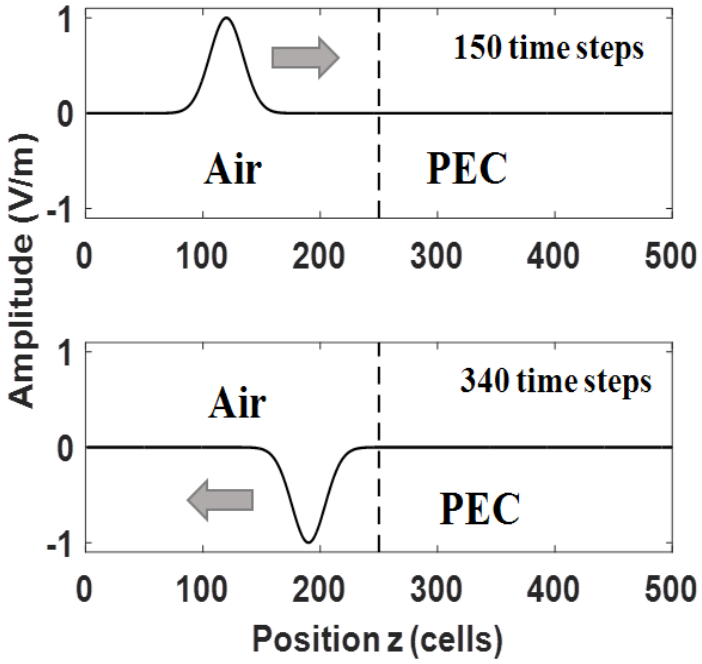

Figure 3.5: Time history of propagation with a Gaussian pulse in free space and PEC case.

Since the 1-D Propagator method equations are the exact electric and magnetic field solutions to Maxwell's equations, the numerical expression for both electric and magnetic field at the boundary point in an inhomogeneous medium has been developed. However, the exact boundary conditions in 2-D and 3-D cannot be derived because they have been numerically developed. Furthermore, the boundary equations based on the Cartesian system cannot be easily employed to simulate curved dielectric surfaces.

A simple conformal technique for the time-domain Propagator method, which can be used to analyze curved dielectric surfaces, is presented below. The proposed conformal dielectric algorithm utilizes a linear average concept similar to the FDTD conformal technique [38]. This technique does not require calculations of areas or volumes. Our conformal technique takes into account a ratio of the area in 2-D or volume in 3-D in a

cell occupied by the two different dielectric regions as well as a time interval along axes embedded in multiple mediums.

We present here the 2-D conformal technique for the time-domain Propagator method algorithm as an example. Fig. 3.6 illustrates the 2-D numerical grid scheme that includes a curved dielectric surface. The gray and white areas indicate two regions, designated 1 and 2, with different dielectric constants, and the red line represents the intersection between the two regions.

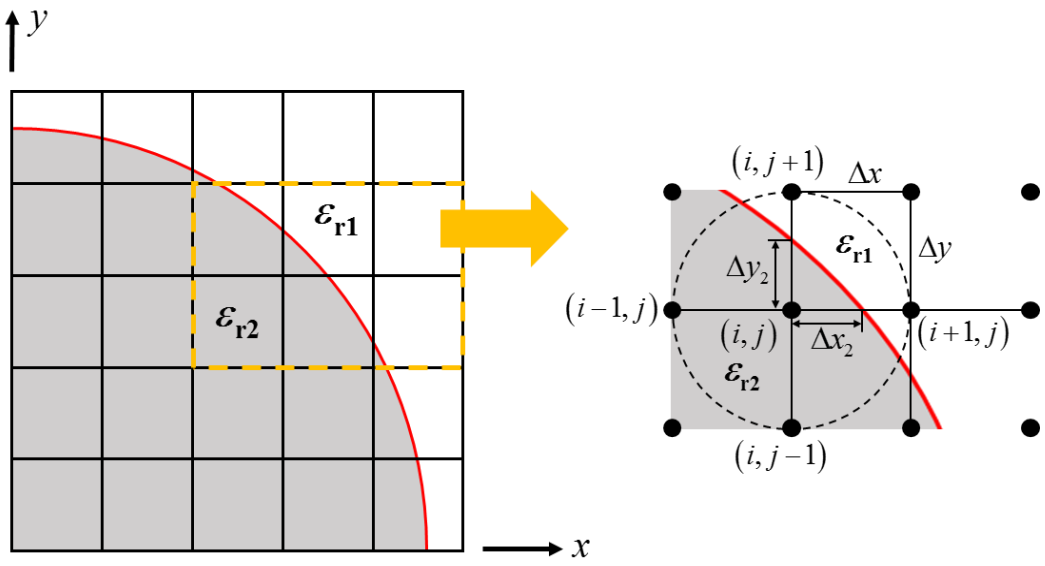

(a) (b)

Figure 3.6: (a) The 2-D numerical scheme including the curved dielectric surface and (b) the enlarged area of the dotted line section.

Consider the time-updating field at the grid point (i, j) in Fig. 3.6 (b). We note in Fig. 3.6 (b) that the circular area consisting of the four grid points at $(i-1, j)$, $(i+1, j)$, $(i, j-1)$, and $(i, j+1)$ overlays two dielectric regions. The ratio of occupied areas for each

region can be simply estimated with a linear average in *x*- and *y*-directions. Effective dielectric constants, $\varepsilon_{x1}^{\text{eff}}(i,j)$ and $\varepsilon_{y1}^{\text{eff}}(i,j)$, for medium coefficients are defined as

$$\varepsilon_{x1}^{\text{eff}}(i,j)=\frac{\left[\Delta x+\Delta x_2(i,j)\right]\varepsilon_{\text{r2}}+\left[\Delta x-\Delta x_2(i,j)\right]\varepsilon_{\text{r1}}}{2\Delta x} \tag{3.10a}$$

$$\varepsilon_{y1}^{\text{eff}}(i,j)=\frac{\left[\Delta y+\Delta y_2(i,j)\right]\varepsilon_{\text{r2}}+\left[\Delta y-\Delta y_2(i,j)\right]\varepsilon_{\text{r1}}}{2\Delta y} \tag{3.10b}$$

where Δx and Δy are the cell sizes along the *x*- and *y*-directions, respectively.

With (3.10), the time-stepping equations for the 2-D TM_z electric and magnetic fields are expressed as

$$\begin{aligned}E_z\big|_{i,j}^{n}=&\frac{1}{4}\left[E_z\big|_{i+1,j}^{n-1}+E_z\big|_{i-1,j}^{n-1}+E_z\big|_{i,j+1}^{n-1}+E_z\big|_{i,j-1}^{n-1}\right]\\&-\frac{1}{2\sqrt{2}}\frac{\eta_0}{\sqrt{\varepsilon_{y1}^{\text{eff}}(i,j)}}\left[H_x\big|_{i,j+1}^{n-1}-H_x\big|_{i,j-1}^{n-1}\right]+\frac{1}{2\sqrt{2}}\frac{\eta_0}{\sqrt{\varepsilon_{x1}^{\text{eff}}(i,j)}}\left[H_y\big|_{i+1,j}^{n-1}-H_y\big|_{i-1,j}^{n-1}\right]\end{aligned} \tag{3.11a}$$

$$\begin{aligned}H_x\big|_{i,j}^{n}=&\frac{1}{4}\left[H_x\big|_{i+1,j}^{n-1}+H_x\big|_{i-1,j}^{n-1}+H_x\big|_{i,j+1}^{n-1}+H_x\big|_{i,j-1}^{n-1}\right]\\&-\frac{1}{2\sqrt{2}}\frac{\sqrt{\varepsilon_{y1}^{\text{eff}}(i,j)}}{\eta_0}\left[E_z\big|_{i,j+1}^{n-1}-E_z\big|_{i,j-1}^{n-1}\right]\end{aligned} \tag{3.11b}$$

$$\begin{aligned}H_y\big|_{i,j}^{n}=&\frac{1}{4}\left[H_y\big|_{i+1,j}^{n-1}+H_y\big|_{i-1,j}^{n-1}+H_y\big|_{i,j+1}^{n-1}+H_y\big|_{i,j-1}^{n-1}\right]\\&+\frac{1}{2\sqrt{2}}\frac{\sqrt{\varepsilon_{x1}^{\text{eff}}(i,j)}}{\eta_0}\left[E_z\big|_{i+1,j}^{n-1}-E_z\big|_{i-1,j}^{n-1}\right]\end{aligned} \tag{3.11c}$$

Another consideration is that the previous time electric and magnetic fields require the extrapolation procedure with effective relative permittivity. As mentioned in section 3.2, the previous time fields surrounding the center point contribute to the present time

field by traveling with a phase velocity determined by the medium constitutive parameter. As shown in Fig. 3.6, the path to the point (i, j) from $(i-1, j)$ and $(i, j-1)$ is located entirely within the region 2, whose relative permittivity is $\varepsilon_{\mathrm{r}2}$, thus the previous time fields at $(i-1, j)$ and $(i, j-1)$ travel with the phase velocity, $v_p = c/\sqrt{\varepsilon_{\mathrm{r}2}}$. However, the path to (i, j) from $(i+1, j)$ and $(i, j+1)$ occupies the two regions, whose dielectric constants are respectively $\varepsilon_{\mathrm{r}1}$ and $\varepsilon_{\mathrm{r}2}$, therefore additional effective dielectric constants for the extrapolation procedure need to be defined. The effective dielectric constants with a linear average for the extrapolation process are defined as

$$\varepsilon_{x2}^{\mathrm{eff}}(i, j) = \frac{\Delta x_2(i, j)\,\varepsilon_{\mathrm{r}2} + \left[\Delta x - \Delta x_2(i, j)\right]\varepsilon_{\mathrm{r}1}}{\Delta x} \tag{3.12a}$$

$$\varepsilon_{y2}^{\mathrm{eff}}(i, j) = \frac{\Delta y_2(i, j)\,\varepsilon_{\mathrm{r}2} + \left[\Delta y - \Delta y_2(i, j)\right]\varepsilon_{\mathrm{r}1}}{\Delta y} \tag{3.12b}$$

In (3.11), the previous time fields $E_z(i+1, j)$, $H_x(i+1, j)$, and $H_y(i+1, j)$ are extrapolated using (3.12a), and the fields $E_z(i, j+1)$, $H_x(i, j+1)$, and $H_y(i, j+1)$ are extrapolated using (3.12b). Note that the time-updating equations (3.11) are identical to the form used in the conventional Propagator method algorithm, except that it uses effective dielectric constants (3.10) and (3.12). This conformal technique can be directly extended to the 3-D case by taking into account a ratio of volumes.

The example of calculating the radar cross section of a circular dielectric cylinder will be presented in chapter 5. This demonstrates the validity of the proposed conformal approach by comparing with analytical results.

3.4 Absorbing Boundary Condition

One of the main issues with numerical methods that solve electromagnetic wave interaction problems is that the computational domain should be truncated in order not to have reflection of numerical waves from the outer boundary. Therefore, absorbing boundary conditions (ABCs) are needed that allow outward propagating waves to be absorbed as if the simulation is being carried out on an infinite computational domain.

Like other time-domain numerical methods, the time-domain Propagator method requires ABCs that prevent outward traveling waves from reflecting from the outer boundary of the computation space. In general, ABCs fall into three categories: (1) boundary integral methods in which a Green's function integral accounts for the open environment outside the numerical grid [39], (2) numerical-averaging methods such as the Liao ABC [40], and (3) absorbing-layer methods such as the perfectly matched layer (PML) developed by Berenger [41].

To these we add the ABC that is described as a null boundary condition, which is uniquely suited for the numerical implementation with the propagator equations, which offer field coincidence in time as well as space. The null boundary condition is realized by simply setting all electromagnetic fields on the numerical outer boundary to zero.

The effectiveness of the null boundary condition has been investigated by placing a source for both the total and incident field at the center of 2-D numerical space. The point source was excited by a Gaussian pulse. The inner boundary was set to be an ABC for the total electric field and the outer boundary was set to be an ABC for the incident field. The total minus incident field divided by the incident field was recorded along the

inner boundary. As shown in Fig. 3.7, no unpredictable reflections from the outer boundary was visually observed at greater angles. With the null absorbing condition, Fig. 3.8 shows the percent absorption error in terms of wave angles. It is shown that the overall error between the coordinate axis at 0^o and 45^o is less than 0.06 %. This result confirms the effectiveness of the null boundary condition as a first order ABC for outward propagating waves.

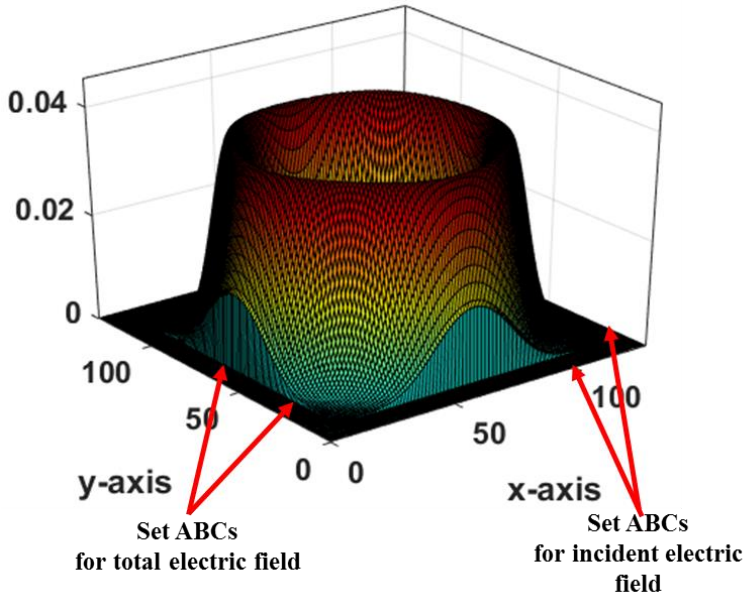

Figure 3.7: Total electric field when setting ABCs on the inner and outer boundary.

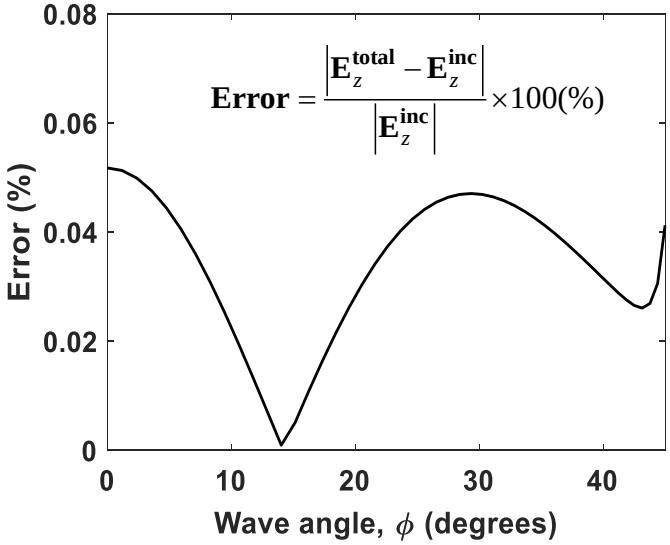

Figure 3.8: Error of total and incident electric fields as a function of ϕ degrees from the source point.

3.5 Numerical Dispersion Relation

A knowledge of the numerical dispersion relation for a time domain numerical method aids in improving the accuracy of the method, in understanding any non-physical artifacts in the numerical solution, and in some cases in establishing a stability condition for the numerical equations. In the following, we develop numerical dispersion relations for the 1-D, 2-D, and 3-D Propagator method based on Von Neumann's method [3]. A derivation of the numerical dispersion relations in multiple dimensions involves substitution of a monochromatic plane wave into the propagator numerical equations.

In 1-D Propagator method, monochromatic expressions for plane wave traveling in the positive *z* direction in the numerical grid for the electric and magnetic field can be expressed as

$$E_x\big|_I^n = E_{x0} e^{j\left(\omega n\Delta t - \tilde{k}_z I\Delta z\right)} \tag{3.13a}$$

$$H_y\Big|_I^n = H_{y0} e^{j\left(\omega n\Delta t - \tilde{k}_z I\Delta z\right)} \tag{3.13b}$$

where I is a node number, n is a time step, $\tilde{k}_z$ is the z component of the numerical wavenumber and ω is a wave angular frequency. By substituting the plane wave expressions (3.13) into the 1-D propagator equations (2.40), the 1-D dispersion relation can be obtained as

$$e^{-j\tilde{k}_z\Delta z} = e^{-j\omega\Delta t} \tag{3.14}$$

Equation (3.14) reduces to

$$\tilde{k}_z = \omega\frac{\Delta t}{\Delta z} = \frac{\omega}{c} = k_0 \tag{3.15}$$

where $\Delta z / \Delta t = c$ is the relationship between numerical time and spatial increments in a free space. This shows that the numerical wavenumber of the 1-D Propagator method is equal to the exact free space wavenumber.

However, as described in the previous chapter, the previous time fields in a dielectric region must be extrapolated by the interpolation procedure. Substituting (3.2) and (3.13) into (2.40), after simplifications, we obtain the following relations:

$$E_{x0} = \frac{\eta H_{y0}\left[1 - P_{1\mathrm{D}}\cos\left(\tilde{k}_z\Delta z\right)\right]}{jP_{1\mathrm{D}}\sin\left(\tilde{k}_z\Delta z\right)} \tag{3.16a}$$

$$H_{y0} = \frac{E_{x0}\left[1 - P_{1\mathrm{D}}\cos\left(\tilde{k}_z\Delta z\right)\right]}{j\eta P_{1\mathrm{D}}\sin\left(\tilde{k}_z\Delta z\right)} \tag{3.16b}$$

where

$$P_{1D} = \left[1 + \beta + \frac{\beta(\beta+1)}{2}\right] e^{-j\omega\Delta t} - \left[\beta(\beta+2)\right] e^{-j\omega 2\Delta t} + \left[\frac{\beta(\beta+1)}{2}\right] e^{-j\omega 3\Delta t} \tag{3.17}$$

Substituting (3.16a) into (3.16b) yields

$$\left[1 - P_{1D}\cos\left(\tilde{k}_z \Delta z\right)\right]^2 = -\left[P_{1D}\sin\left(\tilde{k}_z \Delta z\right)\right]^2 \tag{3.18}$$

Equation (3.18) can be rearranged to give

$$P_{1D} = \cos\left(\tilde{k}_z \Delta z\right) - j\sin\left(\tilde{k}_z \Delta z\right) = e^{-j\tilde{k}_z \Delta z} \tag{3.19}$$

With (3.17) and (3.19), the dispersion relation becomes

$$e^{-j\tilde{k}_z \Delta z} = \left[1 + \beta + \frac{\beta(\beta+1)}{2}\right] e^{-j\omega\Delta t} - \left[\beta(\beta+2)\right] e^{-j\omega 2\Delta t} + \left[\frac{\beta(\beta+1)}{2}\right] e^{-j\omega 3\Delta t} \tag{3.20}$$

Equation (3.20) is the general numerical dispersion relation of the 1-D Propagator algorithm in all dielectric regions of the numerical space. As the dielectric constant approaches that of free space $\beta \to 0$, (3.20) reduces to the exact free space expression (3.14), which is expected because for this special case the numerical equation becomes the exact D'Alembert equation. Alternatively as the space and time increments approach to zero ($\Delta t \to 0$, $\Delta z \to 0$), (3.20) becomes

$$\tilde{k}_z = \omega \frac{\Delta t \sqrt{\varepsilon_r}}{\Delta z} = \frac{\omega}{c}\sqrt{\varepsilon_r} = k \tag{3.21}$$

That is, the 1-D numerical wavenumber becomes the wavenumber of the medium at nodes where the physical time interpolation is applied.

A numerical wavenumber for a dielectric medium can be found by solving (3.20). Fig. 3.9 shows the percent error of the numerical phase velocity relative to the exact phase velocity as a function of dielectric constant for different grid sizes. When the dielectric constant is 1, 4, and 9, the respective numerical phase velocity becomes the exact phase velocity in each case. For other values of dielectric constant, the numerical phase velocity is not the exact phase velocity, resulting in a small third order accurate numerical dispersion. However, as seen in Fig. 3.9, increasing the number of grid points per wavelength significantly improves the phase velocity error.

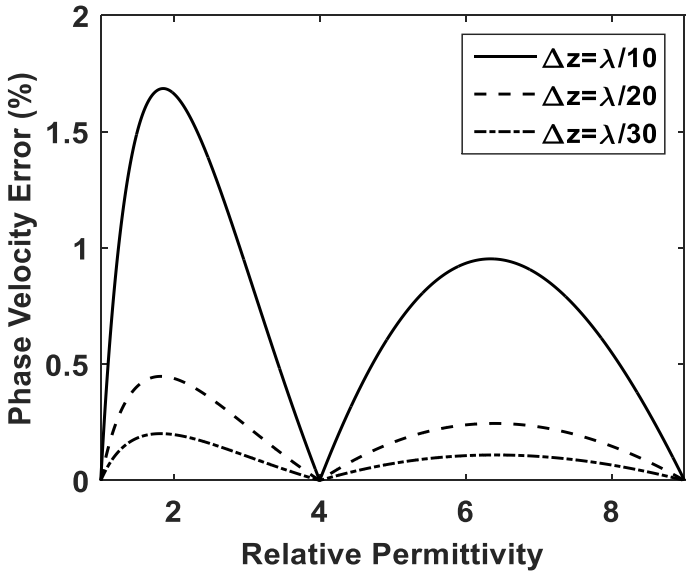

Figure 3.9: Numerical phase velocity error relative to the exact phase velocity as a function of dielectric constant for several grid sizes.

The dispersion analysis presented above can be readily extended to two and three-dimensions. In 2-D case, we begin with monochromatic plane wave expressions for the TM_z mode:

$$E_z\big|_{I,J}^{n} = E_{z0} e^{j\left(\omega n\Delta t - \tilde{k}_x I\Delta x - \tilde{k}_y J\Delta y\right)} \tag{3.22a}$$

$$H_x\big|_{I,J}^{n} = H_{x0} e^{j\left(\omega n\Delta t - \tilde{k}_x I\Delta x - \tilde{k}_y J\Delta y\right)} \tag{3.22b}$$

$$H_y\big|_{I,J}^{n} = H_{y0} e^{j\left(\omega n\Delta t - \tilde{k}_x I\Delta x - \tilde{k}_y J\Delta y\right)} \tag{3.22c}$$

where I and J are respective node numbers for the x- and y-directions, and $\tilde{k}_x$ and $\tilde{k}_y$ are the numerical wavenumbers for x- and y-polarized field components. Substituting (3.22) into (2.54) provides, after simplification, the following relations:

$$E_{z0}\left[1 - P_{2D} e^{-j\omega\Delta t}\right] + H_{x0}\frac{j\eta}{2} e^{-j\omega\Delta t}\sin\left(\tilde{k}_y\Delta y\right) - H_{y0}\frac{j\eta}{2} e^{-j\omega\Delta t}\sin\left(\tilde{k}_x\Delta x\right) = 0 \tag{3.23a}$$

$$E_{z0}\frac{j}{\eta} e^{-j\omega\Delta t}\sin\left(\tilde{k}_y\Delta y\right) + H_{x0}\left[1 - P_{2D} e^{-j\omega\Delta t}\right] = 0 \tag{3.23b}$$

$$E_{z0}\frac{j}{\eta} e^{-j\omega\Delta t}\sin\left(\tilde{k}_x\Delta x\right) - H_{y0}\left[1 - P_{2D} e^{-j\omega\Delta t}\right] = 0 \tag{3.23c}$$

where

$$P_{2D} = \frac{1}{2}\left[\cos\left(\tilde{k}_x\Delta x\right) + \cos\left(\tilde{k}_y\Delta y\right)\right] \tag{3.24}$$

Rearranging (3.23) to a matrix form, we obtain the following homogeneous system of three equations with three unknowns E_{z0}, H_{x0} and H_{y0}:

$$\begin{bmatrix} \left(1 - P_{2D} e^{-j\omega\Delta t}\right) & \frac{j\eta}{2} e^{-j\omega\Delta t}\sin\left(\tilde{k}_y\Delta y\right) & -\frac{j\eta}{2} e^{-j\omega\Delta t}\sin\left(\tilde{k}_x\Delta x\right) \\ \frac{j}{\eta} e^{-j\omega\Delta t}\sin\left(\tilde{k}_y\Delta y\right) & \left(1 - P_{2D} e^{-j\omega\Delta t}\right) & 0 \\ -\frac{j}{\eta} e^{-j\omega\Delta t}\sin\left(\tilde{k}_x\Delta x\right) & 0 & \left(1 - P_{2D} e^{-j\omega\Delta t}\right) \end{bmatrix} \begin{bmatrix} E_{z0} \\ H_{x0} \\ H_{y0} \end{bmatrix} = 0 \tag{3.25}$$

Equating the determinant of this system to zero results in

$$\left[e^{j\omega\Delta t} - P_{2D}\right]^2 = -\frac{1}{2}\left[\sin^2\left(\tilde{k}_x\Delta x\right) + \sin^2\left(\tilde{k}_y\Delta y\right)\right] \tag{3.26}$$

Expanding the left hand side in (3.26) yields

$$\left[e^{j\omega\Delta t} - P_{2D}\right]^2 = \left[P_{2D}^2 - 2P_{2D}\cos\left(\omega\Delta t\right) + \cos\left(2\omega\Delta t\right)\right] + j\left[\sin\left(2\omega\Delta t\right) - 2P_{2D}\sin\left(\omega\Delta t\right)\right] \tag{3.27}$$

Equation (3.27), the left hand side of (3.26), has the real and imaginary parts, whereas the right hand side of (3.26) has only real values. Accordingly, the imaginary part in (3.27) must be zero. Setting the imaginary term in (3.27) equal to zero results in

$$P_{2D} = \cos\left(\omega\Delta t\right) \tag{3.28}$$

After inserting (3.28) into (3.26), (3.26) becomes

$$\sin^2\left(\omega\Delta t\right) = \frac{1}{2}\left[\sin^2\left(\tilde{k}_x\Delta x\right) + \sin^2\left(\tilde{k}_y\Delta y\right)\right] \tag{3.29}$$

Finally, the general numerical dispersion relations of the 2-D TM_z Propagator algorithm are

$$\cos\left(\omega\Delta t\right) = \frac{1}{2}\left[\cos\left(\tilde{k}_x\Delta x\right) + \cos\left(\tilde{k}_y\Delta y\right)\right] \tag{3.30a}$$

$$\sin^2\left(\omega\Delta t\right) = \frac{1}{2}\left[\sin^2\left(\tilde{k}_x\Delta x\right) + \sin^2\left(\tilde{k}_y\Delta y\right)\right] \tag{3.30b}$$

Consider the special case of a square cell gridding with $\Delta x = \Delta y = \Delta$, then take the limit as Δ and Δt approach zero. Equation (3.30a) reduces to

$$\left(\omega\Delta t\right)^2 = \frac{\Delta^2}{2}\left[\tilde{k}_x^2 + \tilde{k}_y^2\right] \tag{3.31}$$

by taking first two terms of infinite series expansion of the cosine function. We note that the numerical time step for the 2-D Propagator is $\Delta t = \Delta / (\sqrt{2}c)$. By inserting this time increment into (3.31), (3.31) becomes to the ideal dispersion case:

$$\left(\frac{\omega}{c}\right)^2 = (k)^2 = \left(\tilde{k}_x\right)^2 + \left(\tilde{k}_y\right)^2 \tag{3.32}$$

Similarly, the dispersion relation (3.30b) also reduces to (3.32) by taking first term of infinite series of the sine function and inserting the 2-D numerical time increment. This shows that numerical dispersion can be reduced to any degree if we use a finer grid sampling. This can also be verified by calculating a numerical phase velocity using the numerical dispersion relations.

Fig. 3.10 shows the normalized numerical phase velocity in terms of wave propagation angle ϕ with respect to the axes. The phase velocity is calculated by the same method used in the FDTD [3]. As shown in Fig. 3.10, as the sampling density increases, the numerical phase velocity approaches that of free space having a maximum at $\phi = 45^\circ$.

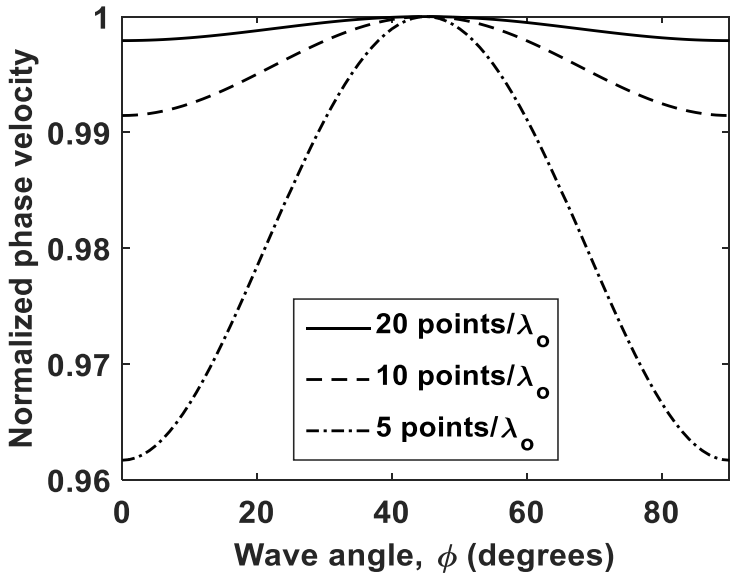

Figure 3.10: 2-D Propagator variation of numerical phase velocity for three sampling densities of the square unit cells.

The dispersion analysis is now extended to the full three-dimensional case that includes all six coupled electric and magnetic field components. To derive the numerical dispersion relations of the 3-D Propagator method, we start with a monochromatic plane wave expressions for the six electric and magnetic field components. Substituting the plane wave expressions into (2.52)-(2.53) yields, after simplifications and rearrangement, the following homogeneous system of six equations along with six unknowns:

$$\begin{bmatrix} a_{11} & 0 & 0 & 0 & a_{15} & a_{16} \\ 0 & a_{22} & 0 & a_{24} & 0 & a_{26} \\ 0 & 0 & a_{33} & a_{34} & a_{35} & 0 \\ 0 & a_{42} & a_{43} & a_{44} & 0 & 0 \\ a_{51} & 0 & a_{53} & 0 & a_{55} & 0 \\ a_{61} & a_{62} & 0 & 0 & 0 & a_{66} \end{bmatrix} \begin{bmatrix} E_{x0} \\ E_{y0} \\ E_{z0} \\ H_{x0} \\ H_{y0} \\ H_{z0} \end{bmatrix} = 0 \tag{3.33}$$

where

$$
\begin{aligned}
a_{11} &= a_{22} = a_{33} = a_{44} = a_{55} = a_{66} = \left(1 - P_{3D} e^{-j\omega\Delta t}\right) \\
a_{15} &= -a_{24} = -\eta^2 a_{42} = \eta^2 a_{51} = j\eta e^{-j\omega\Delta t} \sin\left(\tilde{k}_z \Delta z\right) \\
a_{16} &= -a_{34} = -\eta^2 a_{43} = \eta^2 a_{61} = -j\eta e^{-j\omega\Delta t} \sin\left(\tilde{k}_y \Delta y\right) \\
a_{26} &= -a_{35} = -\eta^2 a_{53} = \eta^2 a_{62} = j\eta e^{-j\omega\Delta t} \sin\left(\tilde{k}_x \Delta x\right)
\end{aligned}
\tag{3.34}
$$

with

$$
P_{3D} = \frac{1}{3}\left[\cos\left(\tilde{k}_x \Delta x\right) + \cos\left(\tilde{k}_y \Delta y\right) + \cos\left(\tilde{k}_z \Delta z\right)\right] \tag{3.35}
$$

Solving the determinant in (3.33) and equating it to zero results in

$$
\left[e^{j\omega\Delta t} - P_{3D}\right]^2 = -\frac{1}{3}\left[\sin^2\left(\tilde{k}_x \Delta x\right) + \sin^2\left(\tilde{k}_y \Delta y\right) + \sin^2\left(\tilde{k}_z \Delta z\right)\right] \tag{3.36}
$$

When the left hand side in (3.36) is expanded, it is shown to contain real and imaginary terms. However, the imaginary part must be zero because the right hand side of (3.36) is a real-valued. The imaginary term provides the following condition:

$$
\cos\left(\omega\Delta t\right) = P_{3D} = \frac{1}{3}\left[\cos\left(\tilde{k}_x \Delta x\right) + \cos\left(\tilde{k}_y \Delta y\right) + \cos\left(\tilde{k}_z \Delta z\right)\right] \tag{3.37}
$$

Upon substituting (3.37) into (3.36), we obtain

$$
\sin^2\left(\omega\Delta t\right) = \frac{1}{3}\left[\sin^2\left(\tilde{k}_x \Delta x\right) + \sin^2\left(\tilde{k}_y \Delta y\right) + \sin^2\left(\tilde{k}_z \Delta z\right)\right] \tag{3.38}
$$

Equations (3.37) and (3.38) are the general form of the numerical dispersion relations for the 3-D Propagator method.

Consider the special case of a cubic-cell lattice with $\Delta x = \Delta y = \Delta z = \Delta$, then take the limit as Δ and Δt go to zero. Both (3.37) and (3.38) reduce to

$$
\left(\omega\Delta t\right)^2 = \frac{\Delta^2}{3}\left[\tilde{k}_x^2 + \tilde{k}_y^2 + \tilde{k}_z^2\right] \tag{3.39}
$$

by taking first two terms of infinite series expression of the cosine function in (3.37) and the first term of the infinite series of the sine function in (3.38). Equation (3.39) also reduces to the ideal free space wave condition:

$$\left(\frac{\omega}{c}\right)^2 = (k)^2 = \left(\tilde{k}_x\right)^2 + \left(\tilde{k}_y\right)^2 + \left(\tilde{k}_z\right)^2 \tag{3.40}$$

by inserting the 3-D numerical time step $\Delta t = \Delta / (\sqrt{3}c)$ into the left term of (3.39). This also illustrates that taking a finer grid sampling can minimize dispersion.

3.6 Stability Condition

The 1-D Propagator numerical equation is unconditionally stable, however, 2-D and 3-D equations have stability conditions that can be developed from the numerical dispersion relations. In this section, the stability condition will be investigated based upon complex-frequency analysis [3].

We first start with the 3-D Propagator equation. It was stated in section 2.5 that the coefficient $1/\sqrt{3}$ in (2.52)-(2.53) has been added to meet the stability condition. The following stability analysis shows the necessity of adding that coefficient. Consider the initially derived 3-D numerical expression (2.51) for the *x*-component of the electric field:

$$\begin{aligned} E_x\big|_{i,j,k}^{n} = \frac{1}{6}\Big[& E_x\big|_{i+1,j,k}^{n-1} + E_x\big|_{i-1,j,k}^{n-1} + E_x\big|_{i,j+1,k}^{n-1} + E_x\big|_{i,j-1,k}^{n-1} + E_x\big|_{i,j,k+1}^{n-1} + E_x\big|_{i,j,k-1}^{n-1} \Big] \\ & - \frac{\eta}{2}\Big[H_y\big|_{i,j,k+1}^{n-1} - H_y\big|_{i,j,k-1}^{n-1} \Big] + \frac{\eta}{2}\Big[H_z\big|_{i,j+1,k}^{n-1} - H_z\big|_{i,j-1,k}^{n-1} \Big] \end{aligned} \tag{3.41}$$

The numerical dispersion relation from (3.41) and other field components can be written as

$$\sin^2\left(\tilde{\omega}\Delta t\right)=\left[\sin^2\left(\tilde{k}_x\Delta x\right)+\sin^2\left(\tilde{k}_y\Delta y\right)+\sin^2\left(\tilde{k}_z\Delta z\right)\right] \tag{3.42}$$

where $\tilde{\omega}$ is the numerical angular frequency. We first solve (3.42) for $\tilde{\omega}$. This yields

$$\tilde{\omega}=\frac{1}{\Delta t}\sin^{-1}\left(\psi\right) \tag{3.43}$$

where

$$\psi=\sqrt{\sin^2\left(\tilde{k}_x\Delta x\right)+\sin^2\left(\tilde{k}_y\Delta y\right)+\sin^2\left(\tilde{k}_z\Delta z\right)} \tag{3.44}$$

Here we allow for the possibility of a complex-valued numerical angular frequency, $\tilde{\omega}=\tilde{\omega}_{real}+j\tilde{\omega}_{imag}$. We note that the imaginary values of $\tilde{\omega}$ will cause the field amplitude to exponentially decrease ($\tilde{\omega}_{imag}>0$) or increase ($\tilde{\omega}_{imag}<0$) with time. Given this basis, the numerical angular frequency $\tilde{\omega}$ will have a complex value if ψ in (3.43) exceeds 1. In (3.44), the range of ψ is $0\le\psi\le\sqrt{3}$, resulting in a complex-valued $\tilde{\omega}$. In order to have a real-valued $\tilde{\omega}$ ($\tilde{\omega}_{imag}=0$), the additional coefficient $1/\sqrt{3}$ is required in front of the square root of (3.44). This modification gives

$$\psi=\sqrt{\frac{1}{3}\left\{\sin^2\left(\tilde{k}_x\Delta x\right)+\sin^2\left(\tilde{k}_y\Delta y\right)+\sin^2\left(\tilde{k}_z\Delta z\right)\right\}} \tag{3.45}$$

After adding the coefficient $1/\sqrt{3}$, the range of ψ in (3.45) became the range of $0\le\psi\le1$, hence real values of $\tilde{\omega}$ are obtained in (3.43) since $\sin^{-1}(\psi)$ is a real value. The addition of $1/\sqrt{3}$ not only provides the stable 3-D numerical expressions, but also it gives the numerical time step, given by

$$\Delta t_{3D}=\frac{\Delta}{\sqrt{3}c} \tag{3.46}$$

In a manner analogous to the above 3-D case, the stability analysis for the 2-D Propagator method starts with the originally found numerical expression that did not contain $1/\sqrt{2}$ in front of the magnetic fields, given by

$$\begin{aligned} E_z\big|_{i,j}^{n} = \frac{1}{4}\Big[& E_z\big|_{i+1,j}^{n-1} + E_z\big|_{i-1,j}^{n-1} + E_z\big|_{i,j+1}^{n-1} + E_z\big|_{i,j-1}^{n-1} \Big] \\ & - \frac{\eta}{2}\Big[H_x\big|_{i,j+1}^{n-1} - H_x\big|_{i,j-1}^{n-1} \Big] + \frac{\eta}{2}\Big[H_y\big|_{i+1,j}^{n-1} - H_y\big|_{i-1,j}^{n-1} \Big] \end{aligned} \tag{3.47}$$

With (3.47), the numerical dispersion relation is obtained as

$$\sin^2\left(\tilde{\omega}\Delta t\right) = \left[\sin^2\left(\tilde{k}_x \Delta x\right) + \sin^2\left(\tilde{k}_y \Delta y\right) \right] \tag{3.48}$$

Solving (3.48) for $\tilde{\omega}$ yields

$$\tilde{\omega} = \frac{1}{\Delta t}\sin^{-1}\left(\psi\right) \tag{3.49}$$

where

$$\psi = \sqrt{\sin^2\left(\tilde{k}_x \Delta x\right) + \sin^2\left(\tilde{k}_y \Delta y\right)} \tag{3.50}$$

In (3.50), ψ has the range of $0 \le \psi \le \sqrt{2}$, resulting in the possibility of having a complex value of $\tilde{\omega}$, which gives rise to numerical instability. In order to be in a stable range of ψ, the coefficient $1/\sqrt{2}$ is required in front of the square root of (3.50). With this adjustment, the modified ψ becomes

$$\psi = \sqrt{\frac{1}{2}\left\{\sin^2\left(\tilde{k}_x \Delta x\right) + \sin^2\left(\tilde{k}_y \Delta y\right)\right\}} \tag{3.51}$$

Equation (3.51) now is in the range of $0 \le \psi \le 1$, and therefore $\tilde{\omega}$ will be a real value. Adding the coefficient $1/\sqrt{2}$ gives rise to the stable 2-D numerical expressions as well as

the numerical time step, given by

$$\Delta t_{2\mathrm{D}} = \frac{\Delta}{\sqrt{2}c} \tag{3.52}$$

Based upon the above stability analysis condition, the additional coefficients $1/\sqrt{3}$ and $1/\sqrt{2}$ have been respectively added into the 3-D and 2-D Propagator method equations. Therefore, (3.46) and (3.52) are the stability conditions for our 3-D and 2-D numerical expressions respectively.

We now consider the possibility of having an alternate value of the additional coefficient in the stable range. We first rewrite the 3-D equation for E_x field component, given by

$$\begin{aligned} E_x\big|_{i,j,k}^{n} = \frac{1}{6}\Big[& E_x\big|_{i+1,j,k}^{n-1} + E_x\big|_{i-1,j,k}^{n-1} + E_x\big|_{i,j+1,k}^{n-1} + E_x\big|_{i,j-1,k}^{n-1} + E_x\big|_{i,j,k+1}^{n-1} + E_x\big|_{i,j,k-1}^{n-1} \Big] \\ & - \frac{\eta}{2S_{3\mathrm{D}}}\Big[H_y\big|_{i,j,k+1}^{n-1} - H_y\big|_{i,j,k-1}^{n-1} \Big] + \frac{\eta}{2S_{3\mathrm{D}}}\Big[H_z\big|_{i,j+1,k}^{n-1} - H_z\big|_{i,j-1,k}^{n-1} \Big] \end{aligned} \tag{3.53}$$

where S represents the stability limit coefficient that requires to be added. From (3.53) and numerical equations of other field components, the dispersion relation becomes

$$\sin^2\left(\tilde{\omega}\Delta t\right) = \frac{1}{S_{3\mathrm{D}}}\left[\sin^2\left(\tilde{k}_x\Delta x\right) + \sin^2\left(\tilde{k}_y\Delta y\right) + \sin^2\left(\tilde{k}_z\Delta z\right)\right] \tag{3.54}$$

Solving for $\tilde{\omega}$, the numerical angular frequency is

$$\tilde{\omega} = \frac{1}{\Delta t}\sin^{-1}\left(\psi\right) \tag{3.55}$$

where

$$\psi = \frac{1}{S_{3\mathrm{D}}}\sqrt{\left\{\sin^2\left(\tilde{k}_x\Delta x\right) + \sin^2\left(\tilde{k}_y\Delta y\right) + \sin^2\left(\tilde{k}_z\Delta z\right)\right\}} \tag{3.56}$$

From (3.55)-(3.56), S_{3D} should be $S_{3D} \geq \sqrt{3}$ to maintain in the stable range, $0 \leq \psi \leq 1$. In other words, (3.53) will be unstable if $S_{3D} < \sqrt{3}$. We now present examples that show the stability limit for S_{3D} is violated where $S_{3D} < \sqrt{3}$.

Fig. 3.11 visualizes the propagation of a Gaussian plane wave pulse in *x*-plane cut when $S_{3D} = 1.0$, 1.4 and $\sqrt{3}$ at $n = 100$ time steps. It is clearly seen that the pulse becomes unstable almost instantly in the case where $S_{3D} = 1.0$ and its amplitude gradually increases when $S_{3D} = 1.4$. The case where $S_{3D} = \sqrt{3}$, on the other hand, preserves pulse propagation. Therefore, it is evident that the additional coefficient, which should be $S_{3D} \geq \sqrt{3}$, is required.

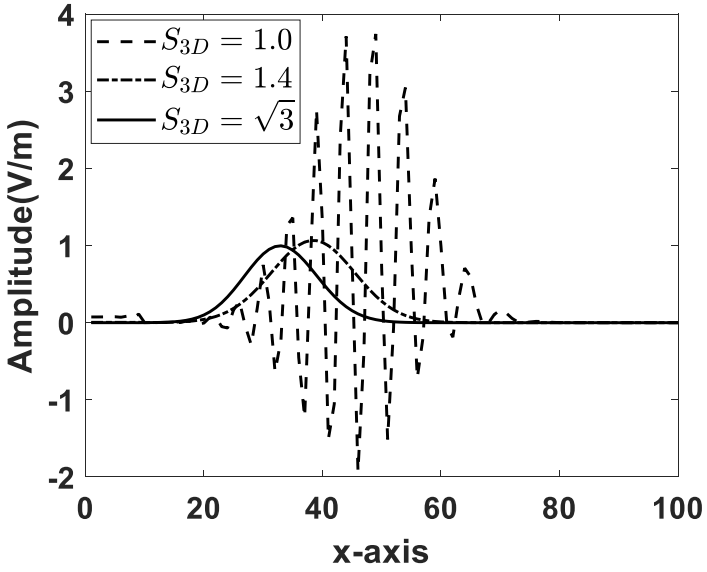

Figure 3.11: Propagation of plane wave pulse in *x*-plane cut for several values of S_{3D} in the unstable range at $n = 100$ time steps.

Next, for the stability limit where S_{3D} is in the unstable range, we consider all possible values of S_{3D} in the stable range, $S_{3D} \geq \sqrt{3}$. Fig. 3.12 shows the 3-D Gaussian plane wave propagated up to 150 time steps in the *x*-plane cut for several values of S_{3D} within $S_{3D} \geq \sqrt{3}$. As shown in Fig. 3.12, the plane wave for $S_{3D} = \sqrt{3}$ is well preserved, whereas for $S_{3D} = 2.0$ and 2.3, which are in the stable range, it decays in amplitude and the pulse velocity alters depending upon the value of S_{3D}. This result shows that any value of S_{3D} in the stable bounds, other than $S_{3D} = \sqrt{3}$, cannot be a possible coefficient. This determines the 3-D numerical time increment, $\Delta t = \Delta / (S_{3D} \times c)$.

From the results of Figs. 3.11 and 3.12, we conclude that the only possible 3-D coefficient is $S_{3D} = \sqrt{3}$ and (2.52)-(2.53) are the ideal 3-D numerical expressions.

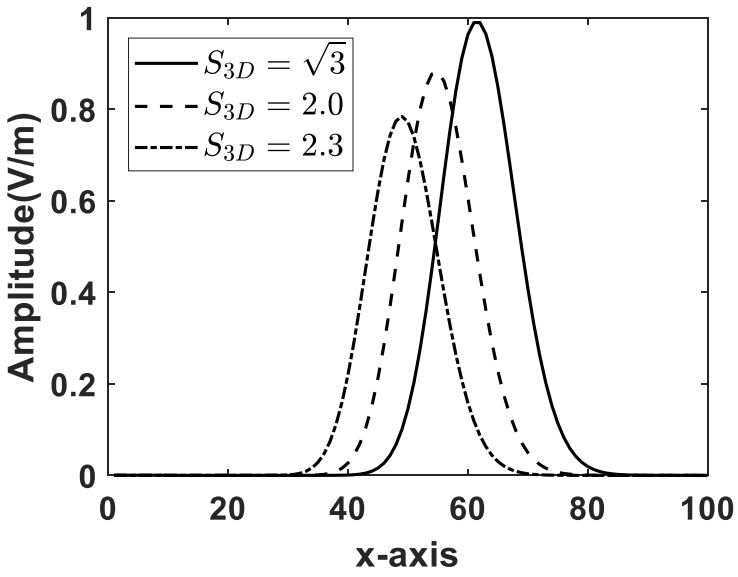

Figure 3.12: Propagation of plane wave pulse in *x*-plane cut for several values of S_{3D} in the stable range at $n = 150$ time steps.

Similarly with the 3-D case, it can be shown that the only possible 2-D stability coefficient is $S_{2D} = \sqrt{2}$ as below. The numerical equation of E_z field component for the 2-D TM$_z$ case with the 2-D stability limit coefficient S_{2D} can be written as

$$\begin{aligned} E_z\big|_{i,j}^{n} = \frac{1}{4}\Big[& E_z\big|_{i+1,j}^{n-1} + E_z\big|_{i-1,j}^{n-1} + E_z\big|_{i,j+1}^{n-1} + E_z\big|_{i,j-1}^{n-1} \Big] \\ & - \frac{\eta}{2S_{2D}}\Big[H_x\big|_{i,j+1}^{n-1} - H_x\big|_{i,j-1}^{n-1} \Big] + \frac{\eta}{2S_{2D}}\Big[H_y\big|_{i+1,j}^{n-1} - H_y\big|_{i-1,j}^{n-1} \Big] \end{aligned} \tag{3.57}$$

The numerical dispersion relation is

$$\sin^2\left(\tilde{\omega}\Delta t\right) = \frac{1}{S_{2D}}\left[\sin^2\left(\tilde{k}_x \Delta x\right) + \sin^2\left(\tilde{k}_y \Delta y\right) \right] \tag{3.58}$$

From (3.58), the numerical angular frequency $\tilde{\omega}$ is

$$\tilde{\omega} = \frac{1}{\Delta t}\sin^{-1}\left(\psi\right) \tag{3.59}$$

where

$$\psi = \frac{1}{S_{2D}}\sqrt{\left\{ \sin^2\left(\tilde{k}_x \Delta x\right) + \sin^2\left(\tilde{k}_y \Delta y\right) \right\}} \tag{3.60}$$

In the unstable range where $S_{2D} < \sqrt{2}$, the propagation of a Gaussian plane wave at $n = 130$ time steps is examined as shown in Fig. 3.13. Fig. 3.13 illustrates the 2-D Gaussian plane wave propagated up to 130 time steps in the *x*-plane cut for several values within $S_{2D} < \sqrt{2}$ and $S_{2D} = \sqrt{2}$. The pulse becomes instantly unstable for $S_{2D} = 1.0$ and its amplitude for $S_{2D} = 1.2$ increases and becomes unstable as it propagates further time steps. On the other hand, the pulse for $S_{2D} = \sqrt{2}$ travels as expected.

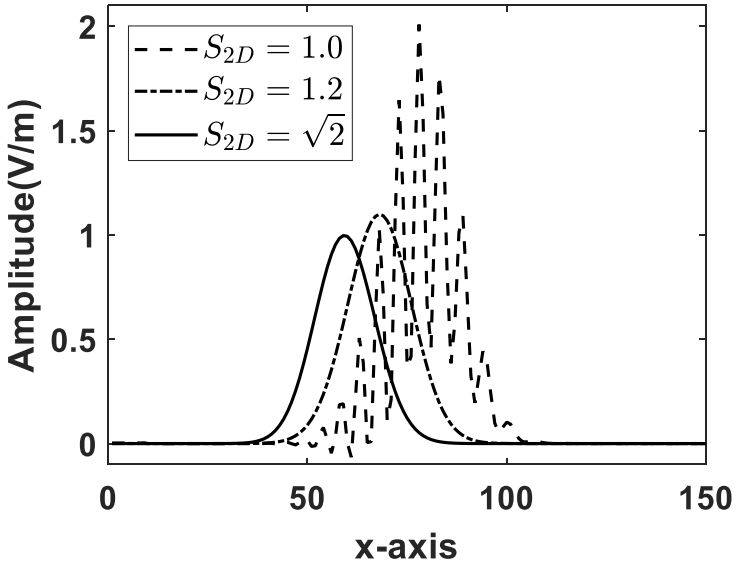

Figure 3.13: Propagation of plane wave pulse in *x*-plane cut for several values of S_{2D} in the unstable range at $n = 130$ time steps.

Next we consider the cases in the stable range where $S_{2D} \geq \sqrt{2}$. As shown in Fig. 3.14, all values including $S_{2D} = \sqrt{2}$, 1.5 and 1.6 do not become unstable as expected. However the amplitude of the pulse for the cases where $S_{2D} = 1.5$ and 1.6 decays as it propagates and the value $S_{2D} = \sqrt{2}$ preserves the pulse propagation. In addition to the stability, the pulse velocity changes depending on the value of S_{2D}. For example, the plane wave for $S_{2D} = \sqrt{2}$ propagated $99\Delta x$ spatial increments, from $10\Delta x$ to $109\Delta x$, during $140\Delta t$ time steps, from $60\Delta t$ to $200\Delta t$, which gives rise to the velocity $v = (99\Delta x / 140\Delta t) \approx \Delta x / (\sqrt{2}\Delta t)$, and for the value of $S_{2D} = 1.6$ its velocity becomes $v = (87\Delta x / 140\Delta t) \approx \Delta x / (1.6\Delta t)$ since it traveled $87\Delta x$ in space during $140\Delta t$ time steps. As a result, it can be concluded from these results that $S_{2D} = \sqrt{2}$ is the only possible

coefficient, the numerical time step is $\Delta t = \Delta / (S_{2D} \times c)$, and (2.54) are the ideal numerical expressions for the 2-D TM_z case.

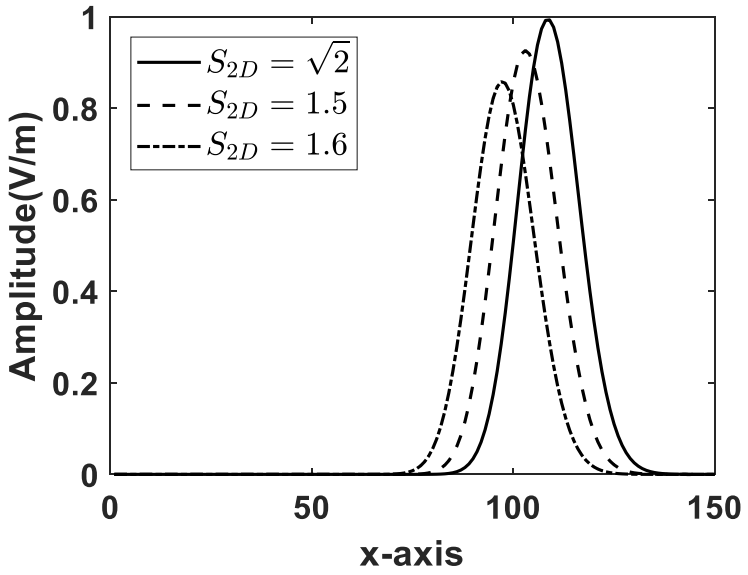

Figure 3.14: Propagation of plane wave pulse in *x*-plane cut for several values of S_{2D} in the stable range at $n = 200$ time steps.

3.7 Summary

In this chapter, the key numerical aspects of the Propagator method were presented for simulating diverse electromagnetic problems in multiple dimensions. These included: (1) the introduction of a physical time increment in a dielectric medium using Newton's third order difference extrapolation technique in time, (2) the derivation of the exact 1-D boundary condition and application of the conformal boundary conditions for the 2-D and 3-D cases, (3) the simple and effective null boundary condition, (4) the derivation of numerical dispersion relations in all dimensions, and (5) numerical stability conditions derived using a complex-frequency analysis.

4. TOTAL-FIELD / SCATTERED-FIELD FORMULATION

4.1 Introduction

The total-field / scattered-field (TF / SF) formulation not only aims at realizing a plane-wave source, but it also provides a number of features that allow an arbitrary incident wave, a wide computational dynamic range and an absorbing boundary condition at the outermost lattice points [3]. The TF / SF technique was successfully applied to the FDTD algorithm and it remains in use today. The time-domain Propagator modeling also requires the TF / SF technique in order to effectively generate a plane-wave source and achieve the null boundary condition.

To illustrate the idea of the TF / SF formulation, the total-field / scattered-field zoning in a space lattice is shown in Fig. 4.1. In region 1, the total-field zone, we assume that total-field vector components including the interaction of the incident and scattered waves from any objects exist. A virtual surface that separates regions 1 and 2 is assumed to be included in the total-field region, and the interacting object is embedded within this region. In region 2, the scattered-field zone, we assume that only scattered-field vector components, total fields minus incident fields, exist. The outer lattice planes of region 2 are truncated by the absorbing boundary condition.

In this chapter, each dimensional TF / SF formulation for the time-domain Propagator method will be presented.

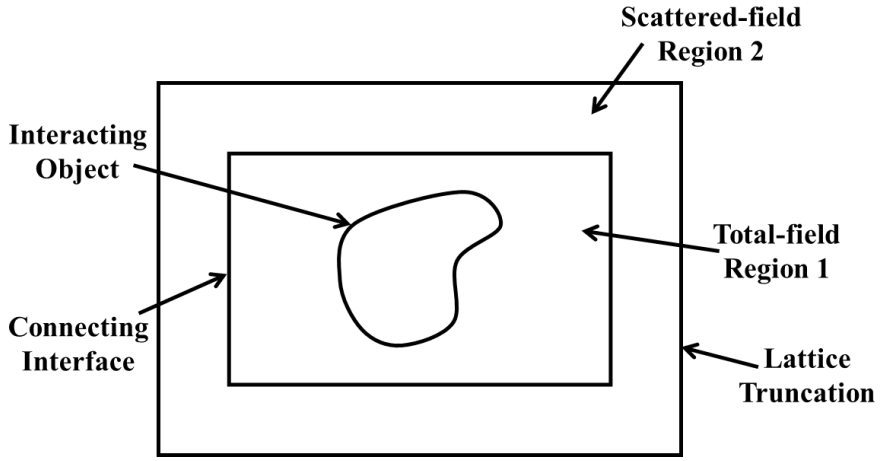

Figure 4.1: Total-field / scattered-field regions.

4.2 One-dimensional formulation

To illustrate the TF / SF formulation of the 1-D Propagator method, consider the 1-D grid scheme containing E_x and H_y field components, as shown in Fig. 4.2. In Fig. 4.2, upward directed arrows and solid circles represent respectively E_x and H_y fields. Assume that the boundary grid cells i_0 and i_1 between regions 1 and 2 are included in a total-field zone and the grid points $i_0 - 1$ and $i_1 + 1$, just outside of region 1, are in a scattered-field zone.

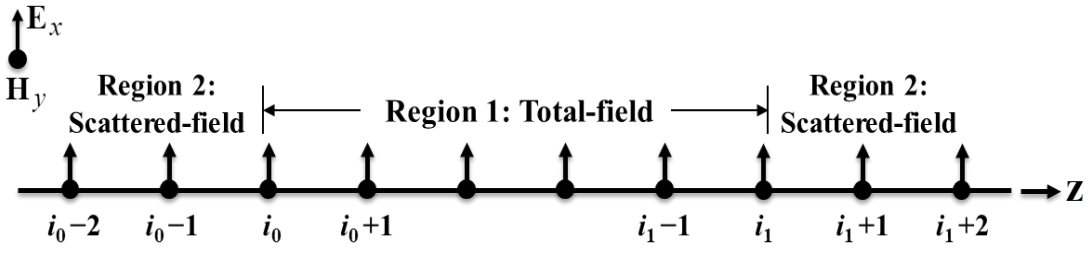

Figure 4.2: Total-field / scattered-field regions of the 1-D Propagator grid scheme.

First, consider a time-stepping E_x component at grid point i_0, the left boundary point between regions 1 and 2. Using the 1-D Propagator equation (2.40), the E_x field located at i_0 is calculated by

$$E_{x,\text{total}}\Big|_{i_0}^{n} = \frac{1}{2}\left[E_{x,\text{total}}\Big|_{i_0+1}^{n-1} + E_{x,\text{scat}}\Big|_{i_0-1}^{n-1} \right] - \frac{\eta}{2}\left[H_{y,\text{total}}\Big|_{i_0+1}^{n-1} - H_{y,\text{scat}}\Big|_{i_0-1}^{n-1} \right] \tag{4.1}$$

In (4.1), the fields at $i_0 + 1$ are assumed to be stored as a total field, whereas the fields at $i_0 - 1$ are assumed to be stored as a scattered field. However, if the grid points $i_0 - 1$, i_0, and $i_0 + 1$ are in region 1 of Fig. 4.2, (4.1) is inconsistent with the equation:

$$E_{x,\text{total}}\Big|_{i_0}^{n} = \frac{1}{2}\left[E_{x,\text{total}}\Big|_{i_0+1}^{n-1} + E_{x,\text{total}}\Big|_{i_0-1}^{n-1} \right] - \frac{\eta}{2}\left[H_{y,\text{total}}\Big|_{i_0+1}^{n-1} - H_{y,\text{total}}\Big|_{i_0-1}^{n-1} \right] \tag{4.2}$$

Consistency of (4.2) can be realized by adding the incident field terms into (4.1), which are assumed to be stored in the computer memory. The modified E_x component at the point i_0 is written as

$$E_{x,\text{total}}\Big|_{i_0}^{n} = \frac{1}{2}\left[E_{x,\text{total}}\Big|_{i_0+1}^{n-1} + \left(E_{x,\text{scat}}\Big|_{i_0-1}^{n-1} + E_{x,\text{inc}}\Big|_{i_0-1}^{n-1} \right) \right] - \frac{\eta}{2}\left[H_{y,\text{total}}\Big|_{i_0+1}^{n-1} - \left(H_{y,\text{scat}}\Big|_{i_0-1}^{n-1} + H_{y,\text{inc}}\Big|_{i_0-1}^{n-1} \right) \right] \tag{4.3}$$

since

$$E_{x,\text{scat}}\Big|_{i_0-1}^{n-1} + E_{x,\text{inc}}\Big|_{i_0-1}^{n-1} = E_{x,\text{total}}\Big|_{i_0-1}^{n-1} \tag{4.4a}$$

$$H_{y,\text{scat}}\Big|_{i_0-1}^{n-1} + H_{y,\text{inc}}\Big|_{i_0-1}^{n-1} = H_{y,\text{total}}\Big|_{i_0-1}^{n-1} \tag{4.4b}$$

Equation (4.3) can be rewritten as a compact expression:

Left boundary point of Region 1 ($i = i_0$)

$$E_x\Big|_i^n = \left\{E_x\Big|_i^n\right\}_{(2.40a)} + \underbrace{\left[\frac{1}{2}E_{x,\mathrm{inc}}\Big|_{i-1}^{n-1} + \frac{\eta}{2}H_{y,\mathrm{inc}}\Big|_{i-1}^{n-1}\right]}_{\text{correction term}} \tag{4.5a}$$

$$H_y\Big|_i^n = \left\{H_y\Big|_i^n\right\}_{(2.40b)} + \underbrace{\left[\frac{1}{2}H_{y,\mathrm{inc}}\Big|_{i-1}^{n-1} + \frac{1}{2\eta}E_{x,\mathrm{inc}}\Big|_{i-1}^{n-1}\right]}_{\text{correction term}} \tag{4.5b}$$

where the curly bracket term denotes the time-stepping field to be calculated before adding the incident field correction term. The remaining H_y field component at the point i_0 is obtained in an analogous manner of (4.1)-(4.4).

Regarding with the grid point i_1, the right boundary point between regions 1 and 2 in Fig. 4.2, the modified field components at the right boundary point of region 1 can be acquired in a similar way as explained above, by adding the incident wave correction terms located at point $i_1 + 1$ in the scattered-field region.

Right boundary point of Region 1 ($i = i_1$)

$$E_x\Big|_i^n = \left\{E_x\Big|_i^n\right\}_{(2.40a)} + \underbrace{\left[\frac{1}{2}E_{x,\mathrm{inc}}\Big|_{i+1}^{n-1} - \frac{\eta}{2}H_{y,\mathrm{inc}}\Big|_{i+1}^{n-1}\right]}_{\text{correction term}} \tag{4.6a}$$

$$H_y\Big|_i^n = \left\{H_y\Big|_i^n\right\}_{(2.40b)} + \underbrace{\left[\frac{1}{2}H_{y,\mathrm{inc}}\Big|_{i+1}^{n-1} - \frac{1}{2\eta}E_{x,\mathrm{inc}}\Big|_{i+1}^{n-1}\right]}_{\text{correction term}} \tag{4.6b}$$

Next, consider the time-stepping E_x component at the grid point $i_0 - 1$ located in the scattered-field zone, just outside left face of region 1 in Fig. 4.2. The E_x component at $i_0 - 1$ is updated by the equation:

$$E_{x,\text{scat}}\Big|_{i_0-1}^{n} = \frac{1}{2}\left[E_{x,\text{total}}\Big|_{i_0}^{n-1} + E_{x,\text{scat}}\Big|_{i_0-2}^{n-1} \right] - \frac{\eta}{2}\left[H_{y,\text{total}}\Big|_{i_0}^{n-1} - H_{y,\text{scat}}\Big|_{i_0-2}^{n-1} \right] \tag{4.7}$$

In (4.7), the fields at i_0 are assumed to be stored as a total field, whereas the fields at $i_0 - 2$ are assumed to be stored as a scattered field. However, if the grid points $i_0 - 2$, $i_0 - 1$, and i_0 are in the scattered-field region 2, (4.7) is inconsistent with the equation:

$$E_{x,\text{scat}}\Big|_{i_0-1}^{n} = \frac{1}{2}\left[E_{x,\text{scat}}\Big|_{i_0}^{n-1} + E_{x,\text{scat}}\Big|_{i_0-2}^{n-1} \right] - \frac{\eta}{2}\left[H_{y,\text{scat}}\Big|_{i_0}^{n-1} - H_{y,\text{scat}}\Big|_{i_0-2}^{n-1} \right] \tag{4.8}$$

The consistency condition of (4.8) can be achieved by subtracting the incident field terms into (4.7). The corrected E_x component at the point $i_0 - 1$ is expressed as

$$E_{x,\text{scat}}\Big|_{i_0-1}^{n} = \frac{1}{2}\left[\left(E_{x,\text{total}}\Big|_{i_0}^{n-1} - E_{x,\text{inc}}\Big|_{i_0}^{n-1} \right) + E_{x,\text{scat}}\Big|_{i_0-2}^{n-1} \right] - \frac{\eta}{2}\left[\left(H_{y,\text{total}}\Big|_{i_0}^{n-1} - H_{y,\text{inc}}\Big|_{i_0}^{n-1} \right) - H_{y,\text{scat}}\Big|_{i_0-2}^{n-1} \right] \tag{4.9}$$

since

$$E_{x,\text{total}}\Big|_{i_0}^{n-1} - E_{x,\text{inc}}\Big|_{i_0}^{n-1} = E_{x,\text{scat}}\Big|_{i_0}^{n-1} \tag{4.10a}$$

$$H_{y,\text{total}}\Big|_{i_0}^{n-1} - H_{y,\text{inc}}\Big|_{i_0}^{n-1} = H_{y,\text{scat}}\Big|_{i_0}^{n-1} \tag{4.10b}$$

Therefore, the corrected equations of field components at the points $i_0 - 1$ and $i_1 + 1$, just outside of region 1, are expressed as

Outside left face of Region 1 ($i = i_0 - 1$)

$$E_x\Big|_i^n = \left\{ E_x\Big|_i^n \right\}_{(2.40a)} - \underbrace{\left[\frac{1}{2} E_{x,\text{inc}}\Big|_{i+1}^{n-1} - \frac{\eta}{2} H_{y,\text{inc}}\Big|_{i+1}^{n-1} \right]}_{\text{correction term}} \tag{4.11a}$$

$$H_y\Big|_i^n = \left\{ H_y\Big|_i^n \right\}_{(2.40b)} - \underbrace{\left[\frac{1}{2} H_{y,\text{inc}}\Big|_{i+1}^{n-1} - \frac{1}{2\eta} E_{x,\text{inc}}\Big|_{i+1}^{n-1} \right]}_{\text{correction term}} \tag{4.11b}$$

Outside right face of Region 1 ($i = i_1 + 1$)

$$E_x\big|_i^n = \left\{ E_x\big|_i^n \right\}_{(2.40a)} - \underbrace{\left[\frac{1}{2} E_{x,\mathrm{inc}}\Big|_{i-1}^{n-1} + \frac{\eta}{2} H_{y,\mathrm{inc}}\Big|_{i-1}^{n-1} \right]}_{\text{correction term}} \tag{4.12a}$$

$$H_y\big|_i^n = \left\{ H_y\big|_i^n \right\}_{(2.40b)} - \underbrace{\left[\frac{1}{2} H_{y,\mathrm{inc}}\Big|_{i-1}^{n-1} + \frac{1}{2\eta} E_{x,\mathrm{inc}}\Big|_{i-1}^{n-1} \right]}_{\text{correction term}} \tag{4.12b}$$

where the curly bracket term denotes the time-stepping operation before adding the incident field correction terms. Equations (4.5)-(4.6) and (4.11)-(4.12) are the TF / SF formulated equations of 1-D Propagator method.

4.3 Two-dimensional formulation

The TF / SF algorithm for the Propagator method can be extended to build two-dimensional TM and TE problems. As an example of the TF / SF formulation for the 2-D Propagator modeling, this section discusses field modifications for the TM_z mode.

Fig. 4.3 illustrates the field component locations of the 2-D Propagator TM_z TF / SF formulation. Region 1 and 2 are respectively assumed to be in the total-field and scattered-field regions. The interface between regions 1 and 2 is assumed to be included in the total-field region 1 and located in source-free vacuum. For the field notations, the solid circles, right and upward arrows represent respectively E_z, H_x, and H_y fields.

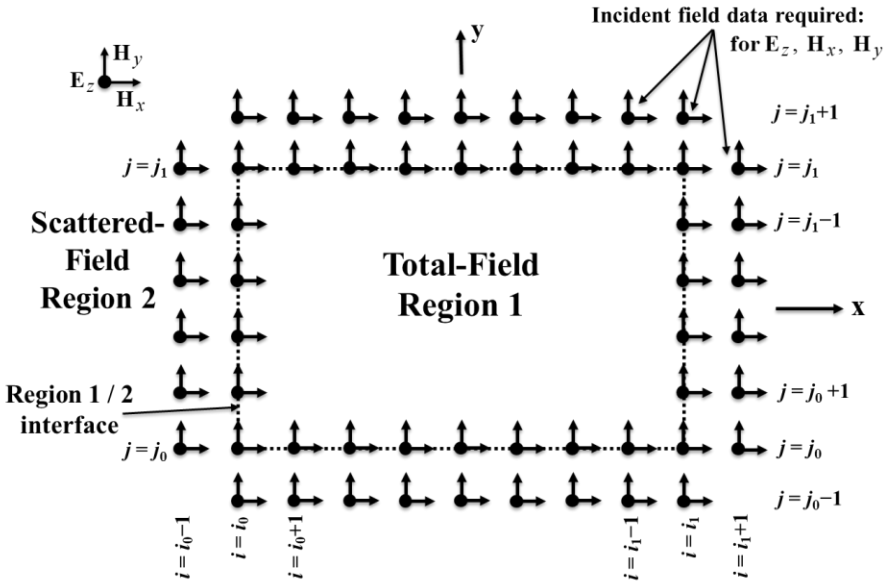

Figure 4.3: Total-field / scattered-field regions of the 2-D Propagator TM_z grid scheme.

In the 2-D Propagator grid scheme, we must account for three zones that involve interfaces, corners and just outside of the region 1 since the 2-D equation includes the fields at four grid points surrounding a center point. First consider the left boundary of region 1 and 2 located at $i = i_0$ excluding two interface corners, (i_0, j_0) and (i_0, j_1). To compute each time-stepping field components at (i_0, j), the previous time fields at $(i_0 - 1, j)$ should be modified since they are in the scattered-field region 2. The total electric and magnetic fields at $(i_0 - 1, j)$ can be decomposed into

$$E_{z,\,\text{total}}\Big|_{i_0-1,\,j} = E_{z,\,\text{scat}}\Big|_{i_0-1,\,j} + E_{z,\,\text{inc}}\Big|_{i_0-1,\,j} \tag{4.13a}$$

$$H_{x,\,\text{total}}\Big|_{i_0-1,\,j} = H_{x,\,\text{scat}}\Big|_{i_0-1,\,j} + H_{x,\,\text{inc}}\Big|_{i_0-1,\,j} \tag{4.13b}$$

$$H_{y,\,\text{total}}\Big|_{i_0-1,\,j} = H_{y,\,\text{scat}}\Big|_{i_0-1,\,j} + H_{y,\,\text{inc}}\Big|_{i_0-1,\,j} \tag{4.13c}$$

for all time steps. To implement the consistency condition, the incident field components at $(i_0 - 1, j)$ need to be added into (2.54) as the correction term. The modified equations at the left boundary of region 1 are given by

Left boundary of Region 1 ($i = i_0\,;\ j = j_0 + 1,\ \ldots,\ j_1 - 1$)

$$E_z\big|_{i,j}^{n} = \left\{ E_z\big|_{i,j}^{n} \right\}_{(2.54a)} + \underbrace{\left[\frac{1}{4} E_{z,\mathrm{inc}}\big|_{i-1,j}^{n-1} - \frac{\eta}{2\sqrt{2}} H_{y,\mathrm{inc}}\big|_{i-1,j}^{n-1} \right]}_{\text{correction term}} \tag{4.14a}$$

$$H_x\big|_{i,j}^{n} = \left\{ H_x\big|_{i,j}^{n} \right\}_{(2.54b)} + \underbrace{\left[\frac{1}{4} H_{x,\mathrm{inc}}\big|_{i-1,j}^{n-1} \right]}_{\text{correction term}} \tag{4.14b}$$

$$H_y\big|_{i,j}^{n} = \left\{ H_y\big|_{i,j}^{n} \right\}_{(2.54c)} + \underbrace{\left[\frac{1}{4} H_{y,\mathrm{inc}}\big|_{i-1,j}^{n-1} - \frac{1}{2\sqrt{2}\eta} E_{z,\mathrm{inc}}\big|_{i-1,j}^{n-1} \right]}_{\text{correction term}} \tag{4.14c}$$

The field components located on the remaining interfaces of region 1 and 2 in Fig. 4.3 can be adjusted in a same way by addition of the incident field terms positioned in the scattered-field zone. The followings are the modified equations at the right, top and bottom boundary of region 1:

Right boundary of Region 1 ($i = i_1\,;\ \ j = j_0 + 1,\ \ldots,\ j_1 - 1$)

$$E_z\big|_{i,j}^{n} = \left\{ E_z\big|_{i,j}^{n} \right\}_{(2.54a)} + \underbrace{\left[\frac{1}{4} E_{z,\mathrm{inc}}\big|_{i+1,j}^{n-1} + \frac{\eta}{2\sqrt{2}} H_{y,\mathrm{inc}}\big|_{i+1,j}^{n-1} \right]}_{\text{correction term}} \tag{4.15a}$$

$$H_x\big|_{i,j}^{n} = \left\{ H_x\big|_{i,j}^{n} \right\}_{(2.54b)} + \underbrace{\left[\frac{1}{4} H_{x,\mathrm{inc}}\big|_{i+1,j}^{n-1} \right]}_{\text{correction term}} \tag{4.15b}$$

$$H_y\Big|_{i,j}^{n} = \left\{H_y\Big|_{i,j}^{n}\right\}_{(2.54c)} + \underbrace{\left[\frac{1}{4}H_{y,\text{inc}}\Big|_{i+1,j}^{n-1} + \frac{1}{2\sqrt{2}\eta}E_{z,\text{inc}}\Big|_{i+1,j}^{n-1}\right]}_{\text{correction term}} \tag{4.15c}$$

Bottom boundary of Region 1 ($j = j_0;\ i = i_0+1,\ \ldots,\ i_1-1$)

$$E_z\Big|_{i,j}^{n} = \left\{E_z\Big|_{i,j}^{n}\right\}_{(2.54a)} + \underbrace{\left[\frac{1}{4}E_{z,\text{inc}}\Big|_{i,j-1}^{n-1} + \frac{\eta}{2\sqrt{2}}H_{y,\text{inc}}\Big|_{i,j-1}^{n-1}\right]}_{\text{correction term}} \tag{4.16a}$$

$$H_x\Big|_{i,j}^{n} = \left\{H_x\Big|_{i,j}^{n}\right\}_{(2.54b)} + \underbrace{\left[\frac{1}{4}H_{x,\text{inc}}\Big|_{i,j-1}^{n-1} + \frac{1}{2\sqrt{2}\eta}E_{z,\text{inc}}\Big|_{i,j-1}^{n-1}\right]}_{\text{correction term}} \tag{4.16b}$$

$$H_y\Big|_{i,j}^{n} = \left\{H_y\Big|_{i,j}^{n}\right\}_{(2.54c)} + \underbrace{\left[\frac{1}{4}H_{y,\text{inc}}\Big|_{i,j-1}^{n-1}\right]}_{\text{correction term}} \tag{4.16c}$$

Top boundary of Region 1 ($j = j_1;\ i = i_0+1,\ \ldots,\ i_1-1$)

$$E_z\Big|_{i,j}^{n} = \left\{E_z\Big|_{i,j}^{n}\right\}_{(2.54a)} + \underbrace{\left[\frac{1}{4}E_{z,\text{inc}}\Big|_{i,j+1}^{n-1} - \frac{\eta}{2\sqrt{2}}H_{y,\text{inc}}\Big|_{i,j+1}^{n-1}\right]}_{\text{correction term}} \tag{4.17a}$$

$$H_x\Big|_{i,j}^{n} = \left\{H_x\Big|_{i,j}^{n}\right\}_{(2.54b)} + \underbrace{\left[\frac{1}{4}H_{x,\text{inc}}\Big|_{i,j+1}^{n-1} - \frac{1}{2\sqrt{2}\eta}E_{z,\text{inc}}\Big|_{i,j+1}^{n-1}\right]}_{\text{correction term}} \tag{4.17b}$$

$$H_y\Big|_{i,j}^{n} = \left\{H_y\Big|_{i,j}^{n}\right\}_{(2.54c)} + \underbrace{\left[\frac{1}{4}H_{y,\text{inc}}\Big|_{i,j+1}^{n-1}\right]}_{\text{correction term}} \tag{4.17c}$$

Next, consider the left bottom corner at (i_0, j_0) in Fig. 4.3. When computing the time-stepping total field at (i_0, j_0), the previous time fields at (i_0+1, j_0) and (i_0, j_0+1), located in the total-field region 1, and at (i_0-1, j_0) and (i_0, j_0-1), located in the

scattered-field region 2, are required. The field components at $(i_0 - 1, j_0)$ and $(i_0, j_0 - 1)$, just outside of the interface, need to be modified. By adding the correction term with the incident fields at $(i_0 - 1, j_0)$ and $(i_0, j_0 - 1)$, the modified time-stepping fields at (i_0, j_0) are expressed as

Left bottom corner of Region 1 $(i = i_0;\ j = j_0)$

$$E_z\big|_{i,j}^{n} = \left\{E_z\big|_{i,j}^{n}\right\}_{(2.54a)} + \underbrace{\left[\frac{1}{4}\left(E_{z,\mathrm{inc}}\big|_{i-1,j}^{n-1} + E_{z,\mathrm{inc}}\big|_{i,j-1}^{n-1}\right) - \frac{\eta}{2\sqrt{2}}\left(H_{y,\mathrm{inc}}\big|_{i-1,j}^{n-1} - H_{x,\mathrm{inc}}\big|_{i,j-1}^{n-1}\right)\right]}_{\text{correction term}} \quad (4.18a)$$

$$H_x\big|_{i,j}^{n} = \left\{H_x\big|_{i,j}^{n}\right\}_{(2.54b)} + \underbrace{\left[\frac{1}{4}\left(H_{x,\mathrm{inc}}\big|_{i-1,j}^{n-1} + H_{x,\mathrm{inc}}\big|_{i,j-1}^{n-1}\right) + \frac{1}{2\sqrt{2}\eta}E_{z,\mathrm{inc}}\big|_{i,j-1}^{n-1}\right]}_{\text{correction term}} \quad (4.18b)$$

$$H_y\big|_{i,j}^{n} = \left\{H_y\big|_{i,j}^{n}\right\}_{(2.54c)} + \underbrace{\left[\frac{1}{4}\left(H_{y,\mathrm{inc}}\big|_{i-1,j}^{n-1} + H_{y,\mathrm{inc}}\big|_{i,j-1}^{n-1}\right) - \frac{1}{2\sqrt{2}\eta}E_{z,\mathrm{inc}}\big|_{i-1,j}^{n-1}\right]}_{\text{correction term}} \quad (4.18c)$$

With an analogous manner of (4.18), the field components located on the remaining corners at (i_0, j_1), (i_1, j_0) and (i_1, j_1) are written as

Left top corner of Region 1 $(i = i_0;\ j = j_1)$

$$E_z\big|_{i,j}^{n} = \left\{E_z\big|_{i,j}^{n}\right\}_{(2.54a)} + \underbrace{\left[\frac{1}{4}\left(E_{z,\mathrm{inc}}\big|_{i-1,j}^{n-1} + E_{z,\mathrm{inc}}\big|_{i,j+1}^{n-1}\right) - \frac{\eta}{2\sqrt{2}}\left(H_{y,\mathrm{inc}}\big|_{i-1,j}^{n-1} + H_{x,\mathrm{inc}}\big|_{i,j+1}^{n-1}\right)\right]}_{\text{correction term}} \quad (4.19a)$$

$$H_x\big|_{i,j}^{n} = \left\{H_x\big|_{i,j}^{n}\right\}_{(2.54b)} + \underbrace{\left[\frac{1}{4}\left(H_{x,\mathrm{inc}}\big|_{i-1,j}^{n-1} + H_{x,\mathrm{inc}}\big|_{i,j+1}^{n-1}\right) - \frac{1}{2\sqrt{2}\eta}E_{z,\mathrm{inc}}\big|_{i,j+1}^{n-1}\right]}_{\text{correction term}} \quad (4.19b)$$

$$H_y\Big|_{i,j}^{n} = \left\{H_y\Big|_{i,j}^{n}\right\}_{(2.54c)} + \underbrace{\left[\frac{1}{4}\left(H_{y,\mathrm{inc}}\Big|_{i-1,j}^{n-1} + H_{y,\mathrm{inc}}\Big|_{i,j+1}^{n-1}\right) - \frac{1}{2\sqrt{2}\eta}E_{z,\mathrm{inc}}\Big|_{i-1,j}^{n-1}\right]}_{\text{correction term}} \tag{4.19c}$$

Right bottom corner of Region 1 ($i = i_1;\ j = j_0$)

$$E_z\Big|_{i,j}^{n} = \left\{E_z\Big|_{i,j}^{n}\right\}_{(2.54a)} + \underbrace{\left[\frac{1}{4}\left(E_{z,\mathrm{inc}}\Big|_{i+1,j}^{n-1} + E_{z,\mathrm{inc}}\Big|_{i,j-1}^{n-1}\right) + \frac{\eta}{2\sqrt{2}}\left(H_{y,\mathrm{inc}}\Big|_{i+1,j}^{n-1} + H_{x,\mathrm{inc}}\Big|_{i,j-1}^{n-1}\right)\right]}_{\text{correction term}} \tag{4.20a}$$

$$H_x\Big|_{i,j}^{n} = \left\{H_x\Big|_{i,j}^{n}\right\}_{(2.54b)} + \underbrace{\left[\frac{1}{4}\left(H_{x,\mathrm{inc}}\Big|_{i+1,j}^{n-1} + H_{x,\mathrm{inc}}\Big|_{i,j-1}^{n-1}\right) + \frac{1}{2\sqrt{2}\eta}E_{z,\mathrm{inc}}\Big|_{i,j-1}^{n-1}\right]}_{\text{correction term}} \tag{4.20b}$$

$$H_y\Big|_{i,j}^{n} = \left\{H_y\Big|_{i,j}^{n}\right\}_{(2.54c)} + \underbrace{\left[\frac{1}{4}\left(H_{y,\mathrm{inc}}\Big|_{i+1,j}^{n-1} + H_{y,\mathrm{inc}}\Big|_{i,j-1}^{n-1}\right) + \frac{1}{2\sqrt{2}\eta}E_{z,\mathrm{inc}}\Big|_{i-1,j}^{n-1}\right]}_{\text{correction term}} \tag{4.20c}$$

Right top corner of Region 1 ($i = i_1;\ j = j_1$)

$$E_z\Big|_{i,j}^{n} = \left\{E_z\Big|_{i,j}^{n}\right\}_{(2.54a)} + \underbrace{\left[\frac{1}{4}\left(E_{z,\mathrm{inc}}\Big|_{i+1,j}^{n-1} + E_{z,\mathrm{inc}}\Big|_{i,j+1}^{n-1}\right) + \frac{\eta}{2\sqrt{2}}\left(H_{y,\mathrm{inc}}\Big|_{i+1,j}^{n-1} - H_{x,\mathrm{inc}}\Big|_{i,j+1}^{n-1}\right)\right]}_{\text{correction term}} \tag{4.21a}$$

$$H_x\Big|_{i,j}^{n} = \left\{H_x\Big|_{i,j}^{n}\right\}_{(2.54b)} + \underbrace{\left[\frac{1}{4}\left(H_{x,\mathrm{inc}}\Big|_{i+1,j}^{n-1} + H_{x,\mathrm{inc}}\Big|_{i,j+1}^{n-1}\right) - \frac{1}{2\sqrt{2}\eta}E_{z,\mathrm{inc}}\Big|_{i,j+1}^{n-1}\right]}_{\text{correction term}} \tag{4.21b}$$

$$H_y\Big|_{i,j}^{n} = \left\{H_y\Big|_{i,j}^{n}\right\}_{(2.54c)} + \underbrace{\left[\frac{1}{4}\left(H_{y,\mathrm{inc}}\Big|_{i+1,j}^{n-1} + H_{y,\mathrm{inc}}\Big|_{i,j+1}^{n-1}\right) + \frac{1}{2\sqrt{2}\eta}E_{z,\mathrm{inc}}\Big|_{i+1,j}^{n-1}\right]}_{\text{correction term}} \tag{4.21c}$$

We have modified equations of each field component positioned on the interfaces including corners between regions 1 and 2. In addition to the grid points on the boundary, we should take the grid cells located outside of region 1 into account. For outside four

faces of region 1, consistency conditions can be achieved by subtracting the incident field terms positioned on the interfaces.

Outside left face of Region 1 ($i = i_0 - 1;\ j = j_0, \ldots, j_1$)

$$E_z\big|_{i,j}^{n} = \left\{ E_z\big|_{i,j}^{n} \right\}_{(2.54a)} - \underbrace{\left[\frac{1}{4} E_{z,\mathrm{inc}}\big|_{i+1,j}^{n-1} + \frac{\eta}{2\sqrt{2}} H_{y,\mathrm{inc}}\big|_{i+1,j}^{n-1} \right]}_{\text{correction term}} \tag{4.22a}$$

$$H_x\big|_{i,j}^{n} = \left\{ H_x\big|_{i,j}^{n} \right\}_{(2.54b)} - \underbrace{\left[\frac{1}{4} H_{x,\mathrm{inc}}\big|_{i+1,j}^{n-1} \right]}_{\text{correction term}} \tag{4.22b}$$

$$H_y\big|_{i,j}^{n} = \left\{ H_y\big|_{i,j}^{n} \right\}_{(2.54c)} - \underbrace{\left[\frac{1}{4} H_{y,\mathrm{inc}}\big|_{i+1,j}^{n-1} + \frac{1}{2\sqrt{2}\eta} E_{z,\mathrm{inc}}\big|_{i+1,j}^{n-1} \right]}_{\text{correction term}} \tag{4.22c}$$

Outside right face of Region 1 ($i = i_1 + 1;\ j = j_0, \ldots, j_1$)

$$E_z\big|_{i,j}^{n} = \left\{ E_z\big|_{i,j}^{n} \right\}_{(2.54a)} - \underbrace{\left[\frac{1}{4} E_{z,\mathrm{inc}}\big|_{i-1,j}^{n-1} - \frac{\eta}{2\sqrt{2}} H_{y,\mathrm{inc}}\big|_{i-1,j}^{n-1} \right]}_{\text{correction term}} \tag{4.23a}$$

$$H_x\big|_{i,j}^{n} = \left\{ H_x\big|_{i,j}^{n} \right\}_{(2.54b)} - \underbrace{\left[\frac{1}{4} H_{x,\mathrm{inc}}\big|_{i-1,j}^{n-1} \right]}_{\text{correction term}} \tag{4.23b}$$

$$H_y\big|_{i,j}^{n} = \left\{ H_y\big|_{i,j}^{n} \right\}_{(2.54c)} - \underbrace{\left[\frac{1}{4} H_{y,\mathrm{inc}}\big|_{i-1,j}^{n-1} - \frac{1}{2\sqrt{2}\eta} E_{z,\mathrm{inc}}\big|_{i-1,j}^{n-1} \right]}_{\text{correction term}} \tag{4.23c}$$

Outside bottom face of Region 1 ($j = j_0 - 1;\ i = i_0, \ldots, i_1$)

$$E_z\big|_{i,j}^{n} = \left\{ E_z\big|_{i,j}^{n} \right\}_{(2.54a)} - \underbrace{\left[\frac{1}{4} E_{z,\mathrm{inc}}\big|_{i,j+1}^{n-1} - \frac{\eta}{2\sqrt{2}} H_{y,\mathrm{inc}}\big|_{i,j+1}^{n-1} \right]}_{\text{correction term}} \tag{4.24a}$$

$$H_x\Big|_{i,j}^{n} = \left\{ H_x\Big|_{i,j}^{n} \right\}_{(2.54b)} - \underbrace{\left[\frac{1}{4} H_{x,\mathrm{inc}}\Big|_{i,j+1}^{n-1} - \frac{1}{2\sqrt{2}\eta} E_{z,\mathrm{inc}}\Big|_{i,j+1}^{n-1} \right]}_{\text{correction term}} \tag{4.24b}$$

$$H_y\Big|_{i,j}^{n} = \left\{ H_y\Big|_{i,j}^{n} \right\}_{(2.54c)} - \underbrace{\left[\frac{1}{4} H_{y,\mathrm{inc}}\Big|_{i,j+1}^{n-1} \right]}_{\text{correction term}} \tag{4.24c}$$

Outside top face of Region 1 ($j = j_0 + 1;\ i = i_0,\ \ldots,\ i_1$)

$$E_z\Big|_{i,j}^{n} = \left\{ E_z\Big|_{i,j}^{n} \right\}_{(2.54a)} - \underbrace{\left[\frac{1}{4} E_{z,\mathrm{inc}}\Big|_{i,j-1}^{n-1} + \frac{\eta}{2\sqrt{2}} H_{y,\mathrm{inc}}\Big|_{i,j-1}^{n-1} \right]}_{\text{correction term}} \tag{4.25a}$$

$$H_x\Big|_{i,j}^{n} = \left\{ H_x\Big|_{i,j}^{n} \right\}_{(2.54b)} - \underbrace{\left[\frac{1}{4} H_{x,\mathrm{inc}}\Big|_{i,j-1}^{n-1} + \frac{1}{2\sqrt{2}\eta} E_{z,\mathrm{inc}}\Big|_{i,j-1}^{n-1} \right]}_{\text{correction term}} \tag{4.25b}$$

$$H_y\Big|_{i,j}^{n} = \left\{ H_y\Big|_{i,j}^{n} \right\}_{(2.54c)} - \underbrace{\left[\frac{1}{4} H_{y,\mathrm{inc}}\Big|_{i,j-1}^{n-1} \right]}_{\text{correction term}} \tag{4.25c}$$

The 2-D Propagator TF / SF formulation for TM_z case has been developed above. Although not shown here, the TF / SF formulation for the 2-D Propagator TE_z case can also be developed in the same manner.

As an example of the 2-D TF / SF formulation for the Propagator method, Fig. 4.4 shows the total and scattered fields from a square dielectric cylinder having $\varepsilon_r = 4$ at two different time steps. In Fig. 4.4, the red box represents the boundary between the total-field and scattered-field regions, and the black box indicates the square dielectric cylinder inserted within the total-field region. The total numerical space is discretized with 200×200, and the TF / SF region and object are respectively discretized with 50×50 and

30×30 from a center point. As shown in Fig. 4.4, the computed total and scattered fields are respectively observed in the total-field and scattered-field zones as expected.

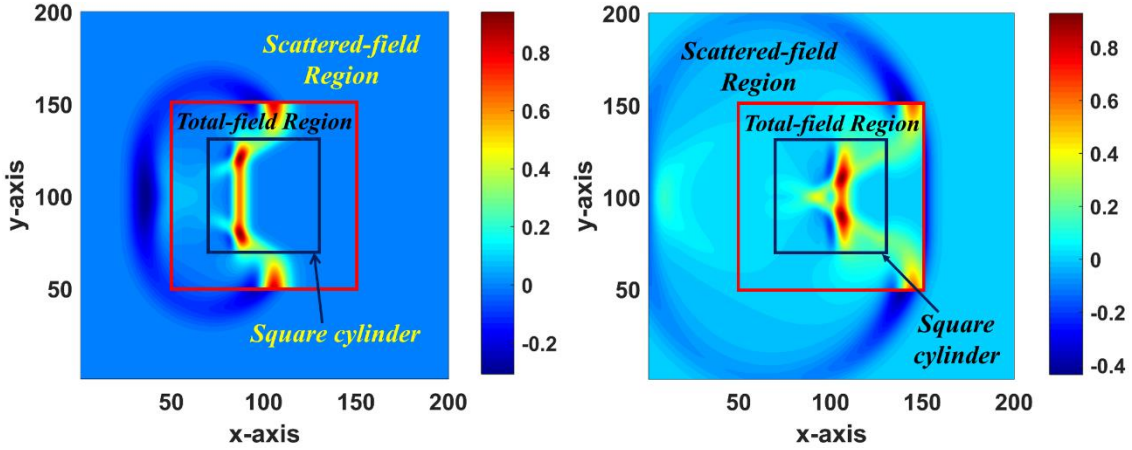

(a) (b)

Figure 4.4: Total and scattered fields at (a) 120 time steps and (b) 175 time steps, from a centered square dielectric cylinder $(\varepsilon_r = 4)$ as an example of the TF / SF formulation for the 2-D Propagator TM_z case.

4.4 Three-dimensional formulation

The TF / SF formulation discussed above can be readily extended to the 3-D Propagator lattices. The TF / SF regions in the 3-D Propagator Method compose six interface surfaces forming a rectangular box, as shown in Fig. 4.5(a) and six surfaces, outside of each face of the TF / SF interfaces. Each interface plane is decomposed into corners, boundary line and one interface surface, as shown in Fig. 4.5(b).

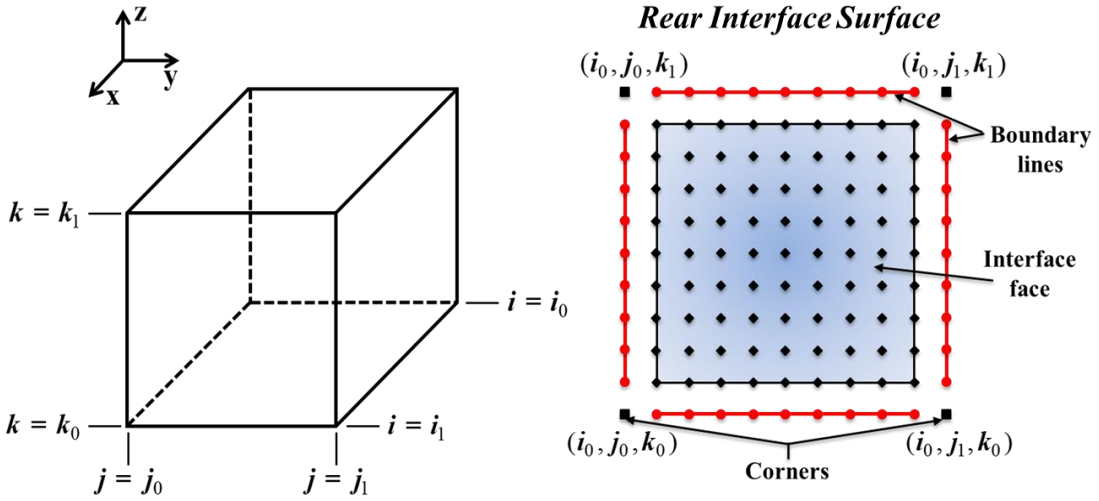

(a) (b)

Figure 4.5: (a) Six interface surfaces and (b) a rear interface surface for the 3-D Propagator TF / SF formulation lattice.

Consider first each surface of the TF / SF interfaces that does not contain boundaries. With the consistency conditions employed in the 2-D TM_z mode above, the modified equations of six field components at each face are given by

Rear surface of Region 1 ($i = i_0;\ j = j_0+1, \ldots, j_1-1;\ k = k_0+1, \ldots, k_1-1$)

$$E_x\big|_{i,j,k}^{n} = \left\{E_x\big|_{i,j,k}^{n}\right\}_{(2.52)} + \underbrace{\left[\frac{1}{6}E_{x,\text{inc}}\big|_{i-1,j,k}^{n-1}\right]}_{\text{correction term}} \tag{4.26a}$$

$$E_y\big|_{i,j,k}^{n} = \left\{E_y\big|_{i,j,k}^{n}\right\}_{(2.53a)} + \underbrace{\left[\frac{1}{6}E_{y,\text{inc}}\big|_{i-1,j,k}^{n-1} + \frac{\eta}{2\sqrt{3}}H_{z,\text{inc}}\big|_{i-1,j,k}^{n-1}\right]}_{\text{correction term}} \tag{4.26b}$$

$$E_z\big|_{i,j,k}^{n} = \left\{E_z\big|_{i,j,k}^{n}\right\}_{(2.53b)} + \underbrace{\left[\frac{1}{6}E_{z,\text{inc}}\big|_{i-1,j,k}^{n-1} - \frac{\eta}{2\sqrt{3}}H_{y,\text{inc}}\big|_{i-1,j,k}^{n-1}\right]}_{\text{correction term}} \tag{4.26c}$$

$$H_x\Big|_{i,j,k}^{n} = \left\{ H_x\Big|_{i,j,k}^{n} \right\}_{(2.53c)} + \underbrace{\left[\frac{1}{6} H_{x,\mathrm{inc}}\Big|_{i-1,j,k}^{n-1} \right]}_{\text{correction term}} \tag{4.26d}$$

$$H_y\Big|_{i,j,k}^{n} = \left\{ H_y\Big|_{i,j,k}^{n} \right\}_{(2.53d)} + \underbrace{\left[\frac{1}{6} H_{y,\mathrm{inc}}\Big|_{i-1,j,k}^{n-1} - \frac{1}{2\sqrt{3}\eta} E_{z,\mathrm{inc}}\Big|_{i-1,j,k}^{n-1} \right]}_{\text{correction term}} \tag{4.26e}$$

$$H_z\Big|_{i,j,k}^{n} = \left\{ H_z\Big|_{i,j,k}^{n} \right\}_{(2.53e)} + \underbrace{\left[\frac{1}{6} H_{z,\mathrm{inc}}\Big|_{i-1,j,k}^{n-1} + \frac{1}{2\sqrt{3}\eta} E_{y,\mathrm{inc}}\Big|_{i-1,j,k}^{n-1} \right]}_{\text{correction term}} \tag{4.26f}$$

Front surface of Region 1 ($i = i_1;\ j = j_0+1, \ldots, j_1-1;\ k = k_0+1, \ldots, k_1-1$)

$$E_x\Big|_{i,j,k}^{n} = \left\{ E_x\Big|_{i,j,k}^{n} \right\}_{(2.52)} + \underbrace{\left[\frac{1}{6} E_{x,\mathrm{inc}}\Big|_{i+1,j,k}^{n-1} \right]}_{\text{correction term}} \tag{4.27a}$$

$$E_y\Big|_{i,j,k}^{n} = \left\{ E_y\Big|_{i,j,k}^{n} \right\}_{(2.53a)} + \underbrace{\left[\frac{1}{6} E_{y,\mathrm{inc}}\Big|_{i+1,j,k}^{n-1} - \frac{\eta}{2\sqrt{3}} H_{z,\mathrm{inc}}\Big|_{i+1,j,k}^{n-1} \right]}_{\text{correction term}} \tag{4.27b}$$

$$E_z\Big|_{i,j,k}^{n} = \left\{ E_z\Big|_{i,j,k}^{n} \right\}_{(2.53b)} + \underbrace{\left[\frac{1}{6} E_{z,\mathrm{inc}}\Big|_{i+1,j,k}^{n-1} + \frac{\eta}{2\sqrt{3}} H_{y,\mathrm{inc}}\Big|_{i+1,j,k}^{n-1} \right]}_{\text{correction term}} \tag{4.27c}$$

$$H_x\Big|_{i,j,k}^{n} = \left\{ H_x\Big|_{i,j,k}^{n} \right\}_{(2.53c)} + \underbrace{\left[\frac{1}{6} H_{x,\mathrm{inc}}\Big|_{i+1,j,k}^{n-1} \right]}_{\text{correction term}} \tag{4.27d}$$

$$H_y\Big|_{i,j,k}^{n} = \left\{ H_y\Big|_{i,j,k}^{n} \right\}_{(2.53d)} + \underbrace{\left[\frac{1}{6} H_{y,\mathrm{inc}}\Big|_{i+1,j,k}^{n-1} + \frac{1}{2\sqrt{3}\eta} E_{z,\mathrm{inc}}\Big|_{i+1,j,k}^{n-1} \right]}_{\text{correction term}} \tag{4.27e}$$

$$H_z\Big|_{i,j,k}^{n} = \left\{ H_z\Big|_{i,j,k}^{n} \right\}_{(2.53e)} + \underbrace{\left[\frac{1}{6} H_{z,\mathrm{inc}}\Big|_{i+1,j,k}^{n-1} - \frac{1}{2\sqrt{3}\eta} E_{y,\mathrm{inc}}\Big|_{i+1,j,k}^{n-1} \right]}_{\text{correction term}} \tag{4.27f}$$

Left surface of Region 1 ($i = i_0 + 1, \ldots, i_1 - 1;\ j = j_0;\ k = k_0 + 1, \ldots, k_1 - 1$)

$$E_x\big|_{i,j,k}^{n} = \left\{ E_x\big|_{i,j,k}^{n} \right\}_{(2.52)} + \underbrace{\left[\frac{1}{6} E_{x,\mathrm{inc}}\big|_{i,j-1,k}^{n-1} - \frac{\eta}{2\sqrt{3}} H_{z,\mathrm{inc}}\big|_{i,j-1,k}^{n-1} \right]}_{\text{correction term}} \tag{4.28a}$$

$$E_y\big|_{i,j,k}^{n} = \left\{ E_y\big|_{i,j,k}^{n} \right\}_{(2.53a)} + \underbrace{\left[\frac{1}{6} E_{y,\mathrm{inc}}\big|_{i,j-1,k}^{n-1} \right]}_{\text{correction term}} \tag{4.28b}$$

$$E_z\big|_{i,j,k}^{n} = \left\{ E_z\big|_{i,j,k}^{n} \right\}_{(2.53b)} + \underbrace{\left[\frac{1}{6} E_{z,\mathrm{inc}}\big|_{i,j-1,k}^{n-1} + \frac{\eta}{2\sqrt{3}} H_{x,\mathrm{inc}}\big|_{i,j-1,k}^{n-1} \right]}_{\text{correction term}} \tag{4.28c}$$

$$H_x\big|_{i,j,k}^{n} = \left\{ H_x\big|_{i,j,k}^{n} \right\}_{(2.53c)} + \underbrace{\left[\frac{1}{6} H_{x,\mathrm{inc}}\big|_{i,j-1,k}^{n-1} + \frac{1}{2\sqrt{3}\eta} E_{z,\mathrm{inc}}\big|_{i,j-1,k}^{n-1} \right]}_{\text{correction term}} \tag{4.28d}$$

$$H_y\big|_{i,j,k}^{n} = \left\{ H_y\big|_{i,j,k}^{n} \right\}_{(2.53d)} + \underbrace{\left[\frac{1}{6} H_{y,\mathrm{inc}}\big|_{i,j-1,k}^{n-1} \right]}_{\text{correction term}} \tag{4.28e}$$

$$H_z\big|_{i,j,k}^{n} = \left\{ H_z\big|_{i,j,k}^{n} \right\}_{(2.53e)} + \underbrace{\left[\frac{1}{6} H_{z,\mathrm{inc}}\big|_{i,j-1,k}^{n-1} - \frac{1}{2\sqrt{3}\eta} E_{x,\mathrm{inc}}\big|_{i,j-1,k}^{n-1} \right]}_{\text{correction term}} \tag{4.28f}$$

Right surface of Region 1 ($i = i_0 + 1, \ldots, i_1 - 1;\ j = j_1;\ k = k_0 + 1, \ldots, k_1 - 1$)

$$E_x\big|_{i,j,k}^{n} = \left\{ E_x\big|_{i,j,k}^{n} \right\}_{(2.52)} + \underbrace{\left[\frac{1}{6} E_{x,\mathrm{inc}}\big|_{i,j+1,k}^{n-1} + \frac{\eta}{2\sqrt{3}} H_{z,\mathrm{inc}}\big|_{i,j+1,k}^{n-1} \right]}_{\text{correction term}} \tag{4.29a}$$

$$E_y\big|_{i,j,k}^{n} = \left\{ E_y\big|_{i,j,k}^{n} \right\}_{(2.53a)} + \underbrace{\left[\frac{1}{6} E_{y,\mathrm{inc}}\big|_{i,j+1,k}^{n-1} \right]}_{\text{correction term}} \tag{4.29b}$$

$$E_z\Big|_{i,j,k}^{n} = \left\{E_z\Big|_{i,j,k}^{n}\right\}_{(2.53b)} + \underbrace{\left[\frac{1}{6}E_{z,\mathrm{inc}}\Big|_{i,j+1,k}^{n-1} - \frac{\eta}{2\sqrt{3}}H_{x,\mathrm{inc}}\Big|_{i,j+1,k}^{n-1}\right]}_{\text{correction term}} \tag{4.29c}$$

$$H_x\Big|_{i,j,k}^{n} = \left\{H_x\Big|_{i,j,k}^{n}\right\}_{(2.53c)} + \underbrace{\left[\frac{1}{6}H_{x,\mathrm{inc}}\Big|_{i,j+1,k}^{n-1} - \frac{1}{2\sqrt{3}\eta}E_{z,\mathrm{inc}}\Big|_{i,j+1,k}^{n-1}\right]}_{\text{correction term}} \tag{4.29d}$$

$$H_y\Big|_{i,j,k}^{n} = \left\{H_y\Big|_{i,j,k}^{n}\right\}_{(2.53d)} + \underbrace{\left[\frac{1}{6}H_{y,\mathrm{inc}}\Big|_{i,j+1,k}^{n-1}\right]}_{\text{correction term}} \tag{4.29e}$$

$$H_z\Big|_{i,j,k}^{n} = \left\{H_z\Big|_{i,j,k}^{n}\right\}_{(2.53e)} + \underbrace{\left[\frac{1}{6}H_{z,\mathrm{inc}}\Big|_{i,j+1,k}^{n-1} + \frac{1}{2\sqrt{3}\eta}E_{x,\mathrm{inc}}\Big|_{i,j+1,k}^{n-1}\right]}_{\text{correction term}} \tag{4.29f}$$

Bottom surface of Region 1 ($i = i_0+1,\ \ldots,\ i_1-1;\ j = j_0+1,\ \ldots,\ j_1-1;\ k = k_0$)

$$E_x\Big|_{i,j,k}^{n} = \left\{E_x\Big|_{i,j,k}^{n}\right\}_{(2.52)} + \underbrace{\left[\frac{1}{6}E_{x,\mathrm{inc}}\Big|_{i,j,k-1}^{n-1} + \frac{\eta}{2\sqrt{3}}H_{y,\mathrm{inc}}\Big|_{i,j,k-1}^{n-1}\right]}_{\text{correction term}} \tag{4.30a}$$

$$E_y\Big|_{i,j,k}^{n} = \left\{E_y\Big|_{i,j,k}^{n}\right\}_{(2.53a)} + \underbrace{\left[\frac{1}{6}E_{y,\mathrm{inc}}\Big|_{i,j,k-1}^{n-1} - \frac{\eta}{2\sqrt{3}}H_{x,\mathrm{inc}}\Big|_{i,j,k-1}^{n-1}\right]}_{\text{correction term}} \tag{4.30b}$$

$$E_z\Big|_{i,j,k}^{n} = \left\{E_z\Big|_{i,j,k}^{n}\right\}_{(2.53b)} + \underbrace{\left[\frac{1}{6}E_{z,\mathrm{inc}}\Big|_{i,j,k-1}^{n-1}\right]}_{\text{correction term}} \tag{4.30c}$$

$$H_x\Big|_{i,j,k}^{n} = \left\{H_x\Big|_{i,j,k}^{n}\right\}_{(2.53c)} + \underbrace{\left[\frac{1}{6}H_{x,\mathrm{inc}}\Big|_{i,j,k-1}^{n-1} - \frac{1}{2\sqrt{3}\eta}E_{y,\mathrm{inc}}\Big|_{i,j,k-1}^{n-1}\right]}_{\text{correction term}} \tag{4.30d}$$

$$H_y\Big|_{i,j,k}^{n} = \left\{H_y\Big|_{i,j,k}^{n}\right\}_{(2.53d)} + \underbrace{\left[\frac{1}{6}H_{y,\mathrm{inc}}\Big|_{i,j,k-1}^{n-1} + \frac{1}{2\sqrt{3}\eta}E_{x,\mathrm{inc}}\Big|_{i,j,k-1}^{n-1}\right]}_{\text{correction term}} \tag{4.30e}$$

$$H_z\Big|_{i,j,k}^{n} = \left\{ H_z\Big|_{i,j,k}^{n} \right\}_{(2.53e)} + \underbrace{\left[\frac{1}{6} H_{z,\mathrm{inc}}\Big|_{i,j,k-1}^{n-1} \right]}_{\text{correction term}} \tag{4.30f}$$

Top surface of Region 1 ($i = i_0 + 1, \ldots, i_1 - 1;\ j = j_0 + 1, \ldots, j_1 - 1;\ k = k_1$)

$$E_x\Big|_{i,j,k}^{n} = \left\{ E_x\Big|_{i,j,k}^{n} \right\}_{(2.52)} + \underbrace{\left[\frac{1}{6} E_{x,\mathrm{inc}}\Big|_{i,j,k+1}^{n-1} - \frac{\eta}{2\sqrt{3}} H_{y,\mathrm{inc}}\Big|_{i,j,k+1}^{n-1} \right]}_{\text{correction term}} \tag{4.31a}$$

$$E_y\Big|_{i,j,k}^{n} = \left\{ E_y\Big|_{i,j,k}^{n} \right\}_{(2.53a)} + \underbrace{\left[\frac{1}{6} E_{y,\mathrm{inc}}\Big|_{i,j,k+1}^{n-1} + \frac{\eta}{2\sqrt{3}} H_{x,\mathrm{inc}}\Big|_{i,j,k+1}^{n-1} \right]}_{\text{correction term}} \tag{4.31b}$$

$$E_z\Big|_{i,j,k}^{n} = \left\{ E_z\Big|_{i,j,k}^{n} \right\}_{(2.53b)} + \underbrace{\left[\frac{1}{6} E_{z,\mathrm{inc}}\Big|_{i,j,k+1}^{n-1} \right]}_{\text{correction term}} \tag{4.31c}$$

$$H_x\Big|_{i,j,k}^{n} = \left\{ H_x\Big|_{i,j,k}^{n} \right\}_{(2.53c)} + \underbrace{\left[\frac{1}{6} H_{x,\mathrm{inc}}\Big|_{i,j,k+1}^{n-1} + \frac{1}{2\sqrt{3}\eta} E_{y,\mathrm{inc}}\Big|_{i,j,k+1}^{n-1} \right]}_{\text{correction term}} \tag{4.31d}$$

$$H_y\Big|_{i,j,k}^{n} = \left\{ H_y\Big|_{i,j,k}^{n} \right\}_{(2.53d)} + \underbrace{\left[\frac{1}{6} H_{y,\mathrm{inc}}\Big|_{i,j,k+1}^{n-1} - \frac{1}{2\sqrt{3}\eta} E_{x,\mathrm{inc}}\Big|_{i,j,k+1}^{n-1} \right]}_{\text{correction term}} \tag{4.31e}$$

$$H_z\Big|_{i,j,k}^{n} = \left\{ H_z\Big|_{i,j,k}^{n} \right\}_{(2.53e)} + \underbrace{\left[\frac{1}{6} H_{z,\mathrm{inc}}\Big|_{i,j,k+1}^{n-1} \right]}_{\text{correction term}} \tag{4.31f}$$

Next, the consistency conditions for all field components at each boundary line excluding corners are given by

Rear left line of Region 1 ($i = i_0;\ j = j_0;\ k = k_0 + 1, \ldots, k_1 - 1$)

$$E_x\Big|_{i,j,k}^{n} = \left\{E_x\Big|_{i,j,k}^{n}\right\}_{(2.52)} + \underbrace{\left[\frac{1}{6}\left(E_{x,\mathrm{inc}}\Big|_{i-1,j,k}^{n-1} + E_{x,\mathrm{inc}}\Big|_{i,j-1,k}^{n-1}\right) - \frac{\eta}{2\sqrt{3}} H_{z,\mathrm{inc}}\Big|_{i,j-1,k}^{n-1}\right]}_{\text{correction term}} \tag{4.32a}$$

$$E_y\Big|_{i,j,k}^{n} = \left\{E_y\Big|_{i,j,k}^{n}\right\}_{(2.53a)} + \underbrace{\left[\frac{1}{6}\left(E_{y,\mathrm{inc}}\Big|_{i-1,j,k}^{n-1} + E_{y,\mathrm{inc}}\Big|_{i,j-1,k}^{n-1}\right) + \frac{\eta}{2\sqrt{3}} H_{z,\mathrm{inc}}\Big|_{i-1,j,k}^{n-1}\right]}_{\text{correction term}} \tag{4.32b}$$

$$E_z\Big|_{i,j,k}^{n} = \left\{E_z\Big|_{i,j,k}^{n}\right\}_{(2.53b)} + \underbrace{\left[\frac{1}{6}\left(E_{z,\mathrm{inc}}\Big|_{i-1,j,k}^{n-1} + E_{z,\mathrm{inc}}\Big|_{i,j-1,k}^{n-1}\right) + \frac{\eta}{2\sqrt{3}}\left(H_{x,\mathrm{inc}}\Big|_{i,j-1,k}^{n-1} - H_{y,\mathrm{inc}}\Big|_{i-1,j,k}^{n-1}\right)\right]}_{\text{correction term}} \tag{4.32c}$$

$$H_x\Big|_{i,j,k}^{n} = \left\{H_x\Big|_{i,j,k}^{n}\right\}_{(2.53c)} + \underbrace{\left[\frac{1}{6}\left(H_{x,\mathrm{inc}}\Big|_{i-1,j,k}^{n-1} + H_{x,\mathrm{inc}}\Big|_{i,j-1,k}^{n-1}\right) + \frac{1}{2\sqrt{3}\eta} E_{z,\mathrm{inc}}\Big|_{i,j-1,k}^{n-1}\right]}_{\text{correction term}} \tag{4.32d}$$

$$H_y\Big|_{i,j,k}^{n} = \left\{H_y\Big|_{i,j,k}^{n}\right\}_{(2.53d)} + \underbrace{\left[\frac{1}{6}\left(H_{y,\mathrm{inc}}\Big|_{i-1,j,k}^{n-1} + H_{y,\mathrm{inc}}\Big|_{i,j-1,k}^{n-1}\right) - \frac{1}{2\sqrt{3}\eta} E_{z,\mathrm{inc}}\Big|_{i-1,j,k}^{n-1}\right]}_{\text{correction term}} \tag{4.32e}$$

$$H_z\Big|_{i,j,k}^{n} = \left\{H_z\Big|_{i,j,k}^{n}\right\}_{(2.53e)} + \underbrace{\left[\frac{1}{6}\left(H_{z,\mathrm{inc}}\Big|_{i-1,j,k}^{n-1} + H_{z,\mathrm{inc}}\Big|_{i,j-1,k}^{n-1}\right) - \frac{1}{2\sqrt{3}\eta}\left(E_{x,\mathrm{inc}}\Big|_{i,j-1,k}^{n-1} - E_{y,\mathrm{inc}}\Big|_{i-1,j,k}^{n-1}\right)\right]}_{\text{correction term}} \tag{4.32f}$$

Rear right line of Region 1 ($i = i_0;\ j = j_1;\ k = k_0 + 1, \ldots, k_1 - 1$)

$$E_x\Big|_{i,j,k}^{n} = \left\{E_x\Big|_{i,j,k}^{n}\right\}_{(2.52)} + \underbrace{\left[\frac{1}{6}\left(E_{x,\mathrm{inc}}\Big|_{i-1,j,k}^{n-1} + E_{x,\mathrm{inc}}\Big|_{i,j+1,k}^{n-1}\right) + \frac{\eta}{2\sqrt{3}} H_{z,\mathrm{inc}}\Big|_{i,j+1,k}^{n-1}\right]}_{\text{correction term}} \tag{4.33a}$$

$$E_y\Big|_{i,j,k}^{n} = \left\{E_y\Big|_{i,j,k}^{n}\right\}_{(2.53a)} + \underbrace{\left[\frac{1}{6}\left(E_{y,\mathrm{inc}}\Big|_{i-1,j,k}^{n-1} + E_{y,\mathrm{inc}}\Big|_{i,j+1,k}^{n-1}\right) + \frac{\eta}{2\sqrt{3}} H_{z,\mathrm{inc}}\Big|_{i-1,j,k}^{n-1}\right]}_{\text{correction term}} \tag{4.33b}$$

$$E_z\Big|_{i,j,k}^{n} = \left\{E_z\Big|_{i,j,k}^{n}\right\}_{(2.53b)} + \underbrace{\left[\frac{1}{6}\left(E_{z,\mathrm{inc}}\Big|_{i-1,j,k}^{n-1} + E_{z,\mathrm{inc}}\Big|_{i,j+1,k}^{n-1}\right) - \frac{\eta}{2\sqrt{3}}\left(H_{x,\mathrm{inc}}\Big|_{i,j+1,k}^{n-1} + H_{y,\mathrm{inc}}\Big|_{i-1,j,k}^{n-1}\right)\right]}_{\text{correction term}} \quad (4.33c)$$

$$H_x\Big|_{i,j,k}^{n} = \left\{H_x\Big|_{i,j,k}^{n}\right\}_{(2.53c)} + \underbrace{\left[\frac{1}{6}\left(H_{x,\mathrm{inc}}\Big|_{i-1,j,k}^{n-1} + H_{x,\mathrm{inc}}\Big|_{i,j+1,k}^{n-1}\right) - \frac{1}{2\sqrt{3}\eta}E_{z,\mathrm{inc}}\Big|_{i,j+1,k}^{n-1}\right]}_{\text{correction term}} \quad (4.33d)$$

$$H_y\Big|_{i,j,k}^{n} = \left\{H_y\Big|_{i,j,k}^{n}\right\}_{(2.53d)} + \underbrace{\left[\frac{1}{6}\left(H_{y,\mathrm{inc}}\Big|_{i-1,j,k}^{n-1} + H_{y,\mathrm{inc}}\Big|_{i,j+1,k}^{n-1}\right) - \frac{1}{2\sqrt{3}\eta}E_{z,\mathrm{inc}}\Big|_{i-1,j,k}^{n-1}\right]}_{\text{correction term}} \quad (4.33e)$$

$$H_z\Big|_{i,j,k}^{n} = \left\{H_z\Big|_{i,j,k}^{n}\right\}_{(2.53e)} + \underbrace{\left[\frac{1}{6}\left(H_{z,\mathrm{inc}}\Big|_{i-1,j,k}^{n-1} + H_{z,\mathrm{inc}}\Big|_{i,j+1,k}^{n-1}\right) + \frac{1}{2\sqrt{3}\eta}\left(E_{x,\mathrm{inc}}\Big|_{i,j+1,k}^{n-1} + E_{y,\mathrm{inc}}\Big|_{i-1,j,k}^{n-1}\right)\right]}_{\text{correction term}} \quad (4.33f)$$

Front left line of Region 1 ($i = i_1;\ j = j_0;\ k = k_0+1, \ldots, k_1-1$)

$$E_x\Big|_{i,j,k}^{n} = \left\{E_x\Big|_{i,j,k}^{n}\right\}_{(2.52)} + \underbrace{\left[\frac{1}{6}\left(E_{x,\mathrm{inc}}\Big|_{i+1,j,k}^{n-1} + E_{x,\mathrm{inc}}\Big|_{i,j-1,k}^{n-1}\right) - \frac{\eta}{2\sqrt{3}}H_{z,\mathrm{inc}}\Big|_{i,j-1,k}^{n-1}\right]}_{\text{correction term}} \quad (4.34a)$$

$$E_y\Big|_{i,j,k}^{n} = \left\{E_y\Big|_{i,j,k}^{n}\right\}_{(2.53a)} + \underbrace{\left[\frac{1}{6}\left(E_{y,\mathrm{inc}}\Big|_{i+1,j,k}^{n-1} + E_{y,\mathrm{inc}}\Big|_{i,j-1,k}^{n-1}\right) - \frac{\eta}{2\sqrt{3}}H_{z,\mathrm{inc}}\Big|_{i+1,j,k}^{n-1}\right]}_{\text{correction term}} \quad (4.34b)$$

$$E_z\Big|_{i,j,k}^{n} = \left\{E_z\Big|_{i,j,k}^{n}\right\}_{(2.53b)} + \underbrace{\left[\frac{1}{6}\left(E_{z,\mathrm{inc}}\Big|_{i+1,j,k}^{n-1} + E_{z,\mathrm{inc}}\Big|_{i,j-1,k}^{n-1}\right) + \frac{\eta}{2\sqrt{3}}\left(H_{x,\mathrm{inc}}\Big|_{i,j-1,k}^{n-1} + H_{y,\mathrm{inc}}\Big|_{i+1,j,k}^{n-1}\right)\right]}_{\text{correction term}} \quad (4.34c)$$

$$H_x\Big|_{i,j,k}^{n} = \left\{H_x\Big|_{i,j,k}^{n}\right\}_{(2.53c)} + \underbrace{\left[\frac{1}{6}\left(H_{x,\mathrm{inc}}\Big|_{i+1,j,k}^{n-1} + H_{x,\mathrm{inc}}\Big|_{i,j-1,k}^{n-1}\right) + \frac{1}{2\sqrt{3}\eta}E_{z,\mathrm{inc}}\Big|_{i,j-1,k}^{n-1}\right]}_{\text{correction term}} \quad (4.34d)$$

$$H_y\Big|_{i,j,k}^{n} = \left\{H_y\Big|_{i,j,k}^{n}\right\}_{(2.53d)} + \underbrace{\left[\frac{1}{6}\left(H_{y,\mathrm{inc}}\Big|_{i+1,j,k}^{n-1} + H_{y,\mathrm{inc}}\Big|_{i,j-1,k}^{n-1}\right) + \frac{1}{2\sqrt{3}\eta}E_{z,\mathrm{inc}}\Big|_{i+1,j,k}^{n-1}\right]}_{\text{correction term}} \quad (4.34e)$$

$$H_z\Big|_{i,j,k}^{n} = \left\{ H_z\Big|_{i,j,k}^{n} \right\}_{(2.53e)} + \underbrace{\left[\frac{1}{6}\left(H_{z,\mathrm{inc}}\Big|_{i+1,j,k}^{n-1} + H_{z,\mathrm{inc}}\Big|_{i,j-1,k}^{n-1} \right) - \frac{1}{2\sqrt{3}\eta}\left(E_{x,\mathrm{inc}}\Big|_{i,j-1,k}^{n-1} + E_{y,\mathrm{inc}}\Big|_{i+1,j,k}^{n-1} \right) \right]}_{\text{correction term}} \quad (4.34f)$$

Front right line of Region 1 ($i = i_1;\ j = j_1;\ k = k_0 + 1, \ldots, k_1 - 1$)

$$E_x\Big|_{i,j,k}^{n} = \left\{ E_x\Big|_{i,j,k}^{n} \right\}_{(2.52)} + \underbrace{\left[\frac{1}{6}\left(E_{x,\mathrm{inc}}\Big|_{i+1,j,k}^{n-1} + E_{x,\mathrm{inc}}\Big|_{i,j+1,k}^{n-1} \right) + \frac{\eta}{2\sqrt{3}} H_{z,\mathrm{inc}}\Big|_{i,j+1,k}^{n-1} \right]}_{\text{correction term}} \quad (4.35a)$$

$$E_y\Big|_{i,j,k}^{n} = \left\{ E_y\Big|_{i,j,k}^{n} \right\}_{(2.53a)} + \underbrace{\left[\frac{1}{6}\left(E_{y,\mathrm{inc}}\Big|_{i+1,j,k}^{n-1} + E_{y,\mathrm{inc}}\Big|_{i,j+1,k}^{n-1} \right) - \frac{\eta}{2\sqrt{3}} H_{z,\mathrm{inc}}\Big|_{i+1,j,k}^{n-1} \right]}_{\text{correction term}} \quad (4.35b)$$

$$E_z\Big|_{i,j,k}^{n} = \left\{ E_z\Big|_{i,j,k}^{n} \right\}_{(2.53b)} + \underbrace{\left[\frac{1}{6}\left(E_{z,\mathrm{inc}}\Big|_{i+1,j,k}^{n-1} + E_{z,\mathrm{inc}}\Big|_{i,j+1,k}^{n-1} \right) - \frac{\eta}{2\sqrt{3}}\left(H_{x,\mathrm{inc}}\Big|_{i,j+1,k}^{n-1} - H_{y,\mathrm{inc}}\Big|_{i+1,j,k}^{n-1} \right) \right]}_{\text{correction term}} \quad (4.35c)$$

$$H_x\Big|_{i,j,k}^{n} = \left\{ H_x\Big|_{i,j,k}^{n} \right\}_{(2.53c)} + \underbrace{\left[\frac{1}{6}\left(H_{x,\mathrm{inc}}\Big|_{i+1,j,k}^{n-1} + H_{x,\mathrm{inc}}\Big|_{i,j+1,k}^{n-1} \right) - \frac{1}{2\sqrt{3}\eta} E_{z,\mathrm{inc}}\Big|_{i,j+1,k}^{n-1} \right]}_{\text{correction term}} \quad (4.35d)$$

$$H_y\Big|_{i,j,k}^{n} = \left\{ H_y\Big|_{i,j,k}^{n} \right\}_{(2.53d)} + \underbrace{\left[\frac{1}{6}\left(H_{y,\mathrm{inc}}\Big|_{i+1,j,k}^{n-1} + H_{y,\mathrm{inc}}\Big|_{i,j+1,k}^{n-1} \right) + \frac{1}{2\sqrt{3}\eta} E_{z,\mathrm{inc}}\Big|_{i+1,j,k}^{n-1} \right]}_{\text{correction term}} \quad (4.35e)$$

$$H_z\Big|_{i,j,k}^{n} = \left\{ H_z\Big|_{i,j,k}^{n} \right\}_{(2.53e)} + \underbrace{\left[\frac{1}{6}\left(H_{z,\mathrm{inc}}\Big|_{i+1,j,k}^{n-1} + H_{z,\mathrm{inc}}\Big|_{i,j+1,k}^{n-1} \right) + \frac{1}{2\sqrt{3}\eta}\left(E_{x,\mathrm{inc}}\Big|_{i,j+1,k}^{n-1} - E_{y,\mathrm{inc}}\Big|_{i+1,j,k}^{n-1} \right) \right]}_{\text{correction term}} \quad (4.35f)$$

Bottom rear line of Region 1 ($i = i_0;\ j = j_0 + 1, \ldots, j_1 - 1;\ k = k_0$)

$$E_x\Big|_{i,j,k}^{n} = \left\{ E_x\Big|_{i,j,k}^{n} \right\}_{(2.52)} + \underbrace{\left[\frac{1}{6}\left(E_{x,\mathrm{inc}}\Big|_{i-1,j,k}^{n-1} + E_{x,\mathrm{inc}}\Big|_{i,j,k-1}^{n-1} \right) + \frac{\eta}{2\sqrt{3}} H_{y,\mathrm{inc}}\Big|_{i,j,k-1}^{n-1} \right]}_{\text{correction term}} \quad (4.36a)$$

$$E_y\Big|_{i,j,k}^{n} = \left\{E_y\Big|_{i,j,k}^{n}\right\}_{(2.53a)} + \underbrace{\left[\frac{1}{6}\left(E_{y,\mathrm{inc}}\Big|_{i-1,j,k}^{n-1} + E_{y,\mathrm{inc}}\Big|_{i,j,k-1}^{n-1}\right) + \frac{\eta}{2\sqrt{3}}\left(H_{z,\mathrm{inc}}\Big|_{i-1,j,k}^{n-1} - H_{x,\mathrm{inc}}\Big|_{i,j,k-1}^{n-1}\right)\right]}_{\text{correction term}} \quad (4.36b)$$

$$E_z\Big|_{i,j,k}^{n} = \left\{E_z\Big|_{i,j,k}^{n}\right\}_{(2.53b)} + \underbrace{\left[\frac{1}{6}\left(E_{z,\mathrm{inc}}\Big|_{i-1,j,k}^{n-1} + E_{z,\mathrm{inc}}\Big|_{i,j,k-1}^{n-1}\right) - \frac{\eta}{2\sqrt{3}} H_{y,\mathrm{inc}}\Big|_{i-1,j,k}^{n-1}\right]}_{\text{correction term}} \quad (4.36c)$$

$$H_x\Big|_{i,j,k}^{n} = \left\{H_x\Big|_{i,j,k}^{n}\right\}_{(2.53c)} + \underbrace{\left[\frac{1}{6}\left(H_{x,\mathrm{inc}}\Big|_{i-1,j,k}^{n-1} + H_{x,\mathrm{inc}}\Big|_{i,j,k-1}^{n-1}\right) - \frac{1}{2\sqrt{3}\eta} E_{y,\mathrm{inc}}\Big|_{i,j,k-1}^{n-1}\right]}_{\text{correction term}} \quad (4.36d)$$

$$H_y\Big|_{i,j,k}^{n} = \left\{H_y\Big|_{i,j,k}^{n}\right\}_{(2.53d)} + \underbrace{\left[\frac{1}{6}\left(H_{y,\mathrm{inc}}\Big|_{i-1,j,k}^{n-1} + H_{y,\mathrm{inc}}\Big|_{i,j,k-1}^{n-1}\right) - \frac{1}{2\sqrt{3}\eta}\left(E_{z,\mathrm{inc}}\Big|_{i-1,j,k}^{n-1} - E_{x,\mathrm{inc}}\Big|_{i,j,k-1}^{n-1}\right)\right]}_{\text{correction term}} \quad (4.36e)$$

$$H_z\Big|_{i,j,k}^{n} = \left\{H_z\Big|_{i,j,k}^{n}\right\}_{(2.53e)} + \underbrace{\left[\frac{1}{6}\left(H_{z,\mathrm{inc}}\Big|_{i-1,j,k}^{n-1} + H_{z,\mathrm{inc}}\Big|_{i,j,k-1}^{n-1}\right) + \frac{1}{2\sqrt{3}\eta} E_{y,\mathrm{inc}}\Big|_{i-1,j,k}^{n-1}\right]}_{\text{correction term}} \quad (4.36f)$$

Bottom front line of Region 1 ($i = i_1;\ j = j_0 + 1, \ldots, j_1 - 1;\ k = k_0$)

$$E_x\Big|_{i,j,k}^{n} = \left\{E_x\Big|_{i,j,k}^{n}\right\}_{(2.52)} + \underbrace{\left[\frac{1}{6}\left(E_{x,\mathrm{inc}}\Big|_{i+1,j,k}^{n-1} + E_{x,\mathrm{inc}}\Big|_{i,j,k-1}^{n-1}\right) + \frac{\eta}{2\sqrt{3}} H_{y,\mathrm{inc}}\Big|_{i,j,k-1}^{n-1}\right]}_{\text{correction term}} \quad (4.37a)$$

$$E_y\Big|_{i,j,k}^{n} = \left\{E_y\Big|_{i,j,k}^{n}\right\}_{(2.53a)} + \underbrace{\left[\frac{1}{6}\left(E_{y,\mathrm{inc}}\Big|_{i+1,j,k}^{n-1} + E_{y,\mathrm{inc}}\Big|_{i,j,k-1}^{n-1}\right) - \frac{\eta}{2\sqrt{3}}\left(H_{z,\mathrm{inc}}\Big|_{i+1,j,k}^{n-1} + H_{x,\mathrm{inc}}\Big|_{i,j,k-1}^{n-1}\right)\right]}_{\text{correction term}} \quad (4.37b)$$

$$E_z\Big|_{i,j,k}^{n} = \left\{E_z\Big|_{i,j,k}^{n}\right\}_{(2.53b)} + \underbrace{\left[\frac{1}{6}\left(E_{z,\mathrm{inc}}\Big|_{i+1,j,k}^{n-1} + E_{z,\mathrm{inc}}\Big|_{i,j,k-1}^{n-1}\right) + \frac{\eta}{2\sqrt{3}} H_{y,\mathrm{inc}}\Big|_{i+1,j,k}^{n-1}\right]}_{\text{correction term}} \quad (4.37c)$$

$$H_x\Big|_{i,j,k}^{n} = \left\{H_x\Big|_{i,j,k}^{n}\right\}_{(2.53c)} + \underbrace{\left[\frac{1}{6}\left(H_{x,\mathrm{inc}}\Big|_{i+1,j,k}^{n-1} + H_{x,\mathrm{inc}}\Big|_{i,j,k-1}^{n-1}\right) - \frac{1}{2\sqrt{3}\eta} E_{y,\mathrm{inc}}\Big|_{i,j,k-1}^{n-1}\right]}_{\text{correction term}} \quad (4.37d)$$

$$H_y\Big|_{i,j,k}^{n} = \left\{H_y\Big|_{i,j,k}^{n}\right\}_{(2.53d)} + \underbrace{\left[\frac{1}{6}\left(H_{y,\mathrm{inc}}\Big|_{i+1,j,k}^{n-1} + H_{y,\mathrm{inc}}\Big|_{i,j,k-1}^{n-1}\right) + \frac{1}{2\sqrt{3}\eta}\left(E_{z,\mathrm{inc}}\Big|_{i+1,j,k}^{n-1} + E_{x,\mathrm{inc}}\Big|_{i,j,k-1}^{n-1}\right)\right]}_{\text{correction term}} \quad (4.37e)$$

$$H_z\Big|_{i,j,k}^{n} = \left\{H_z\Big|_{i,j,k}^{n}\right\}_{(2.53e)} + \underbrace{\left[\frac{1}{6}\left(H_{z,\mathrm{inc}}\Big|_{i+1,j,k}^{n-1} + H_{z,\mathrm{inc}}\Big|_{i,j,k-1}^{n-1}\right) - \frac{1}{2\sqrt{3}\eta}E_{y,\mathrm{inc}}\Big|_{i+1,j,k}^{n-1}\right]}_{\text{correction term}} \quad (4.37f)$$

Bottom left line of Region 1 ($i = i_0 + 1, \ldots, i_1 - 1;\ j = j_0;\ k = k_0$)

$$E_x\Big|_{i,j,k}^{n} = \left\{E_x\Big|_{i,j,k}^{n}\right\}_{(2.52)} + \underbrace{\left[\frac{1}{6}\left(E_{x,\mathrm{inc}}\Big|_{i,j-1,k}^{n-1} + E_{x,\mathrm{inc}}\Big|_{i,j,k-1}^{n-1}\right) + \frac{\eta}{2\sqrt{3}}\left(H_{y,\mathrm{inc}}\Big|_{i,j,k-1}^{n-1} - H_{z,\mathrm{inc}}\Big|_{i,j-1,k}^{n-1}\right)\right]}_{\text{correction term}} \quad (4.38a)$$

$$E_y\Big|_{i,j,k}^{n} = \left\{E_y\Big|_{i,j,k}^{n}\right\}_{(2.53a)} + \underbrace{\left[\frac{1}{6}\left(E_{y,\mathrm{inc}}\Big|_{i,j-1,k}^{n-1} + E_{y,\mathrm{inc}}\Big|_{i,j,k-1}^{n-1}\right) - \frac{\eta}{2\sqrt{3}}H_{x,\mathrm{inc}}\Big|_{i,j,k-1}^{n-1}\right]}_{\text{correction term}} \quad (4.38b)$$

$$E_z\Big|_{i,j,k}^{n} = \left\{E_z\Big|_{i,j,k}^{n}\right\}_{(2.53b)} + \underbrace{\left[\frac{1}{6}\left(E_{z,\mathrm{inc}}\Big|_{i,j-1,k}^{n-1} + E_{z,\mathrm{inc}}\Big|_{i,j,k-1}^{n-1}\right) + \frac{\eta}{2\sqrt{3}}H_{x,\mathrm{inc}}\Big|_{i,j-1,k}^{n-1}\right]}_{\text{correction term}} \quad (4.38c)$$

$$H_x\Big|_{i,j,k}^{n} = \left\{H_x\Big|_{i,j,k}^{n}\right\}_{(2.53c)} + \underbrace{\left[\frac{1}{6}\left(H_{x,\mathrm{inc}}\Big|_{i,j-1,k}^{n-1} + H_{x,\mathrm{inc}}\Big|_{i,j,k-1}^{n-1}\right) - \frac{1}{2\sqrt{3}\eta}\left(E_{y,\mathrm{inc}}\Big|_{i,j,k-1}^{n-1} - E_{z,\mathrm{inc}}\Big|_{i,j-1,k}^{n-1}\right)\right]}_{\text{correction term}} \quad (4.38d)$$

$$H_y\Big|_{i,j,k}^{n} = \left\{H_y\Big|_{i,j,k}^{n}\right\}_{(2.53d)} + \underbrace{\left[\frac{1}{6}\left(H_{y,\mathrm{inc}}\Big|_{i,j-1,k}^{n-1} + H_{y,\mathrm{inc}}\Big|_{i,j,k-1}^{n-1}\right) + \frac{1}{2\sqrt{3}\eta}E_{x,\mathrm{inc}}\Big|_{i,j,k-1}^{n-1}\right]}_{\text{correction term}} \quad (4.38e)$$

$$H_z\Big|_{i,j,k}^{n} = \left\{H_z\Big|_{i,j,k}^{n}\right\}_{(2.53e)} + \underbrace{\left[\frac{1}{6}\left(H_{z,\mathrm{inc}}\Big|_{i,j-1,k}^{n-1} + H_{z,\mathrm{inc}}\Big|_{i,j,k-1}^{n-1}\right) - \frac{1}{2\sqrt{3}\eta}E_{x,\mathrm{inc}}\Big|_{i,j-1,k}^{n-1}\right]}_{\text{correction term}} \quad (4.38f)$$

Bottom right line of Region 1 ($i = i_0 + 1, \ldots, i_1 - 1;\ j = j_1;\ k = k_0$)

$$E_x\Big|_{i,j,k}^{n} = \left\{E_x\Big|_{i,j,k}^{n}\right\}_{(2.52)} + \underbrace{\left[\frac{1}{6}\left(E_{x,\mathrm{inc}}\Big|_{i,j+1,k}^{n-1} + E_{x,\mathrm{inc}}\Big|_{i,j,k-1}^{n-1}\right) + \frac{\eta}{2\sqrt{3}}\left(H_{y,\mathrm{inc}}\Big|_{i,j,k-1}^{n-1} + H_{z,\mathrm{inc}}\Big|_{i,j+1,k}^{n-1}\right)\right]}_{\text{correction term}} \tag{4.39a}$$

$$E_y\Big|_{i,j,k}^{n} = \left\{E_y\Big|_{i,j,k}^{n}\right\}_{(2.53a)} + \underbrace{\left[\frac{1}{6}\left(E_{y,\mathrm{inc}}\Big|_{i,j+1,k}^{n-1} + E_{y,\mathrm{inc}}\Big|_{i,j,k-1}^{n-1}\right) - \frac{\eta}{2\sqrt{3}} H_{x,\mathrm{inc}}\Big|_{i,j,k-1}^{n-1}\right]}_{\text{correction term}} \tag{4.39b}$$

$$E_z\Big|_{i,j,k}^{n} = \left\{E_z\Big|_{i,j,k}^{n}\right\}_{(2.53b)} + \underbrace{\left[\frac{1}{6}\left(E_{z,\mathrm{inc}}\Big|_{i,j+1,k}^{n-1} + E_{z,\mathrm{inc}}\Big|_{i,j,k-1}^{n-1}\right) - \frac{\eta}{2\sqrt{3}} H_{x,\mathrm{inc}}\Big|_{i,j+1,k}^{n-1}\right]}_{\text{correction term}} \tag{4.39c}$$

$$H_x\Big|_{i,j,k}^{n} = \left\{H_x\Big|_{i,j,k}^{n}\right\}_{(2.53c)} + \underbrace{\left[\frac{1}{6}\left(H_{x,\mathrm{inc}}\Big|_{i,j+1,k}^{n-1} + H_{x,\mathrm{inc}}\Big|_{i,j,k-1}^{n-1}\right) - \frac{1}{2\sqrt{3}\eta}\left(E_{y,\mathrm{inc}}\Big|_{i,j,k-1}^{n-1} + E_{z,\mathrm{inc}}\Big|_{i,j+1,k}^{n-1}\right)\right]}_{\text{correction term}} \tag{4.39d}$$

$$H_y\Big|_{i,j,k}^{n} = \left\{H_y\Big|_{i,j,k}^{n}\right\}_{(2.53d)} + \underbrace{\left[\frac{1}{6}\left(H_{y,\mathrm{inc}}\Big|_{i,j+1,k}^{n-1} + H_{y,\mathrm{inc}}\Big|_{i,j,k-1}^{n-1}\right) + \frac{1}{2\sqrt{3}\eta} E_{x,\mathrm{inc}}\Big|_{i,j,k-1}^{n-1}\right]}_{\text{correction term}} \tag{4.39e}$$

$$H_z\Big|_{i,j,k}^{n} = \left\{H_z\Big|_{i,j,k}^{n}\right\}_{(2.53e)} + \underbrace{\left[\frac{1}{6}\left(H_{z,\mathrm{inc}}\Big|_{i,j+1,k}^{n-1} + H_{z,\mathrm{inc}}\Big|_{i,j,k-1}^{n-1}\right) + \frac{1}{2\sqrt{3}\eta} E_{x,\mathrm{inc}}\Big|_{i,j+1,k}^{n-1}\right]}_{\text{correction term}} \tag{4.39f}$$

Top left line of Region 1 ($i = i_0 + 1, \ldots, i_1 - 1;\ j = j_0;\ k = k_1$)

$$E_x\Big|_{i,j,k}^{n} = \left\{E_x\Big|_{i,j,k}^{n}\right\}_{(2.52)} + \underbrace{\left[\frac{1}{6}\left(E_{x,\mathrm{inc}}\Big|_{i,j-1,k}^{n-1} + E_{x,\mathrm{inc}}\Big|_{i,j,k+1}^{n-1}\right) - \frac{\eta}{2\sqrt{3}}\left(H_{y,\mathrm{inc}}\Big|_{i,j,k+1}^{n-1} + H_{z,\mathrm{inc}}\Big|_{i,j-1,k}^{n-1}\right)\right]}_{\text{correction term}} \tag{4.40a}$$

$$E_y\Big|_{i,j,k}^{n} = \left\{E_y\Big|_{i,j,k}^{n}\right\}_{(2.53a)} + \underbrace{\left[\frac{1}{6}\left(E_{y,\mathrm{inc}}\Big|_{i,j-1,k}^{n-1} + E_{y,\mathrm{inc}}\Big|_{i,j,k+1}^{n-1}\right) + \frac{\eta}{2\sqrt{3}} H_{x,\mathrm{inc}}\Big|_{i,j,k+1}^{n-1}\right]}_{\text{correction term}} \tag{4.40b}$$

$$E_z\Big|_{i,j,k}^{n} = \left\{E_z\Big|_{i,j,k}^{n}\right\}_{(2.53b)} + \underbrace{\left[\frac{1}{6}\left(E_{z,\mathrm{inc}}\Big|_{i,j-1,k}^{n-1} + E_{z,\mathrm{inc}}\Big|_{i,j,k+1}^{n-1}\right) + \frac{\eta}{2\sqrt{3}} H_{x,\mathrm{inc}}\Big|_{i,j-1,k}^{n-1}\right]}_{\text{correction term}} \tag{4.40c}$$

$$H_x\Big|_{i,j,k}^{n} = \left\{H_x\Big|_{i,j,k}^{n}\right\}_{(2.53c)} + \underbrace{\left[\frac{1}{6}\left(H_{x,\mathrm{inc}}\Big|_{i,j-1,k}^{n-1} + H_{x,\mathrm{inc}}\Big|_{i,j,k+1}^{n-1}\right) + \frac{1}{2\sqrt{3}\eta}\left(E_{y,\mathrm{inc}}\Big|_{i,j,k+1}^{n-1} + E_{z,\mathrm{inc}}\Big|_{i,j-1,k}^{n-1}\right)\right]}_{\text{correction term}} \tag{4.40d}$$

$$H_y\Big|_{i,j,k}^{n} = \left\{H_y\Big|_{i,j,k}^{n}\right\}_{(2.53d)} + \underbrace{\left[\frac{1}{6}\left(H_{y,\mathrm{inc}}\Big|_{i,j-1,k}^{n-1} + H_{y,\mathrm{inc}}\Big|_{i,j,k+1}^{n-1}\right) - \frac{1}{2\sqrt{3}\eta} E_{x,\mathrm{inc}}\Big|_{i,j,k+1}^{n-1}\right]}_{\text{correction term}} \tag{4.40e}$$

$$H_z\Big|_{i,j,k}^{n} = \left\{H_z\Big|_{i,j,k}^{n}\right\}_{(2.53e)} + \underbrace{\left[\frac{1}{6}\left(H_{z,\mathrm{inc}}\Big|_{i,j-1,k}^{n-1} + H_{z,\mathrm{inc}}\Big|_{i,j,k+1}^{n-1}\right) - \frac{1}{2\sqrt{3}\eta} E_{x,\mathrm{inc}}\Big|_{i,j-1,k}^{n-1}\right]}_{\text{correction term}} \tag{4.40f}$$

Top right line of Region 1 ($i = i_0 + 1, \ldots, i_1 - 1;\ j = j_1;\ k = k_1$)

$$E_x\Big|_{i,j,k}^{n} = \left\{E_x\Big|_{i,j,k}^{n}\right\}_{(2.52)} + \underbrace{\left[\frac{1}{6}\left(E_{x,\mathrm{inc}}\Big|_{i,j+1,k}^{n-1} + E_{x,\mathrm{inc}}\Big|_{i,j,k+1}^{n-1}\right) - \frac{\eta}{2\sqrt{3}}\left(H_{y,\mathrm{inc}}\Big|_{i,j,k+1}^{n-1} - H_{z,\mathrm{inc}}\Big|_{i,j+1,k}^{n-1}\right)\right]}_{\text{correction term}} \tag{4.41a}$$

$$E_y\Big|_{i,j,k}^{n} = \left\{E_y\Big|_{i,j,k}^{n}\right\}_{(2.53a)} + \underbrace{\left[\frac{1}{6}\left(E_{y,\mathrm{inc}}\Big|_{i,j+1,k}^{n-1} + E_{y,\mathrm{inc}}\Big|_{i,j,k+1}^{n-1}\right) + \frac{\eta}{2\sqrt{3}} H_{x,\mathrm{inc}}\Big|_{i,j,k+1}^{n-1}\right]}_{\text{correction term}} \tag{4.41b}$$

$$E_z\Big|_{i,j,k}^{n} = \left\{E_z\Big|_{i,j,k}^{n}\right\}_{(2.53b)} + \underbrace{\left[\frac{1}{6}\left(E_{z,\mathrm{inc}}\Big|_{i,j+1,k}^{n-1} + E_{z,\mathrm{inc}}\Big|_{i,j,k+1}^{n-1}\right) - \frac{\eta}{2\sqrt{3}} H_{x,\mathrm{inc}}\Big|_{i,j+1,k}^{n-1}\right]}_{\text{correction term}} \tag{4.41c}$$

$$H_x\Big|_{i,j,k}^{n} = \left\{H_x\Big|_{i,j,k}^{n}\right\}_{(2.53c)} + \underbrace{\left[\frac{1}{6}\left(H_{x,\mathrm{inc}}\Big|_{i,j+1,k}^{n-1} + H_{x,\mathrm{inc}}\Big|_{i,j,k+1}^{n-1}\right) + \frac{1}{2\sqrt{3}\eta}\left(E_{y,\mathrm{inc}}\Big|_{i,j,k+1}^{n-1} - E_{z,\mathrm{inc}}\Big|_{i,j+1,k}^{n-1}\right)\right]}_{\text{correction term}} \tag{4.41d}$$

$$H_y\Big|_{i,j,k}^{n} = \left\{H_y\Big|_{i,j,k}^{n}\right\}_{(2.53d)} + \underbrace{\left[\frac{1}{6}\left(H_{y,\mathrm{inc}}\Big|_{i,j+1,k}^{n-1} + H_{y,\mathrm{inc}}\Big|_{i,j,k+1}^{n-1}\right) - \frac{1}{2\sqrt{3}\eta} E_{x,\mathrm{inc}}\Big|_{i,j,k+1}^{n-1}\right]}_{\text{correction term}} \tag{4.41e}$$

$$H_z\Big|_{i,j,k}^{n} = \left\{H_z\Big|_{i,j,k}^{n}\right\}_{(2.53e)} + \underbrace{\left[\frac{1}{6}\left(H_{z,\mathrm{inc}}\Big|_{i,j+1,k}^{n-1} + H_{z,\mathrm{inc}}\Big|_{i,j,k+1}^{n-1}\right) + \frac{1}{2\sqrt{3}\eta}E_{x,\mathrm{inc}}\Big|_{i,j+1,k}^{n-1}\right]}_{\text{correction term}} \tag{4.41f}$$

Next, consider eight corners of the 3-D TF / SF interface. The consistency conditions at the corners are given by

Bottom left rear corner of Region 1 ($i = i_0;\ j = j_0;\ k = k_0$)

$$E_x\Big|_{i,j,k}^{n} = \left\{E_x\Big|_{i,j,k}^{n}\right\}_{(2.52)} + \underbrace{\left[\frac{1}{6}\left(E_{x,\mathrm{inc}}\Big|_{i-1,j,k}^{n-1} + E_{x,\mathrm{inc}}\Big|_{i,j-1,k}^{n-1} + E_{x,\mathrm{inc}}\Big|_{i,j,k-1}^{n-1}\right) + \frac{\eta}{2\sqrt{3}}\left(H_{y,\mathrm{inc}}\Big|_{i,j,k-1}^{n-1} - H_{z,\mathrm{inc}}\Big|_{i,j-1,k}^{n-1}\right)\right]}_{\text{correction term}} \tag{4.42a}$$

$$E_y\Big|_{i,j,k}^{n} = \left\{E_y\Big|_{i,j,k}^{n}\right\}_{(2.53a)} + \underbrace{\left[\frac{1}{6}\left(E_{y,\mathrm{inc}}\Big|_{i-1,j,k}^{n-1} + E_{y,\mathrm{inc}}\Big|_{i,j-1,k}^{n-1} + E_{y,\mathrm{inc}}\Big|_{i,j,k-1}^{n-1}\right) + \frac{\eta}{2\sqrt{3}}\left(H_{z,\mathrm{inc}}\Big|_{i-1,j,k}^{n-1} - H_{x,\mathrm{inc}}\Big|_{i,j,k-1}^{n-1}\right)\right]}_{\text{correction term}} \tag{4.42b}$$

$$E_z\Big|_{i,j,k}^{n} = \left\{E_z\Big|_{i,j,k}^{n}\right\}_{(2.53b)} + \underbrace{\left[\frac{1}{6}\left(E_{z,\mathrm{inc}}\Big|_{i-1,j,k}^{n-1} + E_{z,\mathrm{inc}}\Big|_{i,j-1,k}^{n-1} + E_{z,\mathrm{inc}}\Big|_{i,j,k-1}^{n-1}\right) + \frac{\eta}{2\sqrt{3}}\left(H_{x,\mathrm{inc}}\Big|_{i,j-1,k}^{n-1} - H_{y,\mathrm{inc}}\Big|_{i-1,j,k}^{n-1}\right)\right]}_{\text{correction term}} \tag{4.42c}$$

$$H_x\Big|_{i,j,k}^{n} = \left\{H_x\Big|_{i,j,k}^{n}\right\}_{(2.53c)} + \underbrace{\left[\frac{1}{6}\left(H_{x,\mathrm{inc}}\Big|_{i-1,j,k}^{n-1} + H_{x,\mathrm{inc}}\Big|_{i,j-1,k}^{n-1} + H_{x,\mathrm{inc}}\Big|_{i,j,k-1}^{n-1}\right) - \frac{1}{2\sqrt{3}\eta}\left(E_{y,\mathrm{inc}}\Big|_{i,j,k-1}^{n-1} - E_{z,\mathrm{inc}}\Big|_{i,j-1,k}^{n-1}\right)\right]}_{\text{correction term}} \tag{4.42d}$$

$$H_y\Big|_{i,j,k}^{n} = \left\{H_y\Big|_{i,j,k}^{n}\right\}_{(2.53d)} + \underbrace{\left[\frac{1}{6}\left(H_{y,\mathrm{inc}}\Big|_{i-1,j,k}^{n-1} + H_{y,\mathrm{inc}}\Big|_{i,j-1,k}^{n-1} + H_{y,\mathrm{inc}}\Big|_{i,j,k-1}^{n-1}\right) - \frac{1}{2\sqrt{3}\eta}\left(E_{z,\mathrm{inc}}\Big|_{i-1,j,k}^{n-1} - E_{x,\mathrm{inc}}\Big|_{i,j,k-1}^{n-1}\right)\right]}_{\text{correction term}} \tag{4.42e}$$

$$H_z\Big|_{i,j,k}^{n} = \left\{H_z\Big|_{i,j,k}^{n}\right\}_{(2.53e)} + \underbrace{\left[\frac{1}{6}\left(H_{z,\mathrm{inc}}\Big|_{i-1,j,k}^{n-1} + H_{z,\mathrm{inc}}\Big|_{i,j-1,k}^{n-1} + H_{z,\mathrm{inc}}\Big|_{i,j,k-1}^{n-1}\right) - \frac{1}{2\sqrt{3}\eta}\left(E_{x,\mathrm{inc}}\Big|_{i,j-1,k}^{n-1} - E_{y,\mathrm{inc}}\Big|_{i-1,j,k}^{n-1}\right)\right]}_{\text{correction term}} \tag{4.42f}$$

Bottom right rear corner of Region 1 ($i = i_0;\ j = j_1;\ k = k_0$)

$$E_x\Big|_{i,j,k}^{n} = \left\{E_x\Big|_{i,j,k}^{n}\right\}_{(2.52)} + \underbrace{\left[\frac{1}{6}\left(E_{x,\mathrm{inc}}\Big|_{i-1,j,k}^{n-1} + E_{x,\mathrm{inc}}\Big|_{i,j+1,k}^{n-1} + E_{x,\mathrm{inc}}\Big|_{i,j,k-1}^{n-1}\right) + \frac{\eta}{2\sqrt{3}}\left(H_{y,\mathrm{inc}}\Big|_{i,j,k-1}^{n-1} + H_{z,\mathrm{inc}}\Big|_{i,j+1,k}^{n-1}\right)\right]}_{\text{correction term}} \quad (4.43a)$$

$$E_y\Big|_{i,j,k}^{n} = \left\{E_y\Big|_{i,j,k}^{n}\right\}_{(2.53a)} + \underbrace{\left[\frac{1}{6}\left(E_{y,\mathrm{inc}}\Big|_{i-1,j,k}^{n-1} + E_{y,\mathrm{inc}}\Big|_{i,j+1,k}^{n-1} + E_{y,\mathrm{inc}}\Big|_{i,j,k-1}^{n-1}\right) + \frac{\eta}{2\sqrt{3}}\left(H_{z,\mathrm{inc}}\Big|_{i-1,j,k}^{n-1} - H_{x,\mathrm{inc}}\Big|_{i,j,k-1}^{n-1}\right)\right]}_{\text{correction term}} \quad (4.43b)$$

$$E_z\Big|_{i,j,k}^{n} = \left\{E_z\Big|_{i,j,k}^{n}\right\}_{(2.53b)} + \underbrace{\left[\frac{1}{6}\left(E_{z,\mathrm{inc}}\Big|_{i-1,j,k}^{n-1} + E_{z,\mathrm{inc}}\Big|_{i,j+1,k}^{n-1} + E_{z,\mathrm{inc}}\Big|_{i,j,k-1}^{n-1}\right) - \frac{\eta}{2\sqrt{3}}\left(H_{x,\mathrm{inc}}\Big|_{i,j+1,k}^{n-1} + H_{y,\mathrm{inc}}\Big|_{i-1,j,k}^{n-1}\right)\right]}_{\text{correction term}} \quad (4.43c)$$

$$H_x\Big|_{i,j,k}^{n} = \left\{H_x\Big|_{i,j,k}^{n}\right\}_{(2.53c)} + \underbrace{\left[\frac{1}{6}\left(H_{x,\mathrm{inc}}\Big|_{i-1,j,k}^{n-1} + H_{x,\mathrm{inc}}\Big|_{i,j+1,k}^{n-1} + H_{x,\mathrm{inc}}\Big|_{i,j,k-1}^{n-1}\right) - \frac{1}{2\sqrt{3}\eta}\left(E_{y,\mathrm{inc}}\Big|_{i,j,k-1}^{n-1} + E_{z,\mathrm{inc}}\Big|_{i,j+1,k}^{n-1}\right)\right]}_{\text{correction term}} \quad (4.43d)$$

$$H_y\Big|_{i,j,k}^{n} = \left\{H_y\Big|_{i,j,k}^{n}\right\}_{(2.53d)} + \underbrace{\left[\frac{1}{6}\left(H_{y,\mathrm{inc}}\Big|_{i-1,j,k}^{n-1} + H_{y,\mathrm{inc}}\Big|_{i,j+1,k}^{n-1} + H_{y,\mathrm{inc}}\Big|_{i,j,k-1}^{n-1}\right) - \frac{1}{2\sqrt{3}\eta}\left(E_{z,\mathrm{inc}}\Big|_{i-1,j,k}^{n-1} - E_{x,\mathrm{inc}}\Big|_{i,j,k-1}^{n-1}\right)\right]}_{\text{correction term}} \quad (4.43e)$$

$$H_z\Big|_{i,j,k}^{n} = \left\{H_z\Big|_{i,j,k}^{n}\right\}_{(2.53e)} + \underbrace{\left[\frac{1}{6}\left(H_{z,\mathrm{inc}}\Big|_{i-1,j,k}^{n-1} + H_{z,\mathrm{inc}}\Big|_{i,j+1,k}^{n-1} + H_{z,\mathrm{inc}}\Big|_{i,j,k-1}^{n-1}\right) + \frac{1}{2\sqrt{3}\eta}\left(E_{x,\mathrm{inc}}\Big|_{i,j+1,k}^{n-1} + E_{y,\mathrm{inc}}\Big|_{i-1,j,k}^{n-1}\right)\right]}_{\text{correction term}} \quad (4.43f)$$

Bottom left front corner of Region 1 ($i = i_1;\ j = j_0;\ k = k_0$)

$$E_x\Big|_{i,j,k}^{n} = \left\{E_x\Big|_{i,j,k}^{n}\right\}_{(2.52)} + \underbrace{\left[\frac{1}{6}\left(E_{x,\mathrm{inc}}\Big|_{i+1,j,k}^{n-1} + E_{x,\mathrm{inc}}\Big|_{i,j-1,k}^{n-1} + E_{x,\mathrm{inc}}\Big|_{i,j,k-1}^{n-1}\right) + \frac{\eta}{2\sqrt{3}}\left(H_{y,\mathrm{inc}}\Big|_{i,j,k-1}^{n-1} - H_{z,\mathrm{inc}}\Big|_{i,j-1,k}^{n-1}\right)\right]}_{\text{correction term}} \quad (4.44a)$$

$$E_y\Big|_{i,j,k}^{n} = \left\{E_y\Big|_{i,j,k}^{n}\right\}_{(2.53a)} + \underbrace{\left[\frac{1}{6}\left(E_{y,\mathrm{inc}}\Big|_{i+1,j,k}^{n-1} + E_{y,\mathrm{inc}}\Big|_{i,j-1,k}^{n-1} + E_{y,\mathrm{inc}}\Big|_{i,j,k-1}^{n-1}\right) - \frac{\eta}{2\sqrt{3}}\left(H_{z,\mathrm{inc}}\Big|_{i+1,j,k}^{n-1} + H_{x,\mathrm{inc}}\Big|_{i,j,k-1}^{n-1}\right)\right]}_{\text{correction term}} \quad (4.44b)$$

$$E_z\Big|_{i,j,k}^{n} = \left\{E_z\Big|_{i,j,k}^{n}\right\}_{(2.53b)} + \underbrace{\left[\frac{1}{6}\left(E_{z,\mathrm{inc}}\Big|_{i+1,j,k}^{n-1} + E_{z,\mathrm{inc}}\Big|_{i,j-1,k}^{n-1} + E_{z,\mathrm{inc}}\Big|_{i,j,k-1}^{n-1}\right) + \frac{\eta}{2\sqrt{3}}\left(H_{x,\mathrm{inc}}\Big|_{i,j-1,k}^{n-1} + H_{y,\mathrm{inc}}\Big|_{i+1,j,k}^{n-1}\right)\right]}_{\text{correction term}} \quad (4.44c)$$

$$H_x\Big|_{i,j,k}^{n} = \left\{H_x\Big|_{i,j,k}^{n}\right\}_{(2.53c)} + \underbrace{\left[\frac{1}{6}\left(H_{x,\mathrm{inc}}\Big|_{i+1,j,k}^{n-1} + H_{x,\mathrm{inc}}\Big|_{i,j-1,k}^{n-1} + H_{x,\mathrm{inc}}\Big|_{i,j,k-1}^{n-1}\right) - \frac{1}{2\sqrt{3}\eta}\left(E_{y,\mathrm{inc}}\Big|_{i,j,k-1}^{n-1} - E_{z,\mathrm{inc}}\Big|_{i,j-1,k}^{n-1}\right)\right]}_{\text{correction term}} \quad (4.44d)$$

$$H_y\Big|_{i,j,k}^{n} = \left\{H_y\Big|_{i,j,k}^{n}\right\}_{(2.53d)} + \underbrace{\left[\frac{1}{6}\left(H_{y,\mathrm{inc}}\Big|_{i+1,j,k}^{n-1} + H_{y,\mathrm{inc}}\Big|_{i,j-1,k}^{n-1} + H_{y,\mathrm{inc}}\Big|_{i,j,k-1}^{n-1}\right) + \frac{1}{2\sqrt{3}\eta}\left(E_{z,\mathrm{inc}}\Big|_{i+1,j,k}^{n-1} + E_{x,\mathrm{inc}}\Big|_{i,j,k-1}^{n-1}\right)\right]}_{\text{correction term}} \quad (4.44e)$$

$$H_z\Big|_{i,j,k}^{n} = \left\{H_z\Big|_{i,j,k}^{n}\right\}_{(2.53e)} + \underbrace{\left[\frac{1}{6}\left(H_{z,\mathrm{inc}}\Big|_{i+1,j,k}^{n-1} + H_{z,\mathrm{inc}}\Big|_{i,j-1,k}^{n-1} + H_{z,\mathrm{inc}}\Big|_{i,j,k-1}^{n-1}\right) - \frac{1}{2\sqrt{3}\eta}\left(E_{x,\mathrm{inc}}\Big|_{i,j-1,k}^{n-1} + E_{y,\mathrm{inc}}\Big|_{i+1,j,k}^{n-1}\right)\right]}_{\text{correction term}} \quad (4.44f)$$

Bottom right front corner of Region 1 ($i = i_1;\ j = j_1;\ k = k_0$)

$$E_x\Big|_{i,j,k}^{n} = \left\{E_x\Big|_{i,j,k}^{n}\right\}_{(2.52)} + \underbrace{\left[\frac{1}{6}\left(E_{x,\mathrm{inc}}\Big|_{i+1,j,k}^{n-1} + E_{x,\mathrm{inc}}\Big|_{i,j+1,k}^{n-1} + E_{x,\mathrm{inc}}\Big|_{i,j,k-1}^{n-1}\right) + \frac{\eta}{2\sqrt{3}}\left(H_{y,\mathrm{inc}}\Big|_{i,j,k-1}^{n-1} + H_{z,\mathrm{inc}}\Big|_{i,j+1,k}^{n-1}\right)\right]}_{\text{correction term}} \quad (4.45a)$$

$$E_y\Big|_{i,j,k}^{n} = \left\{E_y\Big|_{i,j,k}^{n}\right\}_{(2.53a)} + \underbrace{\left[\frac{1}{6}\left(E_{y,\mathrm{inc}}\Big|_{i+1,j,k}^{n-1} + E_{y,\mathrm{inc}}\Big|_{i,j+1,k}^{n-1} + E_{y,\mathrm{inc}}\Big|_{i,j,k-1}^{n-1}\right) - \frac{\eta}{2\sqrt{3}}\left(H_{z,\mathrm{inc}}\Big|_{i+1,j,k}^{n-1} + H_{x,\mathrm{inc}}\Big|_{i,j,k-1}^{n-1}\right)\right]}_{\text{correction term}} \quad (4.45b)$$

$$E_z\Big|_{i,j,k}^{n} = \left\{E_z\Big|_{i,j,k}^{n}\right\}_{(2.53b)} + \underbrace{\left[\frac{1}{6}\left(E_{z,\mathrm{inc}}\Big|_{i+1,j,k}^{n-1} + E_{z,\mathrm{inc}}\Big|_{i,j+1,k}^{n-1} + E_{z,\mathrm{inc}}\Big|_{i,j,k-1}^{n-1}\right) - \frac{\eta}{2\sqrt{3}}\left(H_{x,\mathrm{inc}}\Big|_{i,j+1,k}^{n-1} - H_{y,\mathrm{inc}}\Big|_{i+1,j,k}^{n-1}\right)\right]}_{\text{correction term}} \quad (4.45c)$$

$$H_x\Big|_{i,j,k}^{n} = \left\{H_x\Big|_{i,j,k}^{n}\right\}_{(2.53c)} + \underbrace{\left[\frac{1}{6}\left(H_{x,\mathrm{inc}}\Big|_{i+1,j,k}^{n-1} + H_{x,\mathrm{inc}}\Big|_{i,j+1,k}^{n-1} + H_{x,\mathrm{inc}}\Big|_{i,j,k-1}^{n-1}\right) - \frac{1}{2\sqrt{3}\eta}\left(E_{y,\mathrm{inc}}\Big|_{i,j,k-1}^{n-1} + E_{z,\mathrm{inc}}\Big|_{i,j+1,k}^{n-1}\right)\right]}_{\text{correction term}} \quad (4.45d)$$

$$H_y\Big|_{i,j,k}^{n} = \left\{H_y\Big|_{i,j,k}^{n}\right\}_{(2.53d)} + \underbrace{\left[\frac{1}{6}\left(H_{y,\mathrm{inc}}\Big|_{i+1,j,k}^{n-1} + H_{y,\mathrm{inc}}\Big|_{i,j+1,k}^{n-1} + H_{y,\mathrm{inc}}\Big|_{i,j,k-1}^{n-1}\right) + \frac{1}{2\sqrt{3}\eta}\left(E_{z,\mathrm{inc}}\Big|_{i+1,j,k}^{n-1} + E_{x,\mathrm{inc}}\Big|_{i,j,k-1}^{n-1}\right)\right]}_{\text{correction term}} \quad (4.45e)$$

$$H_z\Big|_{i,j,k}^{n} = \left\{H_z\Big|_{i,j,k}^{n}\right\}_{(2.53e)} + \underbrace{\left[\frac{1}{6}\left(H_{z,\mathrm{inc}}\Big|_{i+1,j,k}^{n-1} + H_{z,\mathrm{inc}}\Big|_{i,j+1,k}^{n-1} + H_{z,\mathrm{inc}}\Big|_{i,j,k-1}^{n-1}\right) + \frac{1}{2\sqrt{3}\eta}\left(E_{x,\mathrm{inc}}\Big|_{i,j+1,k}^{n-1} - E_{y,\mathrm{inc}}\Big|_{i+1,j,k}^{n-1}\right)\right]}_{\text{correction term}} \quad (4.45f)$$

Top left rear corner of Region 1 ($i = i_0$; $j = j_0$; $k = k_1$)

$$E_x\Big|_{i,j,k}^{n} = \left\{E_x\Big|_{i,j,k}^{n}\right\}_{(2.52)} + \underbrace{\left[\frac{1}{6}\left(E_{x,\mathrm{inc}}\Big|_{i-1,j,k}^{n-1} + E_{x,\mathrm{inc}}\Big|_{i,j-1,k}^{n-1} + E_{x,\mathrm{inc}}\Big|_{i,j,k+1}^{n-1}\right) - \frac{\eta}{2\sqrt{3}}\left(H_{y,\mathrm{inc}}\Big|_{i,j,k+1}^{n-1} + H_{z,\mathrm{inc}}\Big|_{i,j-1,k}^{n-1}\right)\right]}_{\text{correction term}} \quad (4.46a)$$

$$E_y\Big|_{i,j,k}^{n} = \left\{E_y\Big|_{i,j,k}^{n}\right\}_{(2.53a)} + \underbrace{\left[\frac{1}{6}\left(E_{y,\mathrm{inc}}\Big|_{i-1,j,k}^{n-1} + E_{y,\mathrm{inc}}\Big|_{i,j-1,k}^{n-1} + E_{y,\mathrm{inc}}\Big|_{i,j,k+1}^{n-1}\right) + \frac{\eta}{2\sqrt{3}}\left(H_{z,\mathrm{inc}}\Big|_{i-1,j,k}^{n-1} + H_{x,\mathrm{inc}}\Big|_{i,j,k+1}^{n-1}\right)\right]}_{\text{correction term}} \quad (4.46b)$$

$$E_z\Big|_{i,j,k}^{n} = \left\{E_z\Big|_{i,j,k}^{n}\right\}_{(2.53b)} + \underbrace{\left[\frac{1}{6}\left(E_{z,\mathrm{inc}}\Big|_{i-1,j,k}^{n-1} + E_{z,\mathrm{inc}}\Big|_{i,j-1,k}^{n-1} + E_{z,\mathrm{inc}}\Big|_{i,j,k+1}^{n-1}\right) + \frac{\eta}{2\sqrt{3}}\left(H_{x,\mathrm{inc}}\Big|_{i,j-1,k}^{n-1} - H_{y,\mathrm{inc}}\Big|_{i-1,j,k}^{n-1}\right)\right]}_{\text{correction term}} \quad (4.46c)$$

$$H_x\Big|_{i,j,k}^{n} = \left\{H_x\Big|_{i,j,k}^{n}\right\}_{(2.53c)} + \underbrace{\left[\frac{1}{6}\left(H_{x,\mathrm{inc}}\Big|_{i-1,j,k}^{n-1} + H_{x,\mathrm{inc}}\Big|_{i,j-1,k}^{n-1} + H_{x,\mathrm{inc}}\Big|_{i,j,k+1}^{n-1}\right) + \frac{1}{2\sqrt{3}\eta}\left(E_{y,\mathrm{inc}}\Big|_{i,j,k+1}^{n-1} + E_{z,\mathrm{inc}}\Big|_{i,j-1,k}^{n-1}\right)\right]}_{\text{correction term}} \quad (4.46d)$$

$$H_y\Big|_{i,j,k}^{n} = \left\{H_y\Big|_{i,j,k}^{n}\right\}_{(2.53d)} + \underbrace{\left[\frac{1}{6}\left(H_{y,\mathrm{inc}}\Big|_{i-1,j,k}^{n-1} + H_{y,\mathrm{inc}}\Big|_{i,j-1,k}^{n-1} + H_{y,\mathrm{inc}}\Big|_{i,j,k+1}^{n-1}\right) - \frac{1}{2\sqrt{3}\eta}\left(E_{z,\mathrm{inc}}\Big|_{i-1,j,k}^{n-1} + E_{x,\mathrm{inc}}\Big|_{i,j,k+1}^{n-1}\right)\right]}_{\text{correction term}} \quad (4.46e)$$

$$H_z\Big|_{i,j,k}^{n} = \left\{H_z\Big|_{i,j,k}^{n}\right\}_{(2.53e)} + \underbrace{\left[\frac{1}{6}\left(H_{z,\mathrm{inc}}\Big|_{i-1,j,k}^{n-1} + H_{z,\mathrm{inc}}\Big|_{i,j-1,k}^{n-1} + H_{z,\mathrm{inc}}\Big|_{i,j,k+1}^{n-1}\right) - \frac{1}{2\sqrt{3}\eta}\left(E_{x,\mathrm{inc}}\Big|_{i,j-1,k}^{n-1} - E_{y,\mathrm{inc}}\Big|_{i-1,j,k}^{n-1}\right)\right]}_{\text{correction term}} \quad (4.46f)$$

Top right rear corner of Region 1 ($i = i_0$; $j = j_1$; $k = k_1$)

$$E_x\Big|_{i,j,k}^{n} = \left\{E_x\Big|_{i,j,k}^{n}\right\}_{(2.52)} + \underbrace{\left[\frac{1}{6}\left(E_{x,\mathrm{inc}}\Big|_{i-1,j,k}^{n-1} + E_{x,\mathrm{inc}}\Big|_{i,j+1,k}^{n-1} + E_{x,\mathrm{inc}}\Big|_{i,j,k+1}^{n-1}\right) - \frac{\eta}{2\sqrt{3}}\left(H_{y,\mathrm{inc}}\Big|_{i,j,k+1}^{n-1} - H_{z,\mathrm{inc}}\Big|_{i,j+1,k}^{n-1}\right)\right]}_{\text{correction term}} \quad (4.47a)$$

$$E_y\Big|_{i,j,k}^{n} = \left\{E_y\Big|_{i,j,k}^{n}\right\}_{(2.53a)} + \underbrace{\left[\frac{1}{6}\left(E_{y,\mathrm{inc}}\Big|_{i-1,j,k}^{n-1} + E_{y,\mathrm{inc}}\Big|_{i,j+1,k}^{n-1} + E_{y,\mathrm{inc}}\Big|_{i,j,k+1}^{n-1}\right) + \frac{\eta}{2\sqrt{3}}\left(H_{z,\mathrm{inc}}\Big|_{i-1,j,k}^{n-1} + H_{x,\mathrm{inc}}\Big|_{i,j,k+1}^{n-1}\right)\right]}_{\text{correction term}} \quad (4.47b)$$

$$E_z\Big|_{i,j,k}^{n} = \left\{E_z\Big|_{i,j,k}^{n}\right\}_{(2.53b)} + \underbrace{\left[\frac{1}{6}\left(E_{z,\mathrm{inc}}\Big|_{i-1,j,k}^{n-1} + E_{z,\mathrm{inc}}\Big|_{i,j+1,k}^{n-1} + E_{z,\mathrm{inc}}\Big|_{i,j,k+1}^{n-1}\right) - \frac{\eta}{2\sqrt{3}}\left(H_{x,\mathrm{inc}}\Big|_{i,j+1,k}^{n-1} + H_{y,\mathrm{inc}}\Big|_{i-1,j,k}^{n-1}\right)\right]}_{\text{correction term}} \quad (4.47c)$$

$$H_x\Big|_{i,j,k}^{n} = \left\{H_x\Big|_{i,j,k}^{n}\right\}_{(2.53c)} + \underbrace{\left[\frac{1}{6}\left(H_{x,\mathrm{inc}}\Big|_{i-1,j,k}^{n-1} + H_{x,\mathrm{inc}}\Big|_{i,j+1,k}^{n-1} + H_{x,\mathrm{inc}}\Big|_{i,j,k+1}^{n-1}\right) + \frac{1}{2\sqrt{3}\eta}\left(E_{y,\mathrm{inc}}\Big|_{i,j,k+1}^{n-1} - E_{z,\mathrm{inc}}\Big|_{i,j+1,k}^{n-1}\right)\right]}_{\text{correction term}} \quad (4.47d)$$

$$H_y\Big|_{i,j,k}^{n} = \left\{H_y\Big|_{i,j,k}^{n}\right\}_{(2.53d)} + \underbrace{\left[\frac{1}{6}\left(H_{y,\mathrm{inc}}\Big|_{i-1,j,k}^{n-1} + H_{y,\mathrm{inc}}\Big|_{i,j+1,k}^{n-1} + H_{y,\mathrm{inc}}\Big|_{i,j,k+1}^{n-1}\right) - \frac{1}{2\sqrt{3}\eta}\left(E_{z,\mathrm{inc}}\Big|_{i-1,j,k}^{n-1} + E_{x,\mathrm{inc}}\Big|_{i,j,k+1}^{n-1}\right)\right]}_{\text{correction term}} \quad (4.47e)$$

$$H_z\Big|_{i,j,k}^{n} = \left\{H_z\Big|_{i,j,k}^{n}\right\}_{(2.53e)} + \underbrace{\left[\frac{1}{6}\left(H_{z,\mathrm{inc}}\Big|_{i-1,j,k}^{n-1} + H_{z,\mathrm{inc}}\Big|_{i,j+1,k}^{n-1} + H_{z,\mathrm{inc}}\Big|_{i,j,k+1}^{n-1}\right) + \frac{1}{2\sqrt{3}\eta}\left(E_{x,\mathrm{inc}}\Big|_{i,j+1,k}^{n-1} + E_{y,\mathrm{inc}}\Big|_{i-1,j,k}^{n-1}\right)\right]}_{\text{correction term}} \quad (4.47f)$$

Top left front corner of Region 1 ($i = i_1;\ j = j_0;\ k = k_1$)

$$E_x\Big|_{i,j,k}^{n} = \left\{E_x\Big|_{i,j,k}^{n}\right\}_{(2.52)} + \underbrace{\left[\frac{1}{6}\left(E_{x,\mathrm{inc}}\Big|_{i+1,j,k}^{n-1} + E_{x,\mathrm{inc}}\Big|_{i,j-1,k}^{n-1} + E_{x,\mathrm{inc}}\Big|_{i,j,k+1}^{n-1}\right) - \frac{\eta}{2\sqrt{3}}\left(H_{y,\mathrm{inc}}\Big|_{i,j,k+1}^{n-1} + H_{z,\mathrm{inc}}\Big|_{i,j-1,k}^{n-1}\right)\right]}_{\text{correction term}} \quad (4.48a)$$

$$E_y\Big|_{i,j,k}^{n} = \left\{E_y\Big|_{i,j,k}^{n}\right\}_{(2.53a)} + \underbrace{\left[\frac{1}{6}\left(E_{y,\mathrm{inc}}\Big|_{i+1,j,k}^{n-1} + E_{y,\mathrm{inc}}\Big|_{i,j-1,k}^{n-1} + E_{y,\mathrm{inc}}\Big|_{i,j,k+1}^{n-1}\right) - \frac{\eta}{2\sqrt{3}}\left(H_{z,\mathrm{inc}}\Big|_{i+1,j,k}^{n-1} - H_{x,\mathrm{inc}}\Big|_{i,j,k+1}^{n-1}\right)\right]}_{\text{correction term}} \quad (4.48b)$$

$$E_z\Big|_{i,j,k}^{n} = \left\{E_z\Big|_{i,j,k}^{n}\right\}_{(2.53b)} + \underbrace{\left[\frac{1}{6}\left(E_{z,\mathrm{inc}}\Big|_{i+1,j,k}^{n-1} + E_{z,\mathrm{inc}}\Big|_{i,j-1,k}^{n-1} + E_{z,\mathrm{inc}}\Big|_{i,j,k+1}^{n-1}\right) + \frac{\eta}{2\sqrt{3}}\left(H_{x,\mathrm{inc}}\Big|_{i,j-1,k}^{n-1} + H_{y,\mathrm{inc}}\Big|_{i+1,j,k}^{n-1}\right)\right]}_{\text{correction term}} \quad (4.48c)$$

$$H_x\Big|_{i,j,k}^{n} = \left\{H_x\Big|_{i,j,k}^{n}\right\}_{(2.53c)} + \underbrace{\left[\frac{1}{6}\left(H_{x,\mathrm{inc}}\Big|_{i+1,j,k}^{n-1} + H_{x,\mathrm{inc}}\Big|_{i,j-1,k}^{n-1} + H_{x,\mathrm{inc}}\Big|_{i,j,k+1}^{n-1}\right) + \frac{1}{2\sqrt{3}\eta}\left(E_{y,\mathrm{inc}}\Big|_{i,j,k+1}^{n-1} + E_{z,\mathrm{inc}}\Big|_{i,j-1,k}^{n-1}\right)\right]}_{\text{correction term}} \quad (4.48d)$$

$$H_y\Big|_{i,j,k}^{n} = \left\{H_y\Big|_{i,j,k}^{n}\right\}_{(2.53d)} + \underbrace{\left[\frac{1}{6}\left(H_{y,\mathrm{inc}}\Big|_{i+1,j,k}^{n-1} + H_{y,\mathrm{inc}}\Big|_{i,j-1,k}^{n-1} + H_{y,\mathrm{inc}}\Big|_{i,j,k+1}^{n-1}\right) + \frac{1}{2\sqrt{3}\eta}\left(E_{z,\mathrm{inc}}\Big|_{i+1,j,k}^{n-1} - E_{x,\mathrm{inc}}\Big|_{i,j,k+1}^{n-1}\right)\right]}_{\text{correction term}} \quad (4.48e)$$

$$H_z\Big|_{i,j,k}^{n} = \left\{H_z\Big|_{i,j,k}^{n}\right\}_{(2.53e)} + \underbrace{\left[\frac{1}{6}\left(H_{z,\mathrm{inc}}\Big|_{i+1,j,k}^{n-1} + H_{z,\mathrm{inc}}\Big|_{i,j-1,k}^{n-1} + H_{z,\mathrm{inc}}\Big|_{i,j,k+1}^{n-1}\right) - \frac{1}{2\sqrt{3}\eta}\left(E_{x,\mathrm{inc}}\Big|_{i,j-1,k}^{n-1} + E_{y,\mathrm{inc}}\Big|_{i+1,j,k}^{n-1}\right)\right]}_{\text{correction term}} \quad (4.48f)$$

Top right front corner of Region 1 ($i = i_1$; $j = j_1$; $k = k_1$)

$$E_x\Big|_{i,j,k}^{n} = \left\{E_x\Big|_{i,j,k}^{n}\right\}_{(2.52)} + \underbrace{\left[\frac{1}{6}\left(E_{x,\mathrm{inc}}\Big|_{i+1,j,k}^{n-1} + E_{x,\mathrm{inc}}\Big|_{i,j+1,k}^{n-1} + E_{x,\mathrm{inc}}\Big|_{i,j,k+1}^{n-1}\right) - \frac{\eta}{2\sqrt{3}}\left(H_{y,\mathrm{inc}}\Big|_{i,j,k+1}^{n-1} - H_{z,\mathrm{inc}}\Big|_{i,j+1,k}^{n-1}\right)\right]}_{\text{correction term}} \quad (4.49a)$$

$$E_y\Big|_{i,j,k}^{n} = \left\{E_y\Big|_{i,j,k}^{n}\right\}_{(2.53a)} + \underbrace{\left[\frac{1}{6}\left(E_{y,\mathrm{inc}}\Big|_{i+1,j,k}^{n-1} + E_{y,\mathrm{inc}}\Big|_{i,j+1,k}^{n-1} + E_{y,\mathrm{inc}}\Big|_{i,j,k+1}^{n-1}\right) - \frac{\eta}{2\sqrt{3}}\left(H_{z,\mathrm{inc}}\Big|_{i+1,j,k}^{n-1} - H_{x,\mathrm{inc}}\Big|_{i,j,k+1}^{n-1}\right)\right]}_{\text{correction term}} \quad (4.49b)$$

$$E_z\Big|_{i,j,k}^{n} = \left\{E_z\Big|_{i,j,k}^{n}\right\}_{(2.53b)} + \underbrace{\left[\frac{1}{6}\left(E_{z,\mathrm{inc}}\Big|_{i+1,j,k}^{n-1} + E_{z,\mathrm{inc}}\Big|_{i,j+1,k}^{n-1} + E_{z,\mathrm{inc}}\Big|_{i,j,k+1}^{n-1}\right) - \frac{\eta}{2\sqrt{3}}\left(H_{x,\mathrm{inc}}\Big|_{i,j+1,k}^{n-1} - H_{y,\mathrm{inc}}\Big|_{i+1,j,k}^{n-1}\right)\right]}_{\text{correction term}} \quad (4.49c)$$

$$H_x\Big|_{i,j,k}^{n} = \left\{H_x\Big|_{i,j,k}^{n}\right\}_{(2.53c)} + \underbrace{\left[\frac{1}{6}\left(H_{x,\mathrm{inc}}\Big|_{i+1,j,k}^{n-1} + H_{x,\mathrm{inc}}\Big|_{i,j+1,k}^{n-1} + H_{x,\mathrm{inc}}\Big|_{i,j,k+1}^{n-1}\right) + \frac{1}{2\sqrt{3}\eta}\left(E_{y,\mathrm{inc}}\Big|_{i,j,k+1}^{n-1} - E_{z,\mathrm{inc}}\Big|_{i,j+1,k}^{n-1}\right)\right]}_{\text{correction term}} \quad (4.49d)$$

$$H_y\Big|_{i,j,k}^{n} = \left\{H_y\Big|_{i,j,k}^{n}\right\}_{(2.53d)} + \underbrace{\left[\frac{1}{6}\left(H_{y,\mathrm{inc}}\Big|_{i+1,j,k}^{n-1} + H_{y,\mathrm{inc}}\Big|_{i,j+1,k}^{n-1} + H_{y,\mathrm{inc}}\Big|_{i,j,k+1}^{n-1}\right) + \frac{1}{2\sqrt{3}\eta}\left(E_{z,\mathrm{inc}}\Big|_{i+1,j,k}^{n-1} - E_{x,\mathrm{inc}}\Big|_{i,j,k+1}^{n-1}\right)\right]}_{\text{correction term}} \quad (4.49e)$$

$$H_z\Big|_{i,j,k}^{n} = \left\{H_z\Big|_{i,j,k}^{n}\right\}_{(2.53e)} + \underbrace{\left[\frac{1}{6}\left(H_{z,\mathrm{inc}}\Big|_{i+1,j,k}^{n-1} + H_{z,\mathrm{inc}}\Big|_{i,j+1,k}^{n-1} + H_{z,\mathrm{inc}}\Big|_{i,j,k+1}^{n-1}\right) + \frac{1}{2\sqrt{3}\eta}\left(E_{x,\mathrm{inc}}\Big|_{i,j+1,k}^{n-1} - E_{y,\mathrm{inc}}\Big|_{i+1,j,k}^{n-1}\right)\right]}_{\text{correction term}} \quad (4.49f)$$

Consistency conditions on the TF / SF interfaces were developed as above. Each plane outside of the TF / SF interfaces also needs to be modified by subtracting the incident

field term positioned on the interface. The consistency conditions on outside planes of region 1 are given by

Outside rear face of Region 1 ($i = i_0 - 1;\ j = j_0, \ldots, j_1;\ k = k_0, \ldots, k_1$)

$$E_x\Big|_{i,j,k}^{n} = \left\{E_x\Big|_{i,j,k}^{n}\right\}_{(2.52)} - \underbrace{\left[\frac{1}{6}E_{x,\mathrm{inc}}\Big|_{i+1,j,k}^{n-1}\right]}_{\text{correction term}} \tag{4.50a}$$

$$E_y\Big|_{i,j,k}^{n} = \left\{E_y\Big|_{i,j,k}^{n}\right\}_{(2.53a)} - \underbrace{\left[\frac{1}{6}E_{y,\mathrm{inc}}\Big|_{i+1,j,k}^{n-1} - \frac{\eta}{2\sqrt{3}}H_{z,\mathrm{inc}}\Big|_{i+1,j,k}^{n-1}\right]}_{\text{correction term}} \tag{4.50b}$$

$$E_z\Big|_{i,j,k}^{n} = \left\{E_z\Big|_{i,j,k}^{n}\right\}_{(2.53b)} - \underbrace{\left[\frac{1}{6}E_{z,\mathrm{inc}}\Big|_{i+1,j,k}^{n-1} + \frac{\eta}{2\sqrt{3}}H_{y,\mathrm{inc}}\Big|_{i+1,j,k}^{n-1}\right]}_{\text{correction term}} \tag{4.50c}$$

$$H_x\Big|_{i,j,k}^{n} = \left\{H_x\Big|_{i,j,k}^{n}\right\}_{(2.53c)} - \underbrace{\left[\frac{1}{6}H_{x,\mathrm{inc}}\Big|_{i+1,j,k}^{n-1}\right]}_{\text{correction term}} \tag{4.50d}$$

$$H_y\Big|_{i,j,k}^{n} = \left\{H_y\Big|_{i,j,k}^{n}\right\}_{(2.53d)} - \underbrace{\left[\frac{1}{6}H_{y,\mathrm{inc}}\Big|_{i+1,j,k}^{n-1} + \frac{1}{2\sqrt{3}\eta}E_{z,\mathrm{inc}}\Big|_{i+1,j,k}^{n-1}\right]}_{\text{correction term}} \tag{4.50e}$$

$$H_z\Big|_{i,j,k}^{n} = \left\{H_z\Big|_{i,j,k}^{n}\right\}_{(2.53e)} - \underbrace{\left[\frac{1}{6}H_{z,\mathrm{inc}}\Big|_{i+1,j,k}^{n-1} - \frac{1}{2\sqrt{3}\eta}E_{y,\mathrm{inc}}\Big|_{i+1,j,k}^{n-1}\right]}_{\text{correction term}} \tag{4.50f}$$

Outside front face of Region 1 ($i = i_1 + 1;\ j = j_0, \ldots, j_1;\ k = k_0, \ldots, k_1$)

$$E_x\Big|_{i,j,k}^{n} = \left\{E_x\Big|_{i,j,k}^{n}\right\}_{(2.52)} - \underbrace{\left[\frac{1}{6}E_{x,\mathrm{inc}}\Big|_{i-1,j,k}^{n-1}\right]}_{\text{correction term}} \tag{4.51a}$$

$$E_y\Big|_{i,j,k}^{n} = \left\{E_y\Big|_{i,j,k}^{n}\right\}_{(2.53a)} - \underbrace{\left[\frac{1}{6}E_{y,\mathrm{inc}}\Big|_{i-1,j,k}^{n-1} + \frac{\eta}{2\sqrt{3}}H_{z,\mathrm{inc}}\Big|_{i-1,j,k}^{n-1}\right]}_{\text{correction term}} \tag{4.51b}$$

$$E_z\Big|_{i,j,k}^{n} = \left\{E_z\Big|_{i,j,k}^{n}\right\}_{(2.53b)} - \underbrace{\left[\frac{1}{6}E_{z,\mathrm{inc}}\Big|_{i-1,j,k}^{n-1} - \frac{\eta}{2\sqrt{3}}H_{y,\mathrm{inc}}\Big|_{i-1,j,k}^{n-1}\right]}_{\text{correction term}} \tag{4.51c}$$

$$H_x\Big|_{i,j,k}^{n} = \left\{H_x\Big|_{i,j,k}^{n}\right\}_{(2.53c)} - \underbrace{\left[\frac{1}{6}H_{x,\mathrm{inc}}\Big|_{i-1,j,k}^{n-1}\right]}_{\text{correction term}} \tag{4.51d}$$

$$H_y\Big|_{i,j,k}^{n} = \left\{H_y\Big|_{i,j,k}^{n}\right\}_{(2.53d)} - \underbrace{\left[\frac{1}{6}H_{y,\mathrm{inc}}\Big|_{i-1,j,k}^{n-1} - \frac{1}{2\sqrt{3}\eta}E_{z,\mathrm{inc}}\Big|_{i-1,j,k}^{n-1}\right]}_{\text{correction term}} \tag{4.51e}$$

$$H_z\Big|_{i,j,k}^{n} = \left\{H_z\Big|_{i,j,k}^{n}\right\}_{(2.53e)} - \underbrace{\left[\frac{1}{6}H_{z,\mathrm{inc}}\Big|_{i-1,j,k}^{n-1} + \frac{1}{2\sqrt{3}\eta}E_{y,\mathrm{inc}}\Big|_{i-1,j,k}^{n-1}\right]}_{\text{correction term}} \tag{4.51f}$$

Outside left face of Region 1 ($i = i_0, \ldots, i_1;\ j = j_0 - 1;\ k = k_0, \ldots, k_1$)

$$E_x\Big|_{i,j,k}^{n} = \left\{E_x\Big|_{i,j,k}^{n}\right\}_{(2.52)} - \underbrace{\left[\frac{1}{6}E_{x,\mathrm{inc}}\Big|_{i,j+1,k}^{n-1} + \frac{\eta}{2\sqrt{3}}H_{z,\mathrm{inc}}\Big|_{i,j+1,k}^{n-1}\right]}_{\text{correction term}} \tag{4.52a}$$

$$E_y\Big|_{i,j,k}^{n} = \left\{E_y\Big|_{i,j,k}^{n}\right\}_{(2.53a)} - \underbrace{\left[\frac{1}{6}E_{y,\mathrm{inc}}\Big|_{i,j+1,k}^{n-1}\right]}_{\text{correction term}} \tag{4.52b}$$

$$E_z\Big|_{i,j,k}^{n} = \left\{E_z\Big|_{i,j,k}^{n}\right\}_{(2.53b)} - \underbrace{\left[\frac{1}{6}E_{z,\mathrm{inc}}\Big|_{i,j+1,k}^{n-1} - \frac{\eta}{2\sqrt{3}}H_{x,\mathrm{inc}}\Big|_{i,j+1,k}^{n-1}\right]}_{\text{correction term}} \tag{4.52c}$$

$$H_x\Big|_{i,j,k}^{n} = \left\{H_x\Big|_{i,j,k}^{n}\right\}_{(2.53c)} - \underbrace{\left[\frac{1}{6}H_{x,\mathrm{inc}}\Big|_{i,j+1,k}^{n-1} - \frac{1}{2\sqrt{3}\eta}E_{z,\mathrm{inc}}\Big|_{i,j+1,k}^{n-1}\right]}_{\text{correction term}} \tag{4.52d}$$

$$H_y\Big|_{i,j,k}^{n} = \left\{H_y\Big|_{i,j,k}^{n}\right\}_{(2.53d)} \; - \; \underbrace{\left[\frac{1}{6}H_{y,\mathrm{inc}}\Big|_{i,j+1,k}^{n-1}\right]}_{\text{correction term}} \tag{4.52e}$$

$$H_z\Big|_{i,j,k}^{n} = \left\{H_z\Big|_{i,j,k}^{n}\right\}_{(2.53e)} \; - \; \underbrace{\left[\frac{1}{6}H_{z,\mathrm{inc}}\Big|_{i,j+1,k}^{n-1} + \frac{1}{2\sqrt{3}\eta}E_{x,\mathrm{inc}}\Big|_{i,j+1,k}^{n-1}\right]}_{\text{correction term}} \tag{4.52f}$$

Outside right face of Region 1 ($i = i_0, \ldots, i_1;\ j = j_1 + 1;\ k = k_0, \ldots, k_1$)

$$E_x\Big|_{i,j,k}^{n} = \left\{E_x\Big|_{i,j,k}^{n}\right\}_{(2.52)} \; - \; \underbrace{\left[\frac{1}{6}E_{x,\mathrm{inc}}\Big|_{i,j-1,k}^{n-1} - \frac{\eta}{2\sqrt{3}}H_{z,\mathrm{inc}}\Big|_{i,j-1,k}^{n-1}\right]}_{\text{correction term}} \tag{4.53a}$$

$$E_y\Big|_{i,j,k}^{n} = \left\{E_y\Big|_{i,j,k}^{n}\right\}_{(2.53a)} \; - \; \underbrace{\left[\frac{1}{6}E_{y,\mathrm{inc}}\Big|_{i,j-1,k}^{n-1}\right]}_{\text{correction term}} \tag{4.53b}$$

$$E_z\Big|_{i,j,k}^{n} = \left\{E_z\Big|_{i,j,k}^{n}\right\}_{(2.53b)} \; - \; \underbrace{\left[\frac{1}{6}E_{z,\mathrm{inc}}\Big|_{i,j-1,k}^{n-1} + \frac{\eta}{2\sqrt{3}}H_{x,\mathrm{inc}}\Big|_{i,j-1,k}^{n-1}\right]}_{\text{correction term}} \tag{4.53c}$$

$$H_x\Big|_{i,j,k}^{n} = \left\{H_x\Big|_{i,j,k}^{n}\right\}_{(2.53c)} \; - \; \underbrace{\left[\frac{1}{6}H_{x,\mathrm{inc}}\Big|_{i,j-1,k}^{n-1} + \frac{1}{2\sqrt{3}\eta}E_{z,\mathrm{inc}}\Big|_{i,j-1,k}^{n-1}\right]}_{\text{correction term}} \tag{4.53d}$$

$$H_y\Big|_{i,j,k}^{n} = \left\{H_y\Big|_{i,j,k}^{n}\right\}_{(2.53d)} \; - \; \underbrace{\left[\frac{1}{6}H_{y,\mathrm{inc}}\Big|_{i,j-1,k}^{n-1}\right]}_{\text{correction term}} \tag{4.53e}$$

$$H_z\Big|_{i,j,k}^{n} = \left\{H_z\Big|_{i,j,k}^{n}\right\}_{(2.53e)} \; - \; \underbrace{\left[\frac{1}{6}H_{z,\mathrm{inc}}\Big|_{i,j-1,k}^{n-1} - \frac{1}{2\sqrt{3}\eta}E_{x,\mathrm{inc}}\Big|_{i,j-1,k}^{n-1}\right]}_{\text{correction term}} \tag{4.53f}$$

Outside bottom face of Region 1 ($i = i_0, \ldots, i_1;\ j = j_0, \ldots, j_1;\ k = k_0 - 1$)

$$E_x\Big|_{i,j,k}^{n} = \left\{E_x\Big|_{i,j,k}^{n}\right\}_{(2.52)} - \underbrace{\left[\frac{1}{6}E_{x,\mathrm{inc}}\Big|_{i,j,k+1}^{n-1} - \frac{\eta}{2\sqrt{3}}H_{y,\mathrm{inc}}\Big|_{i,j,k+1}^{n-1}\right]}_{\text{correction term}} \tag{4.54a}$$

$$E_y\Big|_{i,j,k}^{n} = \left\{E_y\Big|_{i,j,k}^{n}\right\}_{(2.53a)} - \underbrace{\left[\frac{1}{6}E_{y,\mathrm{inc}}\Big|_{i,j,k+1}^{n-1} + \frac{\eta}{2\sqrt{3}}H_{x,\mathrm{inc}}\Big|_{i,j,k+1}^{n-1}\right]}_{\text{correction term}} \tag{4.54b}$$

$$E_z\Big|_{i,j,k}^{n} = \left\{E_z\Big|_{i,j,k}^{n}\right\}_{(2.53b)} - \underbrace{\left[\frac{1}{6}E_{z,\mathrm{inc}}\Big|_{i,j,k+1}^{n-1}\right]}_{\text{correction term}} \tag{4.54c}$$

$$H_x\Big|_{i,j,k}^{n} = \left\{H_x\Big|_{i,j,k}^{n}\right\}_{(2.53c)} - \underbrace{\left[\frac{1}{6}H_{x,\mathrm{inc}}\Big|_{i,j,k+1}^{n-1} + \frac{1}{2\sqrt{3}\eta}E_{y,\mathrm{inc}}\Big|_{i,j,k+1}^{n-1}\right]}_{\text{correction term}} \tag{4.54d}$$

$$H_y\Big|_{i,j,k}^{n} = \left\{H_y\Big|_{i,j,k}^{n}\right\}_{(2.53d)} - \underbrace{\left[\frac{1}{6}H_{y,\mathrm{inc}}\Big|_{i,j,k+1}^{n-1} - \frac{1}{2\sqrt{3}\eta}E_{x,\mathrm{inc}}\Big|_{i,j,k+1}^{n-1}\right]}_{\text{correction term}} \tag{4.54e}$$

$$H_z\Big|_{i,j,k}^{n} = \left\{H_z\Big|_{i,j,k}^{n}\right\}_{(2.53e)} - \underbrace{\left[\frac{1}{6}H_{z,\mathrm{inc}}\Big|_{i,j,k+1}^{n-1}\right]}_{\text{correction term}} \tag{4.54f}$$

Outside top face of Region 1 ($i = i_0, \ldots, i_1;\ j = j_0, \ldots, j_1;\ k = k_1 + 1$)

$$E_x\Big|_{i,j,k}^{n} = \left\{E_x\Big|_{i,j,k}^{n}\right\}_{(2.52)} - \underbrace{\left[\frac{1}{6}E_{x,\mathrm{inc}}\Big|_{i,j,k-1}^{n-1} + \frac{\eta}{2\sqrt{3}}H_{y,\mathrm{inc}}\Big|_{i,j,k-1}^{n-1}\right]}_{\text{correction term}} \tag{4.55a}$$

$$E_y\Big|_{i,j,k}^{n} = \left\{E_y\Big|_{i,j,k}^{n}\right\}_{(2.53a)} - \underbrace{\left[\frac{1}{6}E_{y,\mathrm{inc}}\Big|_{i,j,k-1}^{n-1} - \frac{\eta}{2\sqrt{3}}H_{x,\mathrm{inc}}\Big|_{i,j,k-1}^{n-1}\right]}_{\text{correction term}} \tag{4.55b}$$

$$E_z\big|_{i,j,k}^{n} = \left\{ E_z\big|_{i,j,k}^{n} \right\}_{\text{(2.53b)}} - \underbrace{\left[\frac{1}{6} E_{z,\text{inc}}\big|_{i,j,k-1}^{n-1} \right]}_{\text{correction term}} \tag{4.55c}$$

$$H_x\big|_{i,j,k}^{n} = \left\{ H_x\big|_{i,j,k}^{n} \right\}_{\text{(2.53c)}} - \underbrace{\left[\frac{1}{6} H_{x,\text{inc}}\big|_{i,j,k-1}^{n-1} - \frac{1}{2\sqrt{3}\eta} E_{y,\text{inc}}\big|_{i,j,k-1}^{n-1} \right]}_{\text{correction term}} \tag{4.55d}$$

$$H_y\big|_{i,j,k}^{n} = \left\{ H_y\big|_{i,j,k}^{n} \right\}_{\text{(2.53d)}} - \underbrace{\left[\frac{1}{6} H_{y,\text{inc}}\big|_{i,j,k-1}^{n-1} + \frac{1}{2\sqrt{3}\eta} E_{x,\text{inc}}\big|_{i,j,k-1}^{n-1} \right]}_{\text{correction term}} \tag{4.55e}$$

$$H_z\big|_{i,j,k}^{n} = \left\{ H_z\big|_{i,j,k}^{n} \right\}_{\text{(2.53e)}} - \underbrace{\left[\frac{1}{6} H_{z,\text{inc}}\big|_{i,j,k-1}^{n-1} \right]}_{\text{correction term}} \tag{4.55f}$$

An example of the 3-D Propagator TF / SF formulation is shown in Fig. 4.6, which illustrates the total and scattered fields in three orthogonal view planes, *x*-*z*, *x*-*y*, and *y*-*z* planes from the centered dielectric cube with a dielectric constant of $\varepsilon_r = 4$. The red box represents the each boundary between the total-field and scattered-field regions, and the dielectric cube is inserted into the total-field region. The entire domain is taken to be $120 \times 120 \times 120$, and the size of the TF / SF region and cube are chosen to be respectively $60 \times 60 \times 60$ and $40 \times 40 \times 40$ from a center point. As shown in Fig. 4.6, the simulated total and scattered fields are respectively observed in the total-field and scattered-field zones as expected.

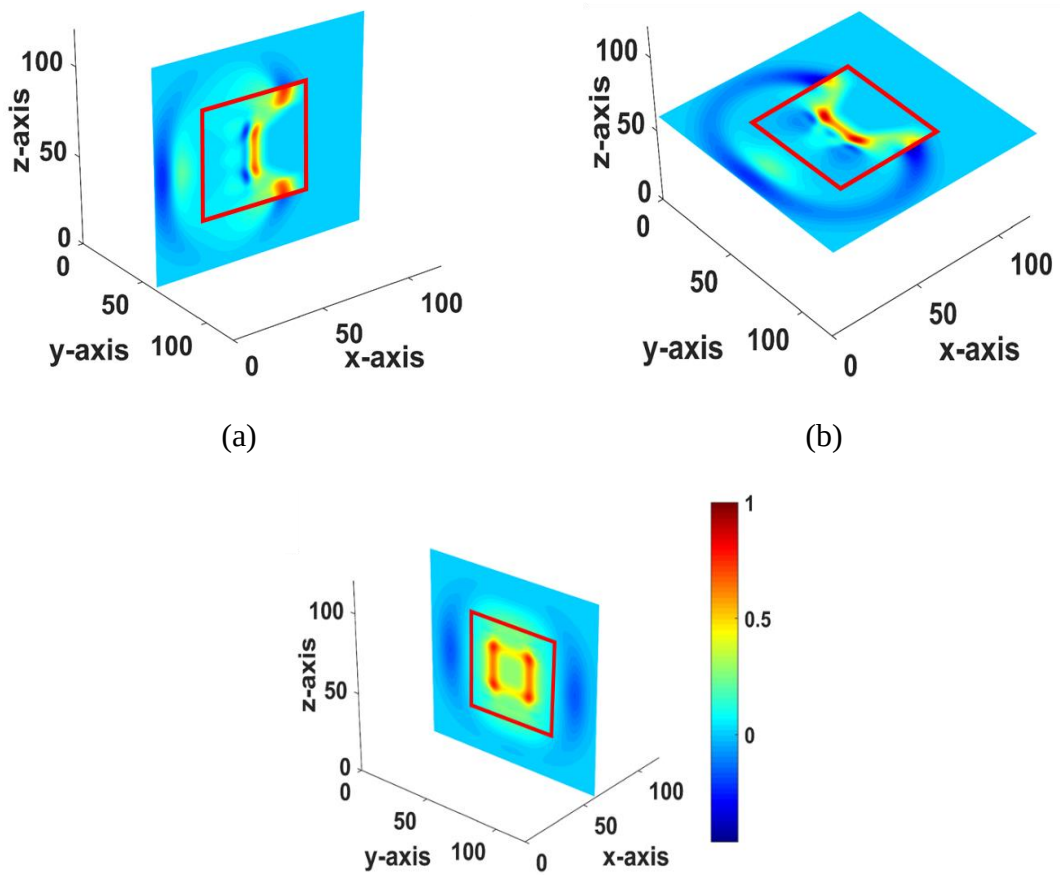

Figure 4.6: Total and scattered fields from the dielectric cube $(\varepsilon_r = 4)$ in (a) *x*-*z* (b) *x*-*y*, and (c) *y*-*z* planes through the center of the box at 120 time steps.

4.5 Summary

In this this chapter each dimensional TF / SF formulation for the time-domain Propagator method was presented. The purpose of the TF / SF implementation is to simulate effectively the plane wave source generation, the null boundary condition, and a wide computational dynamic range. The conventional numerical equations at the lattice point having both the total and scattered fields have been modified by adding or subtracting the incident field terms.

5. NUMERICAL RESULTS*

5.1 Introduction

The complete numerical solution for the full wave time-domain Propagator method has been derived, and numerical techniques including the extrapolation in time, the boundary condition, the absorbing boundary condition, the numerical dispersion and stability condition have been established. In this chapter, the validity and accuracy of the time domain Propagator method are demonstrated by showing various numerical examples.

In 1-D, reflection and transmission coefficients for both lossless and lossy dielectric slabs are computed and compared with the FDTD and analytical solutions. The 1-D Propagator equation is applied to several transmission line problems. In 2-D and 3-D, a Gaussian plane wave propagating in a free-space is first investigated. Then, diffracted and scattered fields from several dielectric objects are simulated and investigated. To demonstrate accuracy, far-field radar cross sections (RCS) of canonical objects using the near-to-far-field transformation technique [3] are calculated and compared with exact solutions and results obtained by other numerical methods.

In each case, unless it is stated, the source is a Gaussian pulse plane wave, given by

---

* Reprinted with permission from "A Propagator analysis of transmission line on an inhomogeneous substrate" by J. Shin and R. D. Nevels, 2017, *Microwave and Optical Technology Letters*, vol. 59, pp. 1411-1416, Copyright 2017 by John Wiley and Sons.
* Reprinted with permission from "A time-domain Propagator numerical method for computational electromagnetics" by J. Shin and R. D. Nevels, 2018, *IEEE Journal on Multiscale and Multiphysics Computational Techniques*, vol. 3, pp. 80-87, Copyright 2018 by IEEE.

$$E_s = \exp\left[-\left[(n-4\kappa)/\kappa\right]^2\right] \tag{5.1}$$

where n is the time step and $\kappa = 10$.

5.2 One-Dimensional Examples

As the first 1-D example, a lossless dielectric slab having a width of 5 cm, a permittivity of $\varepsilon_2 = 4\varepsilon_0$, and permeability of $\mu_2 = \mu_0$ is investigated. The *x*-polarized electric field along with the *y*-directed magnetic field is excited by a Gaussian wave propagating along positive *z*-axis. The numerical space contains 300 grid cells equally divided between the three sections, the dielectric slab and the free space regions on either side. The numerical grid size Δz and time increment $\Delta t = \Delta z / c$ are respectively taken to be 0.5 mm and 1.668 ps.

Fig. 5.1 illustrates a comparison of a Gaussian pulse propagated 600 and 700 time steps with the Propagator method and the FDTD method. In the Propagator method, the previous time fields in the dielectric slab are extrapolated and the fields at the dielectric-free space interfaces are computed by the boundary condition equations (3.7)-(3.8). In the FDTD case, a simple average of the dielectric constants for two different regions is applied on the dielectric interfaces. The pulse computed with the Propagator method equations reflected and refracted at the dielectric boundaries as expected without visible dispersion, whereas the wave calculated with FDTD showed numerical dispersion errors. Fig. 5.2 shows a comparison of reflection coefficients obtained with the Propagator method, the FDTD method and the exact solution. The reflection coefficients are acquired by Fourier

transformation during a single 2,000 time step run of the propagator code. As shown in Fig. 5.2 and Table 5.1, when compared with the exact solution, the Propagator method reflection coefficients have an accuracy of up to five decimal places. Moreover, in the higher frequency range, the Propagator method results are more accurate than the FDTD, specifically by 2.16 % at 14 GHz and 3.7 % at 17 GHz. With respect to a computation time, the Propagator method takes about 20 % more time, than the FDTD does because of additional terms in (2.40) and extrapolating terms (3.2) that are stored in the memory. However, the Propagator method provides very accurate results due to its unique grid meshing and the field coincidence in time and space.

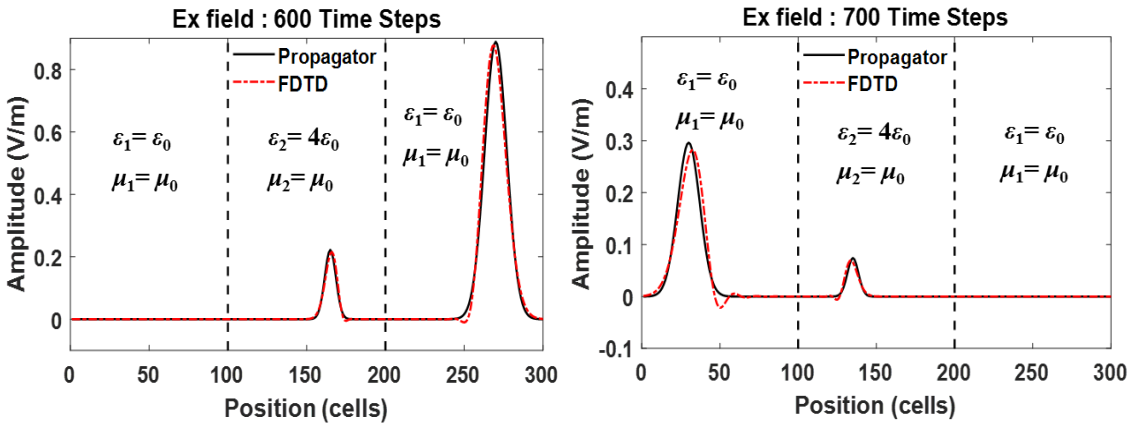

(a) (b)

Figure 5.1: Comparison of total electric field response between the Propagator and FDTD at (a) 600 time steps and (b) 700 time steps.

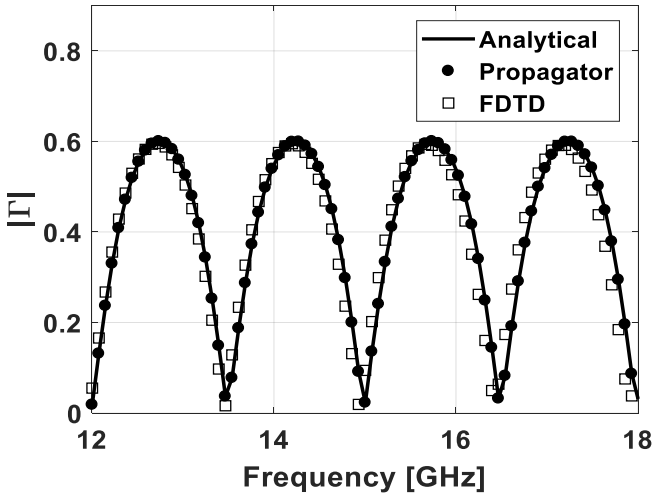

Figure 5.2: Comparison of reflection coefficients for the lossless dielectric slab ($\varepsilon_r = 4$) with the Propagator method, FDTD, and exact solution.

	Reflection coefficients		Computation Time [s]
	At 14 GHz	At 17 GHz	
Theoretical	0.539602	0.541019	
Propagator	0.539594	0.541013	1.0127
FDTD	0.551273	0.561073	0.8441

Table 5.1: Comparison of reflection coefficients and computation time with the Propagator method, FDTD, and exact solution.

Fig. 5.3 illustrates a comparison between the Propagator method and the exact reflection coefficient for plane wave incidence on a lossy dielectric slab having a conductivity of $\sigma = 0.1$ S/m, a dielectric constant of $\varepsilon_r = 4$ (real part) and the same width employed in the previous example. Here the numerical grid size and numerical time increment are respectively chosen to be Δz = 0.25 mm and Δt = 0.834 ps. The results are obtained by the 1-D lossy Propagator method equations [20]. As shown in Fig. 5.3, good agreement with the exact results for a broad frequency range is observed.

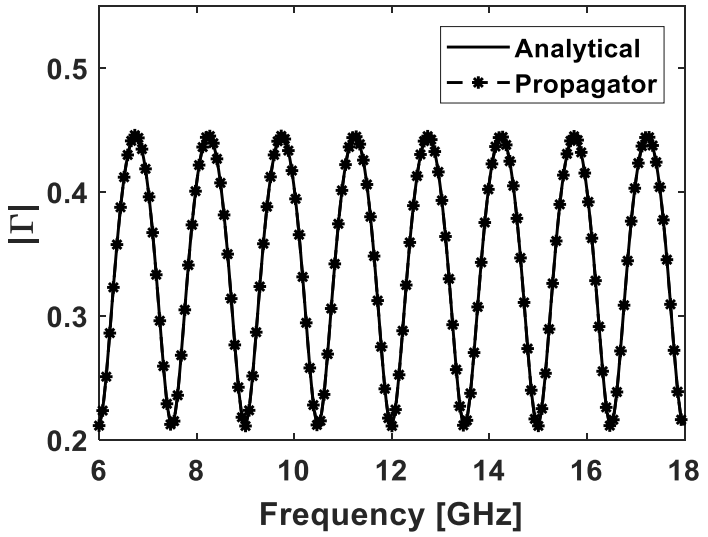

Figure 5.3: Comparison of reflection coefficients for the lossy dielectric slab ($\varepsilon_r = 4$ and $\sigma = 0.1$ S/m) with the Propagator method and exact solution.

The 1-D Propagator equation can be extended to various transmission line problems. As the first example, we investigate a behavior of a pulse excited on a transmission line with multiple dielectric substrates. Fig. 5.4(a) shows a transmission line configuration with two lossless sections, one having Teflon substrate with permittivity of $\varepsilon_1 = 2.1\varepsilon_0$ and permeability of $\mu_1 = \mu_0$, and the other having RT/duroid substrate with permittivity of $\varepsilon_2 = 3.48\varepsilon_0$ and permeability of $\mu_2 = \mu_0$. The distributed inductance is taken to be $L = 0.167$ μH/m in two sections and the capacitance is chosen to be $C = 0.14$ nF/m in the first section and $C = 0.232$ nF/m in the second section. Figs. 5.4(b) and (c) show the rectangular and Gaussian pulses with an initial amplitude of 1 V, having propagated after 150 and 488 time steps. Rectangular and Gaussian pulses were chosen in order to determine the effectiveness of the Propagator method at two extremes in signal input, discontinuous and slowly varying. The total length of the transmission line is 10 cm

with 400 grid cells equally divided between the two substrates. The numerical grid size is therefore $\Delta z = 0.025$ cm and the numerical time increment Δt is 0.834 ps.

In the first substrate, the dielectric constant is $\varepsilon_{r1} = 2.1$, so in one numerical time step Δt the pulse propagates the physical spatial increment $\Delta l_1 = \Delta z / \sqrt{\varepsilon_{r1}} = 0.69\Delta z$. When the leading edge of the incident pulse intersects the material interface at $z = 200\Delta z$, it experiences partial reflection and transmission into the second medium where $\varepsilon_{r2} = 3.48$. The reflection coefficient $\Gamma = 0.126$ is calculated numerically by taking the ratio of the peak values of the reflected and incident pulses. The transmitted pulse propagates with a different velocity so the physical distance traveled in this medium in one numerical time step is $\Delta l_2 = \Delta z / \sqrt{\varepsilon_{r2}} = 0.536\Delta z$. The transmission coefficient $\mathrm{T} = 0.874$ is obtained by taking the ratio of the transmitted and incident pulse amplitudes. The computed reflection and transmission coefficients are accurate up to four decimal places when compared with the exact results although not shown here.

Also, as shown in Fig. 5.4(b), the sharp discontinuities in the leading and trailing edges of the rectangular pulse created in Teflon substrate region experience Gibbs phenomenon when encountering the dielectric discontinuity at the boundary with RT/duroid substrate, as expected to occur in actual practice. Both the rectangular pulse and the Gaussian pulse diffract, reflect, and propagate through the 400 cell numerical distance on the transmission line with two dielectric material substrates without distinguishable numerical dispersion.

(a)

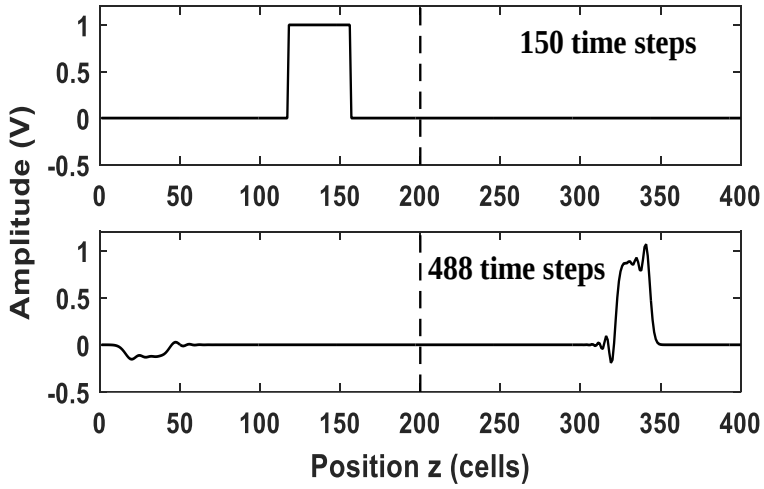

(b)

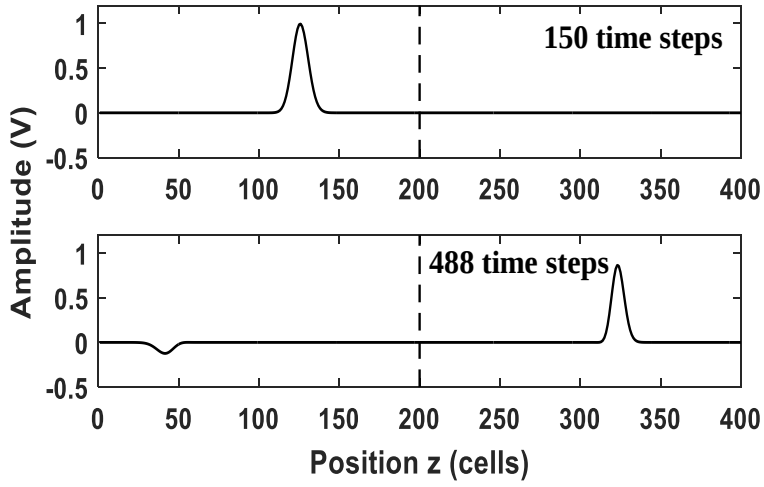

(c)

Figure 5.4: (a) Configuration with two sections of transmission line with different dielectric substrates, $\varepsilon_{r1} = 2.1$ and $\varepsilon_{r2} = 3.48$, and time history of (b) rectangular pulse and (c) Gaussian pulse.

Another example is a transmission line with three sections, a Gallium nitride (GaN) substrate with a dielectric constant of $\varepsilon_{r2} = 8.9$ and relative permeability of $\mu_{r1} = 1$ is sandwiched between two silicon dioxide (SiO_2) substrates with dielectric constant of $\varepsilon_{r1} = 3.9$ and relative permeability of $\mu_{r2} = 1$. All three sections have an equal distributed inductance $L = 0.167$ μH/m , and a center section with a capacitance $C = 0.593$ nF/m is sandwiched between two end sections with $C = 0.26$ nF/m . Here the center section is assumed to be a lossy transmission line with a distributed resistance *R* and the two end sections are lossless. As in the first example, the spatial and time increments are respectively 0.025 cm and 0.834 ps. The total transmission line is numerically discretized with 600 grid points and its length is 15 cm equally divided into three sections. Figs. 5.5(b) and (c) show comparisons of the analytical and propagator numerical reflection and transmission coefficients versus frequency for a low-loss, $R = 0.1\,\Omega$/m, and a high-loss, $R = 100\,\Omega$/m , center section. The broad band frequency domain reflection and transmission coefficient results are obtained by Fourier transformation of the voltage during a single time domain run of the propagator code with a Gaussian excitation function. As expected, the maximum reflection coefficient $\Gamma = 0.39$ and minimum transmission coefficient $T = 0.92$ for a low-loss line occur in odd multiples of a quarter wavelength width of the GaN substrate section. Zero reflection and maximum transmission $T = 1$ occur when the width of the GaN section is a multiple of a half wavelength. The Propagator method and exact results for both low-loss and high-loss cases shown in Figs. 5.5(b) and (c) give excellent agreement over the frequency range 0-15 GHz.

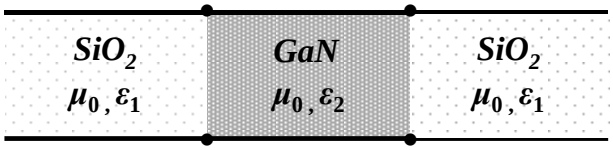

(a)

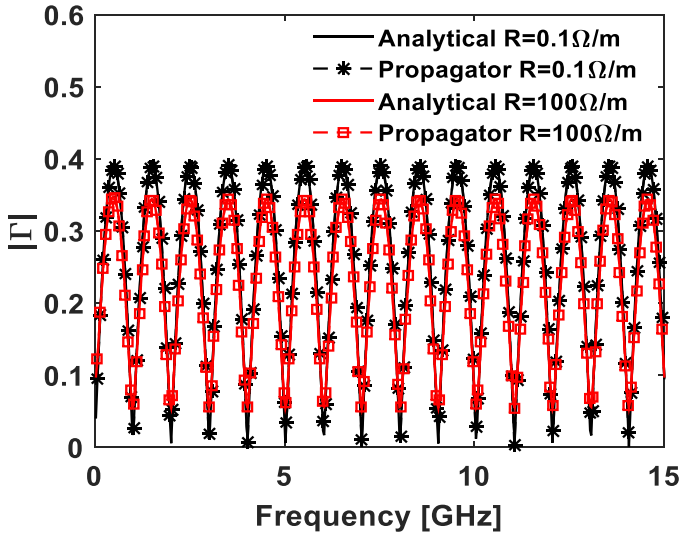

(b)

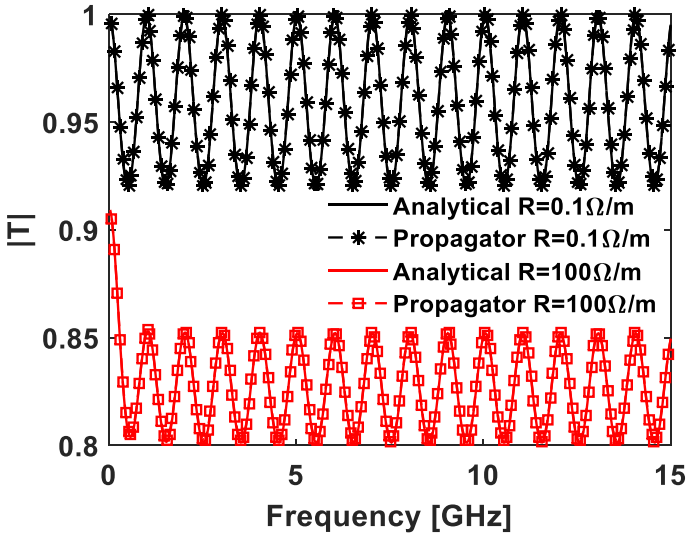

(c)

Figure 5.5: (a) Configuration with three sections of transmission line, and comparison between analytical and Propagator method (b) reflection coefficients and (c) transmission coefficients versus frequency when R=0.1 Ω/m and R=100 Ω/m.

5.3 Two-Dimensional Examples

Recall that the 2-D numerical expression for the time-domain Propagator method cannot be an exact expression, therefore it is expected to have a small numerical dispersion error. In the following, we first generate a plane wave source and observe the manner I which propagates in free space. Then we insert several dielectric objects into a numerical space and investigate how the incident plane wave diffracts and scatters from the objects.

Fig. 5.6 illustrates propagation of the Gaussian plane wave excited by (5.1) with $\kappa = 15$, which is chosen to minimize numerical dispersion error. Fig. 5.6(a) is the generated Gaussian pulse plane wave in 2-D numerical space and Fig. 5.6(b) is the time history of the propagating plane wave in *x*-directed cut. As shown in Fig. 5.6(b), the generated Gaussian plane wave propagates as expected without visible numerical dispersion.

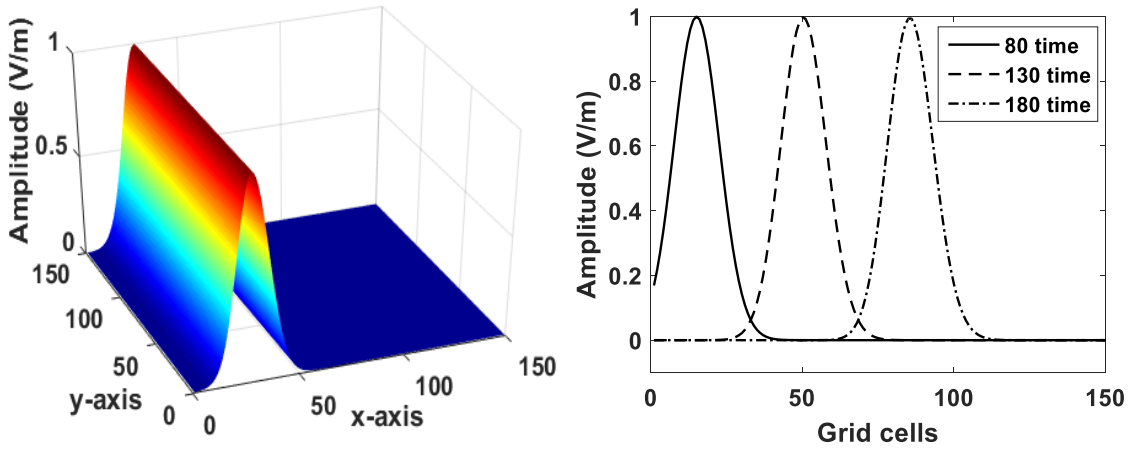

(a) (b)

Figure 5.6: (a) Excited Gaussian pulse plane wave and (b) time history of a traveling plane wave in free space in a 1-D *x*-directed cut at 80, 130, and 180 time steps.

We have simulated the plane wave pulse propagation in free space. We next insert several different dielectric objects into a numerical space for the 2-D TM_z mode. As the first example, a dielectric rectangular cylinder having a dielectric constant of $\varepsilon_r = 4$ and a relative permeability of $\mu_r = 1$ is positioned at the center. Fig. 5.7 illustrates the excited Gaussian plane wave along with the rectangular cylinder and the simulation of the total, incident, and scattered electric field interacting with it at $n = 120$ time steps. The entire numerical region and the cylinder are respectively discretized with 100×100 and 40×40 in *x*- and *y*-axis. The electric and magnetic fields in the dielectric region are extrapolated by (3.2) and the average dielectric constant of the two materials is used on the interfaces. As shown in Fig. 5.7, when the plane wave pulse interacts the cylinder, a portion of it travels through it, some go around, and some of it scatters from the cylinder as expected.

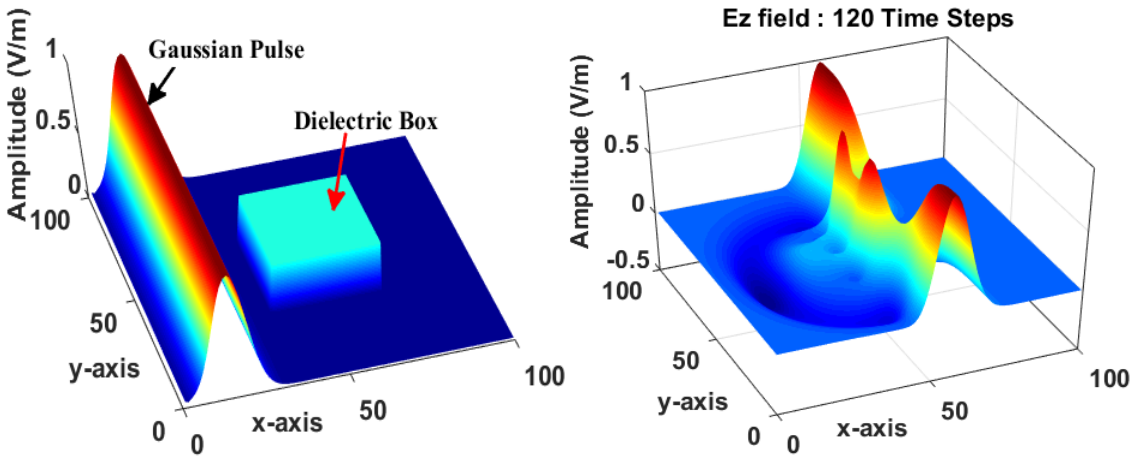

(a) (b)

Figure 5.7: (a) Generated Gaussian plane wave with the centered rectangular dielectric cylinder ($\varepsilon_r = 4$) in a numerical region and (b) the total, incident, and scattered electric field at 120 time steps.

The computed total electric field is then compared with the result acquired by FDTD. A comparison between the Propagator method and FDTD method total electric fields in terms of time steps is illustrated in Fig. 5.8. The numerical time step in both cases is taken to be $\Delta t = \Delta / (\sqrt{2}c)$ and the fields are collected in front of the object along the center axis. Good agreement is observed as shown in Fig. 5.8.

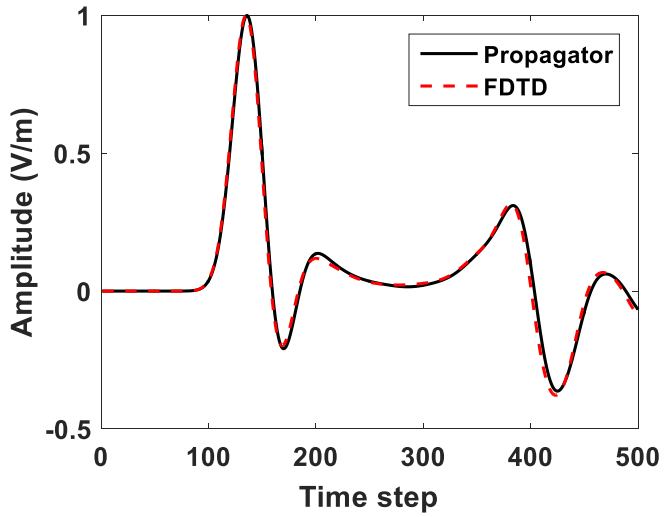

Figure 5.8: Comparison of time history of total electric field by the rectangular dielectric cylinder $(\varepsilon_r = 4)$ between the Propagator method and FDTD results.

The next example is a circular dielectric cylinder, which has a dielectric constant of $\varepsilon_r = 4$ and a curved material boundary. To simulate the plane wave pulse interacting with the dielectric circular cylinder, a simple in-or-out approach is used to determine the material property. Each cell is 'in' a dielectric region if the distance from the dielectric to the center of the cell is less than a cell radius, or 'out' if it is larger than a cell radius. The numerical space is discretized with 100×100 cells and the cylinder radius *r* is 15 grid cells. As shown in Fig. 5.9, the plane wave diffracts and scatters from the cylinder as expected.

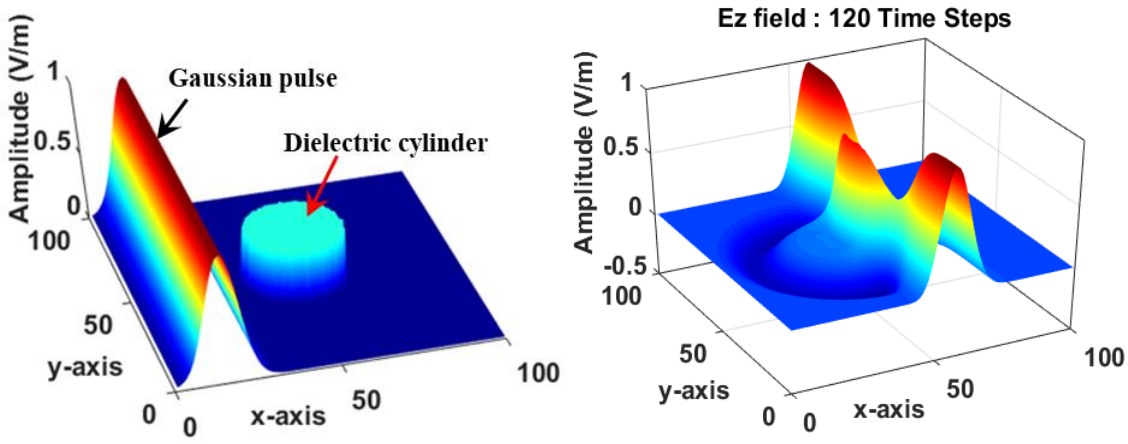

(a) (b)

Figure 5.9: (a) Generated Gaussian plane wave with the centered circular dielectric cylinder ($\varepsilon_r = 4$) in a numerical region and (b) the interacted total electric field from the cylinder at 120 time steps.

In the following, we compute the normalized bistatic RCS in terms of observation angle ϕ for several 2-D dielectric objects. The total-field / scattered-field formulation discussed in chapter 4 is implemented in the Propagator method code and the far-field RCS is obtained by the near-to-far-field transformation [3].

Consider first a square dielectric cylinder having a dielectric constant of $\varepsilon_r = 4$ and a side length $a = \lambda_0 / \pi$. Fig. 5.10 shows a computed RCS between the Propagator method and FDTD method for a plane wave scattered from a square cylinder. The source is a Gaussian plane wave, TM to z and propagating in the x-direction. The numerical spatial increment is chosen to be $\Delta x = \Delta y = 1.06$ cm and numerical time step is taken to be $\Delta t = \Delta / (\sqrt{2}c)$ and $\Delta t = \Delta / (2c)$ respectively for the Propagator method and FDTD method. The total numerical space and the cylinder are respectively discretized with 150×150 and 30×30 cells. The numerical space is truncated by the UPML [3] for the

FDTD and the null boundary condition for the Propagator method. For computation of the fields on the interfaces, a simple average dielectric constant of two regions was used in both the FDTD and Propagator method codes. In the Propagator method, when computing the current time fields, the previous time fields positioned in the dielectric area including the interfaces are extrapolated by (3.2) with $\varepsilon_r = 4$. As shown in Fig. 5.10, the proposed Propagator method algorithm and FDTD are in very good agreement. Regarding the computation time it was 2.574 s for the Propagator method and 2.528 s for FDTD in 800 time step run. In many situations, a drawback of the Propagator method is that, due to additional terms in the numerical expression and the field extrapolation procedure in the dielectric material, up to 10 % more computation time is required than with the FDTD. However, as mentioned earlier, the Propagator method fields at each grid point can be directly meshed with other equations of science, thus avoiding errors and additional computation caused by averaging the fields in space and time, as does the FDTD.

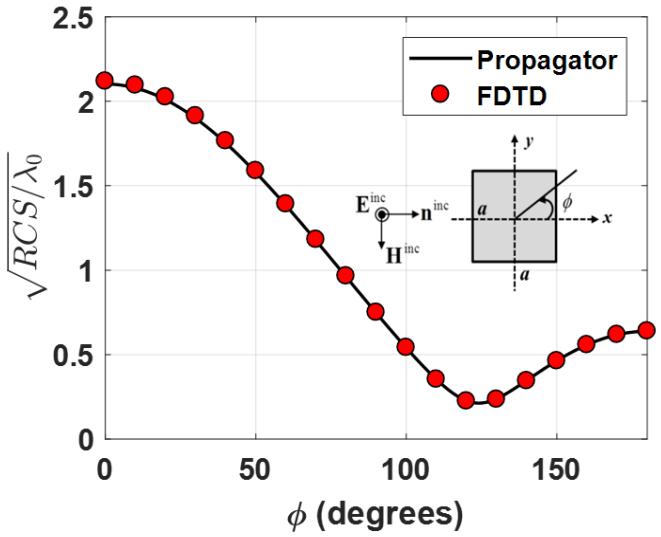

Figure 5.10: Normalized bistatic RCS of a rectangular dielectric cylinder ($\varepsilon_r = 4$, $a = \lambda_0 / \pi$): comparison of the 2-D TM_z Propagator method solution with the FDTD results.

In this example, we compute the normalized far-field RCS of the square dielectric cylinder with a dielectric constant of $\varepsilon_r = 4$ and a side length $a = 0.2\lambda_0$ for the transverse to z electric (TE_z) case, where the vector field components are H_z, E_x, and E_y. A comparison of computed RCS for the square cylinder between the Propagator method and MoM results [42] is shown in Fig. 5.11. Each component of the fields is computed by the 2-D TE_z Propagator equations (2.55). The numerical space and the cylinder are respectively discretized with 200×200 and 40×40 cells. The computed Propagator method RCS gives excellent agreement with the MoM results as shown in Fig. 5.11. We note that, unlike the TM case, for the previous time fields on the interfaces, extrapolating with an average dielectric constant of two mediums gives better results. Based upon our numerous simulations, in the case where the electric field normal to the boundary exists, the previous time field located on the interface would need to be extrapolated with an average dielectric constant of two dielectric materials.

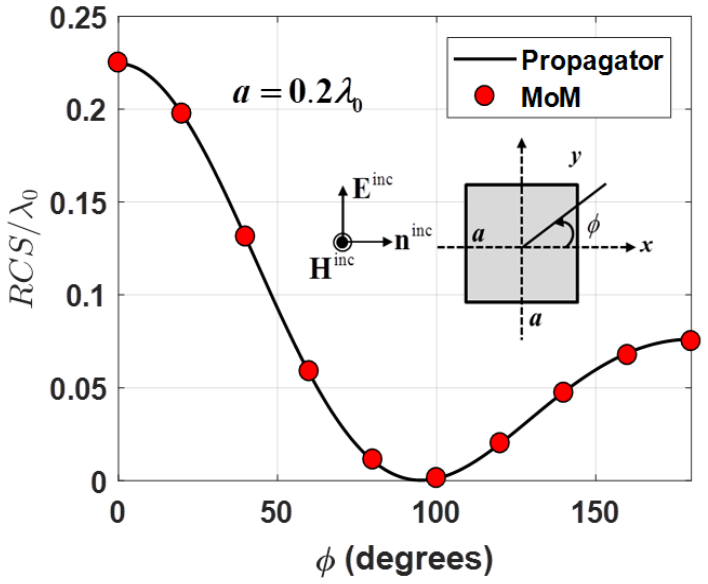

Figure 5.11: Normalized bistatic RCS of a rectangular dielectric cylinder ($\varepsilon_r = 4$, $a = 0.2\lambda_0$) : comparison of the 2-D TE_z Propagator method solution with the MoM results.

Next, we present second example comparing the Propagator method and MoM, the computation of RCS of a thin dielectric slab. Fig. 5.12 shows the comparison of the normalized bistatic RCS between the Propagator method and Richmond's MoM results [43] for the thin dielectric slab having a dielectric constant of $\varepsilon_r = 4$, a thickness of $T = 0.05\lambda_0$, and a width of $W = 2.5\lambda_0$. The grid size of a numerical space is taken to be $\Delta x = \Delta y = 1.25$ cm and the dielectric slab is discretized with 200×4 grid cells in *x*-, and *y*-direction. As seen in Fig. 5.12, there is very good agreement between the two methods even at 0^o edge on incidence.

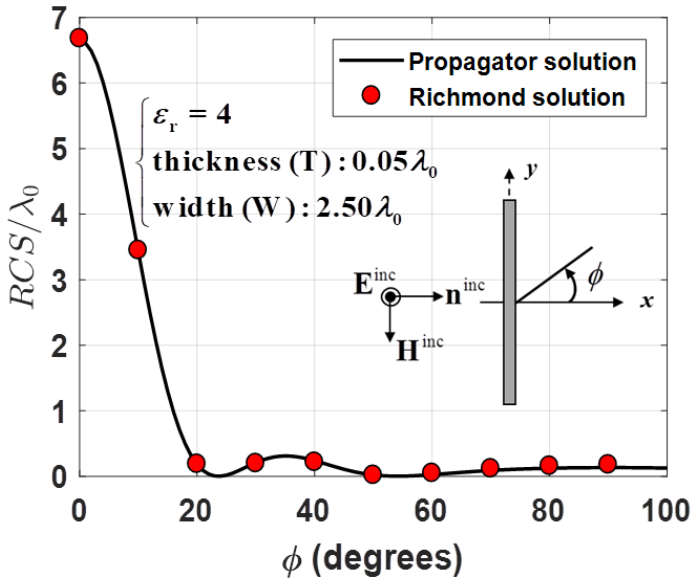

(a)

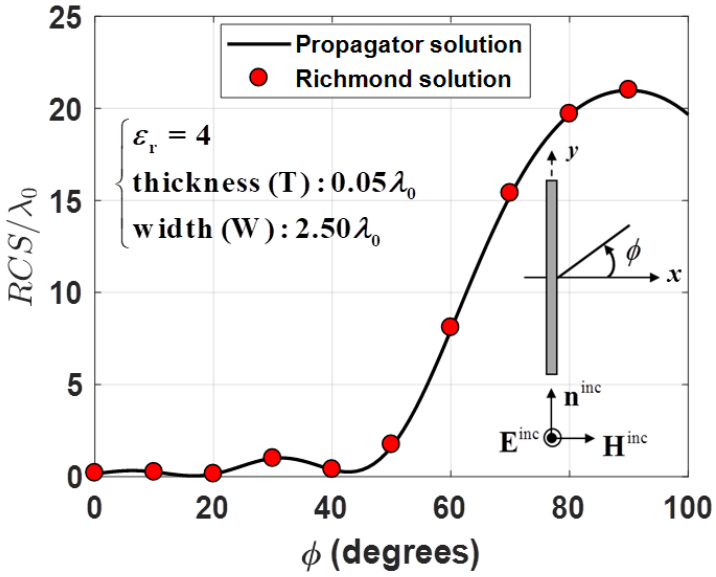

(b)

Figure 5.12: Normalized bistatic RCS of a dielectric slab ($\varepsilon_r = 4$) with a finite thickness and width at (a) normal and (b) grazing incidence: comparison between the 2-D TM_z Propagator method and Richmond's results.

We next investigate the case where there is curvature in a material boundary. Fig. 5.13 shows a comparison between the Propagator method and exact analytical RCS results for a dielectric circular cylinder having a dielectric constant $\varepsilon_r = 2$ and a radius $r = 0.1\lambda_0$ modeled with 30 grid points. Our conformal technique presented in section 3.3 is embedded in the Propagator code to compute the previous time field at grid points on the intersection between the two regions. As shown in Fig. 5.13, the Propagator method RCS is in excellent agreement with the analytical solution. The accuracy of the Propagator method is attributed to the fact that each grid point is the center of a cell and is shared by an additional four neighboring cells in 2-D and an additional six in 3-D. Each cell will intersect the grid point from a different direction and, when the grid point is near the boundary, will contain a different portion of the cylinder, thus providing an average shape and position of the local cylinder boundary.

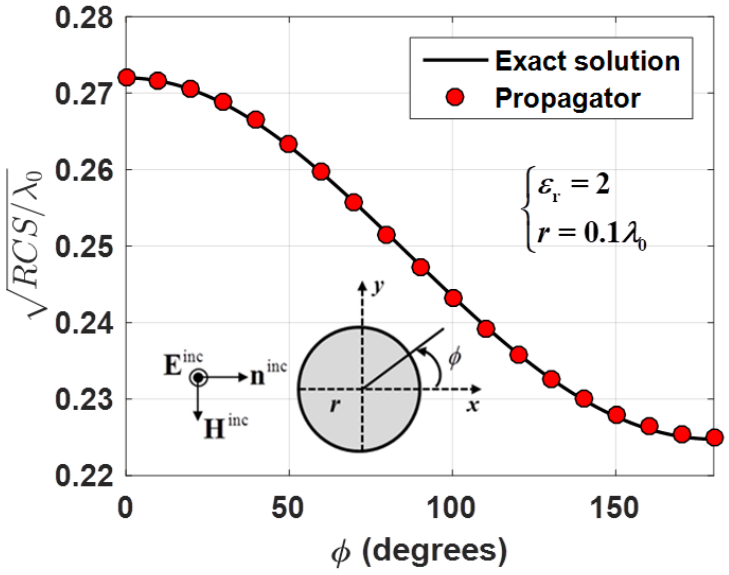

Figure 5.13: Normalized bistatic RCS of a rectangular circular cylinder $(\varepsilon_r = 2,\ r = 0.1\lambda_0)$: comparison of the 2-D TM_z Propagator solution with the exact solution.

5.4 Three-Dimensional Examples

Based upon the numerical dispersion analysis, the 3-D Propagator method numerical expressions (2.52)-(2.53) are subject to have numerical errors. We first observe propagation of a Gaussian pulse plane wave excited by (5.1) using the 3-D Propagator equations (2.52)-(2.53). In (5.1), the value κ is chosen to be $\kappa = 15$ to minimize numerical dispersion. We simulate the incident pulse in free space with an *x*-polarized electric field and a *y*-directed magnetic field, yielding travel in the positive *z*-direction. Fig. 5.14 exhibits the time history of a propagating plane wave in a *z*-directed cut. Referring to Fig. 5.14(b), the incident field amplitude at 160 time steps is slightly decreased by 0.89 % due to numerical dispersion, and the pulse requires 30 time increments, from $n = 130$ to 160 time steps, to propagate 17 grid cells in *z*-direction, from $z = 41\Delta$ to 58Δ, which shows that the velocity in 3-D free space is $v_p = (17\Delta / 30\Delta t) \approx c$ with the 3-D numerical time step $\Delta t_{3D} = \Delta / (\sqrt{3}c)$.

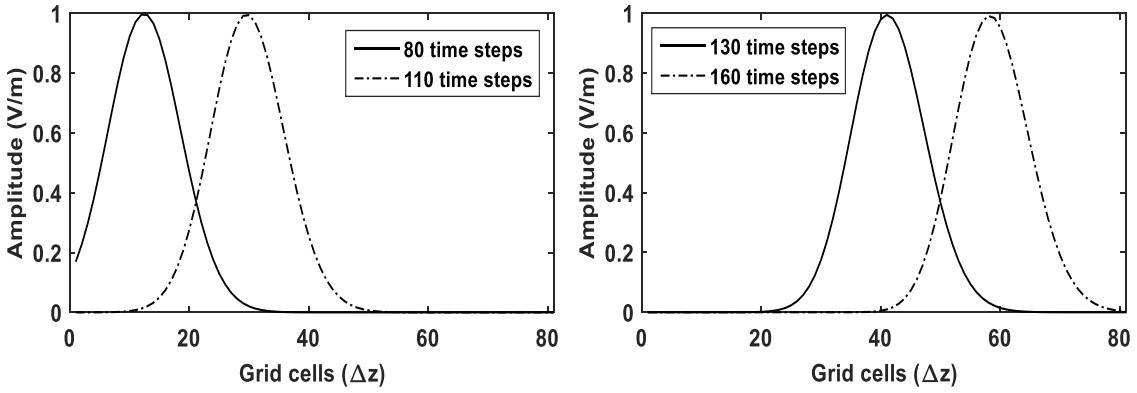

(a) (b)

Figure 5.14: Time history of a Gaussian plane wave traveling to *z*-axis in free space by the 3-D Propagator method.

Next we insert a dielectric cube to investigate how the pulse interacts with the object. The dielectric cube having a dielectric constant of $\varepsilon_r = 4$ and a relative permeability of $\mu_r = 1$ is positioned at the center of a numerical space $60 \times 60 \times 60$ grid points, and it is discretized with $20 \times 20 \times 20$ grid points. Fig. 5.15 illustrates the scattered E_x field, total minus incident field, from the cube in *x*-*z*, *y*-*z*, and *x*-*y* plane views through the center.

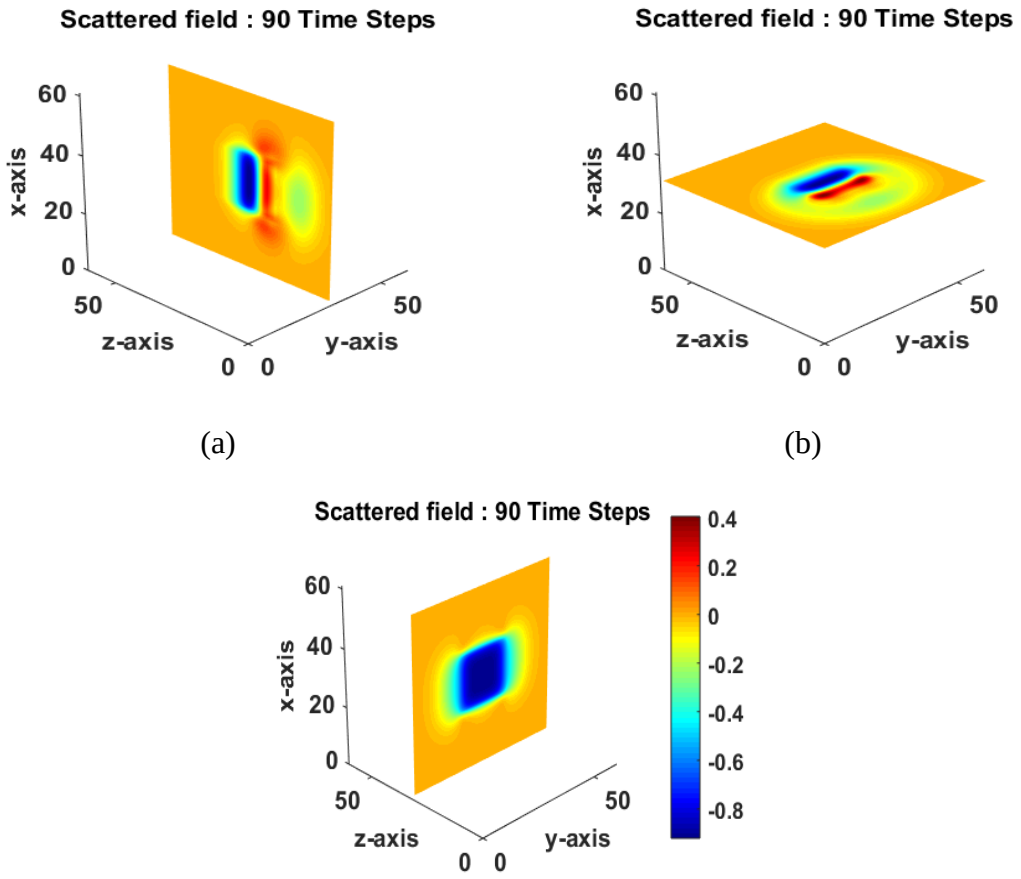

(a) (b)

(c)

Figure 5.15: The electric field scattered from a centered dielectric cube ($\varepsilon_r = 4$) in (a) the *x*-*z*, (b) *y*-*z*, and (c) *x*-*y* planes through the center of the box.

Fig. 5.16 shows the normalized bistatic *x*-*z* plane RCS in *x*-*z* plane and *y*-*z* plane of a 3-D dielectric cube with a dielectric constant of $\varepsilon_r = 4$, at the frequency where each side has a length $a = 0.3\lambda_0$. The Propagator method results are compared with those acquired by the MoM [44] and hybrid FEM-MoM [44]. An incident Gaussian pulse plane wave is traveling in *z*-direction and is *x*-polarized, with a *y*-directed magnetic field. The numerical spatial increment and time step are respectively taken to be $\Delta x = \Delta y = \Delta z = 0.5$ cm and $\Delta t = \Delta / (\sqrt{3}c)$. The numerical space and cube are discretized with $150 \times 150 \times 150$ and $60 \times 60 \times 60$ grid cells, respectively. Good agreement between the three set of results is observed in Fig. 5.16, although as expected MoM provides greater accuracy in the deep null. It was found that the 3-D structure requires a finer grid discretization than the 2-D case.

5.5 Summary

In this chapter, numerical examples were presented in 1-D, 2-D, and 3-D and the validity and accuracy of the time-domain Propagator method was demonstrated. In 1-D, both lossless and lossy cases were considered, and the computed reflection and transmission coefficients showed excellent agreement with the exact results. In the 2-D and 3-D cases, it was showed that the computed RCS of dielectric objects having both flat and curved boundaries via the proposed algorithm were in good agreement with the theoretical results and other numerical methods including the FDTD, MoM, and hybrid FEM-MoM.

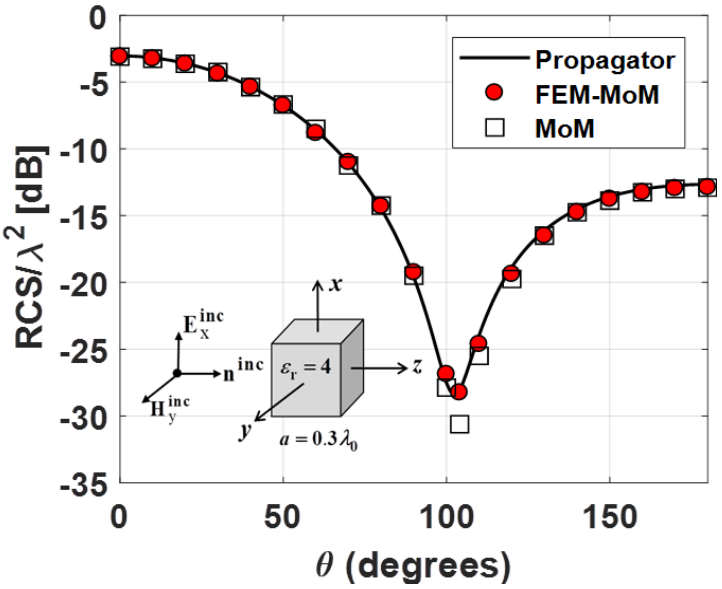

(a)

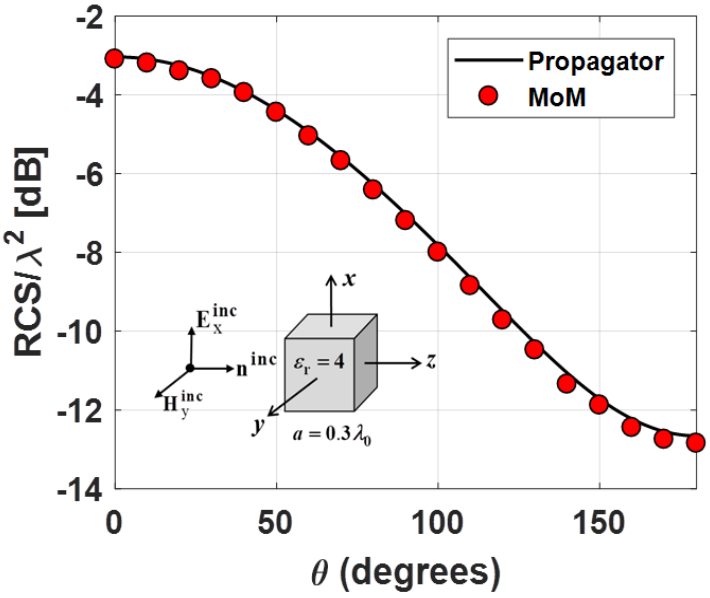

(b)

Figure 5.16: Normalized bistatic RCS of a dielectric cube ($\varepsilon_r = 4$, $a = 0.3\lambda_0$) in (a) *x*-*z* plane ($\phi = 0^o$) and (b) *y*-*z* plane ($\phi = 90^o$): comparison of the 3-D Propagator solution with the hybrid FEM-MoM and MoM results.

6. CONCLUSIONS AND RECOMMENDATIONS

6.1 Conclusions

We proposed the complete full-wave time-domain Propagator method numerical algorithm for electromagnetic fields. The Propagator method is a numerical evaluation of an exact solution to Maxwell's equations in a homogeneous region. The derivation of the compact integral form of propagator and Green's functions in all dimensions has been reviewed. Based on the derived analytical form of the Green's function propagator, numerical equations in 1-D, 2-D, and 3-D have been obtained by numerically evaluating the volume integral containing the Green's function propagator and initial field product. It has been shown that the 1-D solution is both an exact analytical and numerical solution. The 2-D and 3-D propagator solutions have been numerically approximated by evaluation of surface integrations and partial derivatives over the causal boundary, respectively a circle and a sphere. The ideal 2-D and 3-D numerical expressions have been found by an analysis of the numerical dispersion relations and stability conditions.

A primary advantage of the Propagator method is that all electromagnetic field components are computed at each numerical grid point and at the same numerical time. Due to the spatiotemporal coincidence of the field, the 1-D boundary equations were derived and a simple and effective first-order ABC, described as the null boundary condition, was obtained. A conformal boundary condition that takes into account the ratio of areas in 2-D or volumes in 3-D occupied by different dielectric regions have been applied to the proposed method. It has also been shown that the numerical spatial and time

increments can be maintained throughout an inhomogeneous space lattice by applying Newton's third-order backward difference interpolation in time with three consecutive time intervals. This extrapolation technique can be simply extended to higher relative permittivity by moving the time intervals farther back in time.

Numerical dispersion relations have been derived, and it was shown that in free space the 1-D numerical equation has no dispersion, whereas the 2-D and 3-D equations have small dispersion errors, which can be minimized by use of finer sampling. Based on the numerical dispersion relations, stability conditions were investigated and consequently provided additional coefficients in the 2-D and 3-D numerical expressions.

The total-field/scattered-field technique was formulated and incorporated into the Propagator method grid mesh. The advantages of implementing the TFSF formulation are: a robust plane wave source excitation, a null ABC, a wide computational range, and a significant reduction in the number of computations.

Numerical examples have been presented that demonstrate the validity of the proposed Propagator numerical method. It was shown that the 1-D examples provide excellent agreement with exact solutions, up to three to four decimal points, for both lossless and lossy structures. In the 2-D and 3-D cases, electromagnetic wave propagation and scattering from canonical dielectric objects has been investigated. Accuracy was demonstrated by comparing the Propagator method RCS of several dielectric objects, including both flat and curved boundaries, with exact solutions and the results computed by other numerical methods. It is expected that the proposed method can be used to solve

any electromagnetic problem that can be solved by the other standard numerical techniques such as MoM, FDTD and FEM.

6.2 Recommendations for future research

Although we have developed Propagator method numerical expressions and related methods necessary for its numerical implementation in all three dimensions, many issues still remain. First, the boundary condition for dielectric and perfect electric conductor, which has been implemented in 1-D, to 2-D and 3-D cases must be extended. The conformal boundary conditions presented here enabled us to compute the electromagnetic fields in inhomogeneous dielectric regions, however special techniques or the development of tangential and normal boundary conditions in 2-D and 3-D cases are required to handle interfaces and edges of PEC surfaces.

In 2-D and 3-D, we have simulated electromagnetic propagation in free space and in a simple dielectric media. However, there are many cases that have a loss term specified by the conductivity. In a lossy dielectric media, although the 1-D Propagator equations have been derived and verified in [20], due to the complications in the evolution operator matrix, 2-D and 3-D numerical equations have not yet been developed. Therefore the operator matrix and Green's function propagator adding a loss term into Maxwell's equations must be solved.

An effective and viable time-domain numerical method should have the capability to analyze wave propagation in a dispersive material. Generally, frequency-domain methods are better suited to handle frequency dependent material than are time-domain

methods. However, in order to display the time evolution of wave propagation, frequency-domain codes must be run many times in order to cover the frequency spectrum of an input signal. The FDTD method has been applied to dispersive media with a piecewise recursive convolution method developed by Lubbers et.al. [45], [46]. Debye, Lorentz and Drude dispersive media models with the recursive linear interpolation must be incorporated in the Propagator method. This will include mathematical development as well as numerical implementation.

It is also suggested that applications where Schrödinger's equation for quantum mechanics and bio-heat equation for biological applications involve the electromagnetic field should be investigated. The Propagator method mesh having all fields at each grid point and coincident in time is well suited for combining with those equations along with mathematical models. These multi-disciplinary applications could include the interaction of a quantum dot and the plasmonic dipole antenna with Schrödinger's equation [47]–[51] or designing of a microwave heart catheter for ventricular ablation applications adding the bioheat equation [6], [52], [53].

REFERENCES

[1] R. F. Harrington, *Field Computation by Moment Methods*, Piscataway, NJ, USA: IEEE Press, 1993.

[2] J. M. Jin, *The Finite Element Method in Electromagnetics*, 3rd ed., New York, NY, USA: John Wiley & Sons, 2014.

[3] A. Taflove and S. C. Hagness, *Computational Electrodynamics: The Finite-Difference Time-Domain Method*, 2nd ed. Norwood, MA, USA: Artech House, 2000.

[4] K. S. Yee, "Numerical solution of initial boundary value problems involving Maxwell's equations in isotropic media," *IEEE Transactions on Antennas and Propagation*, vol. 14, pp. 302-307, May 1966.

[5] R. P. Feynman and A. R. Hibbs, *Quantum Mechanics and Path Integrals*, New York, NY, USA: McGraw Hill, 1965.

[6] O. Bottauscio, M. Chiampi, and L. Zilberti, "Boundary Element Solution of Electromagnetic and Bioheat Equations for the Simulation of SAR and Temperature Increase in Biological Tissues," *IEEE Transactions on Magnetics*, vol. 48, no. 2, pp. 691-694, Feb. 2012.

[7] J. Schwinger, *Quantum Electrodynamics*, New York, NY, USA: Dover, 1958.

[8] R. Oehme and W. Zimmermann, "Quark and gluon propagators in quantum chromodynamics," *Physical Review D*, vol. 21, pp. 471-484, 1980.

[9] A. Arbouet, A. Mlayah, C. Girard, and G. C. des Francs, “Electron energy losses and cathodoluminescence from complex plasmonic nanostructures: spectra, maps and radiation patterns from a generalized field propagator,” *New Journal of Physics*, vol. 16, 113012, 2014.

[10] X. Du, R. P. Fletcher, and P. J. Fowler, "Pure P-wave propagators versus pseudo-acoustic propagators for RTM in VTI media," *72nd EAGE Conference and Exhibition incorporating SPE EUROPEC*, Jun. 2010.

[11] M. Badiey, I. Jaya, and A. H-D. Ching, “Propagator Matrix for Plane Wave Reflection from Inhomogeneous Anisotropic Poroelastic Seafloor,” *Journal of Computational Acoustics*, vol. 2, no. 11, 1994.

[12] F. Gilbert and G. E. Backus, “Propagator Matrices in Elastic Wave and Vibration Problems,” *Geophysics*, vol. 31, no. 2, pp. 326-332, 1966.

[13] H. Kleinert, *Path Integrals in Quantum Mechanics, Statistics and Polymer Physics*. Singapore: World Scientific, 1990.

[14] L. S. Schulman, *Techniques and Applications of Path Integration*, New York, NY, USA: John Wiley & Sons, 1981.

[15] J. B. Keller and D. W. McLaughlin, “The Feynman Integral,” *The American Mathematical Monthly*, vol. 82, no. 5, pp. 451-465, May 1975.

[16] R. D. Nevels and J. Jeong, “The time domain Green’s function and propagator for Maxwell’s equations,” *IEEE Transactions on Antennas and Propagation*, vol. 52, no. 11, pp. 3012-3018, Nov. 2004.

[17] R. D. Nevels and J. Jeong, "Corrections to 'The complete free space Green's function and propagator for Maxwell's equations," *IEEE Transactions on Antennas and Propagation*, vol. 56, no. 4, pp. 1212-1213, Apr. 2008.

[18] R. D. Nevels and J. Jeong, "Time domain coupled field dyadic Green's function solution for Maxwell's equations," *IEEE Transactions on Antennas and Propagation*, vol. 56, no. 8, pp. 2761-2764, Aug. 2008.

[19] R. D. Nevels and J. Miller, "A simple equation for analysis of nonuniform transmission line," *IEEE Transactions on Microwave Theory and Techniques*, vol. 49, no. 4, pp. 721-724, Apr. 2001.

[20] J. Jeong and R. D. Nevels, "Time domain analysis of a lossy nonuniform transmission line," *IEEE Transactions on Circuits and Systems II: Express Briefs*, vol. 56, no. 2, pp. 157–161, Feb. 2009.

[21] J. Jeong, I. Hong, and R. D. Nevels, "The Time domain propagator method for lossless multiconductor quasi-TEM lines," *IEEE Transactions on Advanced Packaging*, vol. 32, no. 3, pp. 619-626, Aug. 2009.

[22] J. Shin and R. D. Nevels, "A propagator analysis of transmission line on an inhomogeneous substrate," *Microwave and Optical Technology Letters*, vol. 59, no. 6, pp. 1411-1416, Jun. 2017.

[23] H. T. Abbas, J. Shin, and R. D. Nevels, "Numerical Techniques for Evaluating Electromagnetic Field Propagators," *IEEE International Conference on Computational Electromagnetics*, pp. 22-23, Hong Kong, Feb. 2015.

[24] J. Shin, H. T. Abbas, and R. D. Nevels, "A Numerical Method for the Electromagnetic Field Time Domain Propagator Equations," *IEEE AP-S and URSI International Conference on Antennas and Propagation*, pp. 1480-1481, Vancouver, Canada, Jul. 2015.

[25] J. Shin and R. D. Nevels, "Recent Progress in the Development of a Propagator Method for Electromagnetic Fields," *IEEE AP-S and URSI International Conference on Antennas and Propagation*, pp. 1041-1042, Puerto Rico, Jul. 2016.

[26] J. Shin and R. D. Nevels, "Analysis of a time-domain Propagator numerical method for electromagnetic fields," *Texas Symposium on Wireless & Microwave Circuits & Systems*, Waco, TX, Mar. 2017.

[27] J. Shin and R. D. Nevels, "A full wave analysis of a Propagator method for electromagnetic fields," *IEEE AP-S and URSI International Conference on Antennas and Propagation*, pp. 1131-1132, San Diego, CA, Jul. 2017.

[28] J. Shin and R. D. Nevels, "Propagator Methods in Electromagnetics," Chapter in *The World of Applied Electromagnetics*, A. Lakhttakia and C.M. Furse Eds., Springer, 2017.

[29] J. Shin and R. D. Nevels, "Numerical dispersion and stability of the time-domain Propagator numerical algorithm," *IEEE AP-S and URSI International Conference on Antennas and Propagation*, Boston, MA, Jul. 2018.

[30] J. Shin and R. D. Nevels, "A time-domain Propagator numerical method for computational electromagnetics," *IEEE Journal on Multiscale and Multiphysics Computational Techniques*, vol. 3, pp. 80-87, Jun. 2018.

[31] G. Barton, *Elements of Green's Functions and Propagation*, New York, NY, USA: Oxford, 1989.

[32] S. M. Rao and D. R. Wilton, "Transient scattering by conducting surfaces of arbitrary shape," *IEEE Transactions on Antennas and Propagation*, vol. 39, no. 1, pp. 56-61, Jan. 1991.

[33] C. T. Tai, *Dyadic Green Functions in Electromagnetic Theory*, New York, NY, USA: IEEE Press, 1971.

[34] I. A. Maksoud, H. Elkamchouchi, and R.D. Nevels, "On the general tensor solution to Maxwell's equations and its potential as a numerical technique for antennas in complex environments," *IEEE Middle East Conference on Antennas and Propagation*, Cairo, Egypt, Oct. 2010.

[35] H. C. Chen, *Theory of Electromagnetic Waves*, New York, NY, USA: McGraw Hill, 1983.

[36] Y. A. Brychkov and A. P. Prudnikov, *Integral Transforms of Generalized Functions*, New York, NY, USA: Gordon and Breach Science, 1989.

[37] W. Cheney and D. Kincaid, *Approximation by Spline Functions, in Numerical Mathematics and Computing*, 6th ed., Thomson Brooks/Cole, Belmont, CA, pp. 385-399, 2008.

[38] W. Yu and R. Mittra, "A conformal Finite Difference Time Domain technique for modeling curved dielectric structures," *IEEE Microwave and Wireless Components Letters*, vol. 11, no. 1, pp. 25-27, Jan. 2001.

[39] G. Mur, “Absorbing boundary conditions for finite-difference approximation of the time-domain electromagnetic-field equations,” *IEEE Transactions on Electromagnetic Compatibility*, vol. EMC-23, no. 4, pp. 377-382, Nov. 1981.

[40] Z. P. Liao, H. L. Wong, B. P. Yang, and Y. F. Yuan, “A transmitting boundary for transient wave analyses,” *Science in China Series A-Mathematics, Physics, Astronomy & Technological Science*, vol. 27, no. 10, pp. 1063-1076, 1984.

[41] J. P. Berenger, “A perfectly matched layer for the absorption of electromagnetic waves,” *Journal of Computational Physics*, vol. 114, no. 2, pp. 185-200, Oct. 1994.

[42] G. Alsharahi, A. Faize, and A. Driouach, “MOM Application for calculating the RCS Two-Dimensional Dielectric Geometric Shape (TE),” *International Journal of Innovation and Applied Studies*, vol. 11, no. 1, pp. 58-62, Apr. 2015.

[43] J. H. Richmond, “Scattering by a dielectric cylinder of arbitrary cross-section shape,” *IEEE Transactions on Antennas and Propagation*, vol. AP-13, pp. 334-341, May 1965.

[44] M. M. Ilic´, M. Djordjevic´, A. Z. Ilic´, and B. M. Notaroˇs, “Higher order hybrid FEM-MoM technique for analysis of antennas and scatters,” *IEEE Transactions on Antennas and Propagation*, vol. 57, no. 5, pp. 1452-1459, May 2009.

[45] R. J. Lubbers, D. Steich, and K. Kunz, “FDTD calculation of scattering from frequency-dependent materials,” *IEEE Transactions on Antennas and Propagation*, vol. 41, no. 9, pp. 1249-1257, Sep. 1993.

[46] D. F. Kelly and R. J. Lubbers, "Piecewise linear recursive convolution for dispersive media using FDTD," *IEEE Transactions on Antennas and Propagation*, vol. 44, no. 6, pp. 792-797, Jun. 1996.

[47] R. D. Nevels, G. R. Welch, P. S. Cremer, P. Hemmer, T. Phillips, S. Scully, A. V. Sokolov, A. A. Svidzinsky, H. Xia, A. Zheltikov, and M. O. Scully, "Figuration and detection of single molecules," *Molecular Physics*, vol. 110, no. 15-16, pp. 1993-2000, Aug. 2012.

[48] R. D. Nevels and K. A. Michalski, "On the Behavior of Surface Plasmons at a Metallo-Dielectric Interface," *Journal of Lightwave Technology*, vol. 32, no. 19, pp. 3299-3305, Oct. 2014.

[49] R. D. Nevels and H. T. Abbas, "Optical Nanoantennas," Chapter in *Handbook of Antenna Technologies*, Chen Zhi Ning ed., Springer, 2015.

[50] I. Ahmed, E. H. Khoo, E. Li, and R. Mittra, "A Hybrid Approach for Solving Coupled Maxwell and Schrödinger Equations Arising in the Simulation of Nano-Devices," *IEEE Antennas and Wireless Propagation Letters*, vol. 9, pp. 914-917, 2010.

[51] C. J. Ryu, A. Y. Liu, W. E. Sha, and W. C. Chew, "Finite-Difference Time-Domain Simulation of the Maxwell–Schrödinger System," *IEEE Journal on Multiscale and Multiphysics Computational Techniques*, vol. 1, pp. 40-47, Sep. 2016.

[52] R. D. Nevels, D. Arndt, G. Raffoul, J. Carl, and A. Pacifico, "Microwave Catheter Design," *IEEE Transactions on Biomedical Engineering*, vol. 45, no. 7, pp. 885-890, Jul. 1998.

[53] T. Samaras, A. Christ, and N. Kuster, "Effects of geometry discretization aspects on the numerical solution of the bioheat transfer equation with the FDTD technique," *Physics in Medicine and Biology*, vol. 51, no. 11, May 2006.